

**BILATERAL CONTROL - A SLIDING MODE CONTROL  
APPROACH**

by  
**CAGDAS DENIZEL ONAL**

Submitted to the Graduate School of Engineering and Natural Sciences  
in partial fulfillment of  
the requirements for the degree of  
Master of Science  
Sabanci University  
Spring 2005

BILATERAL CONTROL - A SLIDING MODE CONTROL APPROACH

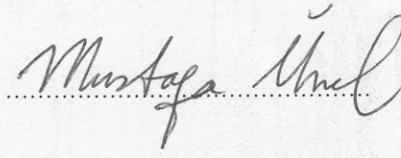
Çağdaş Önal

APPROVED BY

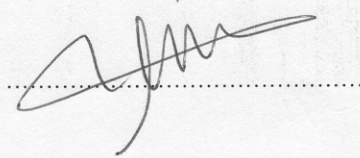
Prof. Dr. Asif SABANOVIC  
(Thesis Supervisor)



Assoc. Prof. Dr. Mustafa UNEL



Assist. Prof. Dr. Ibrahim TEKIN



DATE OF APPROVAL: .....14.07.2025.....

©Cagdas Denizel Onal 2005

All Rights Reserved

*to the time interval between August 2004 and August 2005*

*&*

*all it reminds..*

## Acknowledgments

I wish to express my gratitude to everyone who contributed in any way to the completion of this thesis. Among all, I must single out my supervisor, Prof. Dr. Asif Sabanovic, who initiated the study and didn't abandon his support in any phase of it, in addition to his valuable friendship, patience, and understanding. It has always been nice and enlightening to work with him.

One of the people I owe thanks to is Assoc. Prof. Dr. Mustafa Unel, who has been very helpful in developing a researcher's approach in me and whose motivation and encouragement has added considerably to my graduate experience in Sabanci University as well as the career ahead of me. I appreciate his vast knowledge and skills as well as his ambitious character and insightful comments.

I would also like to thank Assist. Prof. Dr. Ibrahim Tekin from Telecommunications Program, for finding time in his busy schedule to serve as one of my jurors.

I must acknowledge my friends, who have been very supportive and kind to discuss and exchange many ideas throughout the thesis. Among them, the ones that really made a difference for me could be counted as, Khalid Abidi, whose work and ideas have provided me a starting point; Burak Yilmaz, who is probably one of the smartest and caring people I have ever known; Nusrettin Gulec, Fazil Serincan, Ali Nazmi Ozyagci, Emrah Deniz Kunt and Ahmet Altinisik, who made it clear that they were ready for help if ever necessary.

Very special thanks go out to Aylin Aksu, whose influence on me could not possibly be summarized in a paragraph and with whom we seem to communicate on a level beyond words. Simply, she has redefined the term support, for me.

I would also like to thank my family for the backup and understanding they provided me through my entire life and in particular, I must acknowledge my grandfather, who has always expected the best of me and has been so kind to lend me his name. I hope to be able to bring it back to him one day, in person.

## **Abstract**

Bilateral control is bi-directional control of force-position between two systems connected by a communication link. It is typically used for teleoperation with force feedback, such that the master system is handled by an operator. Motions of the operator are fed forward to the slave system, generally remote to the operator and forces encountered are fed back to the master system, enabling a telepresence of the operator in the remote environment. The necessity of bilateral control lies in its applicability to the tasks that cannot be handled by autonomous manipulators and/or reached by human beings.

Main issues of consideration for bilateral control, namely transparency, scaling and time delay, are addressed and two discrete-time sliding-mode approaches are presented as solutions to highly transparent bilateral controllers that support scaling.

First approach has a force-hybrid architecture, where the cascaded sliding mode hybrid force/position controller on the slave side reacts to the external forces directly. Therefore, it provides a protection (reflex) mechanism on the slave side to large external forces, that the operator cannot respond in time due to the time delay.

Second approach has a decentralized nature. Virtual systems are devised by a linear transformation from the plant space to the task space and sliding mode control has been applied to those virtual systems, hence sides of bilateral control are interchangeable. The decentralized structure of the controller makes it possible to generalize the problem to a coordination and/or cooperation of more than two plants.

High precision has been achieved on experiments for both approaches designed and discussed in detail.

# ÇİFT TARAFLI KONTROL - BİR KAYAN KIPLİ KONTROL YAKLAŞIMI

Çağdaş Denizel Önal

## Özet

Çift taraflı kontrol, iletişim ağıyla bağlı iki sistemin kuvvet ve pozisyonlarının çift yönlü olarak kontrolü demektir. Tipik olarak kuvvet geribeslemeli uzaktan kumanda için kullanılır. İki sistemden yakında olanı (efendi sistem) operatör tarafından yönetilir ve hareketleri uzaktaki (köle) sisteme iletilir. Bu hareketlerden doğan kuvvetler ise operatöre geri beslenir. Böylece operatörün uzak ortamda sanal varlığı sağlanır. Çift taraflı kontrolün gerekliliği bağımsız robot kollarının tam olarak çözemediği insanlarınsa erişemediği görevlerde ortaya çıkar.

Çift taraflı kontrol tasarım ve performansının ana etkenleri, şeffaflık, ölçekleme ve gecikme olarak sayılabilir. Bu çalışmada, bahsedilen etkenler ve yol açtıkları problemler hedeflenmiş, yüksek şeffaflığa sahip ve ölçeklemeyi mümkün kılan bir çift taraflı denetleyici için iki kesikli-zaman kayan kipli yaklaşım çözümü getirilmiştir.

İlk yaklaşımın kuvvet-melez yapısı içinde köle sistemi yöneten basamaklı kayan kipli melez kuvvet/pozisyon denetleyicisi dış kuvvetlere doğrudan tepki gösterir. Böylece, uzak sistemde operatörün gecikme nedeniyle zamanında karşılık veremediği yüksek dış kuvvetlere karşı bir korunma (refleks) mekanizması sağlanmaktadır.

İkinci yaklaşım dağıtılmış bir niteliktedir. Bu yaklaşımda sistem uzayından görev uzayına düzlemsel bir dönüşüm ile sanal sistemler elde edilmiş ve kayan kipli kontrol sanal sistemler üzerinde yapılmıştır. Bu denetleyicinin önemi kontrol problemini, görevleri sistemlere bölüştürerek merkezileştirmektense, doğrudan görev gereksinimlerini hedeflemesidir. Böylece çift taraflı kontrolün iki tarafı birbirinin yerine geçebilir olmuştur. Denetleyicinin dağıtılmış yapısı problemi ikiden fazla sistem için işbirliği ya da eşgüdüm gibi problemlere genellemeye imkan sağlamaktadır.

İki yaklaşım için de deneylerle yüksek hassasiyet sağlanmıştır. Tezde kullanılan kesikli zaman kayan kipli denetleyiciler detaylı olarak tasarlanmış ve açıklanmıştır.

## Table of Contents

Acknowledgments	v
Abstract	vi
Ozet	viii
<b>1 Introduction</b>	<b>1</b>
1.1 Objective	2
1.2 Bilateral Control	3
1.3 Hybrid Force/Position Control	5
1.4 Motivation for using Sliding Mode Control	7
1.5 High Precision in Motion Control	8
1.5.1 Piezoelectric Effect	9
<b>2 Sliding Mode Variable Structure Control</b>	<b>14</b>
2.1 Introduction	14
2.2 Sliding Mode in Variable Structure Systems	15
2.3 Sliding Mode Control in Discrete Time	19
2.4 Disturbance Compensation based on Sliding Mode Control	22
<b>3 Implementation of a Discrete Sliding Mode Approach to High Precision Motion Control</b>	<b>26</b>
3.1 Position Control	27
3.2 Force Control	30
3.3 External Force Observer	33
3.4 Disturbance Compensation and Plant Behaviour Dictation using a Sliding Mode Model Reference Controller(SMMRC)	36
3.5 Controller Parameter Adaptation	43
<b>4 A Cascaded Sliding Mode Hybrid Force/Position Controller</b>	<b>47</b>
4.1 Position Error Estimator with respect to External Force Error	48
4.2 Force Controller Stability Analysis	49

4.3	Error Selection for Hybrid Control . . . . .	51
4.4	Experimental Results . . . . .	52
<b>5</b>	<b>Bilateral Control</b>	<b>65</b>
5.1	Transparency . . . . .	66
5.2	Time Delay . . . . .	68
5.3	Scaling . . . . .	68
5.4	Safe Teleoperation with a Reflex Mechanism on the Slave Side . . . .	68
5.4.1	Experimental Results . . . . .	70
5.5	Decentralized Bilateral Control . . . . .	77
5.5.1	Virtual Plant for Position Tracking . . . . .	78
5.5.2	Virtual Plant for Force Tracking . . . . .	79
5.5.3	Task-Based Bilateral Control . . . . .	80
5.5.4	Sliding Mode Controller Derivation for Task Based Bilateral Control . . . . .	81
5.5.5	Experimental Results . . . . .	83
<b>6</b>	<b>Conclusions</b>	<b>86</b>
	<b>Appendix</b>	<b>88</b>
<b>A</b>	<b>Experimental Setup</b>	<b>88</b>
A.1	Maxon RE-40 DC Motor . . . . .	88
A.2	Piezomechanik PSt150/5/60 Piezoelectric actuator . . . . .	89
A.3	Unscaled Bilateral Control Experimental Setup . . . . .	94
A.4	Scaled Bilateral Control Experimental Setup . . . . .	94
	<b>Bibliography</b>	<b>97</b>

## List of Figures

1.1	The general structure of the two subsystems of bilateral control . . .	3
1.2	The general classical force-position architecture of bilateral control . .	4
1.3	Hybrid Control in Two Degrees of Freedom (a)A 2D Manipulator (b)Case 1: Motion Coordinates Parallel to Position, Force Subspaces (c)Case 2: Motion Coordinates Making an Angle to Position, Force Subspaces (d)Case 3: Real-life Case . . . . .	5
1.4	The classical approach to hybrid control . . . . .	6
1.5	Illustration of a PZT Stack Actuator, Image Courtesy of PI Gmbh . .	11
1.6	3-Axis nanopositioning system (Nanocube), PI Gmbh . . . . .	12
1.7	Custom 3-Axis XYZ Stage, DSM . . . . .	12
1.8	Microscope Turret NanoPositioner, PI Gmbh . . . . .	13
1.9	Microscope Objective NanoPositioners, PI Gmbh . . . . .	13
2.1	Sliding Mode Possibilities ( $s = \sigma$ ) (a) Sliding Mode in Discontinuity Surfaces and Their Intersection (b) Sliding Mode only in the Inter- section of Discontinuity Surfaces . . . . .	17
3.1	PEA Position Controller Results . . . . .	29
3.2	PEA: External Force (measured by load cell) Control for a Step Ref- erence . . . . .	32
3.3	PEA: External Force Control for a Step Reference Magnified for $3.1 <$ $t < 3.5$ . . . . .	32
3.4	PEA: External Force (measured by load cell) Control for a Sinusoidal Reference . . . . .	33
3.5	Maxon RE-40: External Torque Control based on Observed Data with Stationary Obstacle . . . . .	35

3.6	Maxon RE-40: External Torque Control based on Observed Data with Moving Obstacle . . . . .	35
3.7	Traditional Model Reference Controller . . . . .	36
3.8	Sliding Mode Model Reference Controller . . . . .	37
3.9	Open Loop Control using SMMRC . . . . .	39
3.10	PEA: SMMRC Open Loop Position Control Model Response for a 1 um Step . . . . .	39
3.11	PEA: Magnified Model Position Error of SMMRC Open Loop Posi- tion Control for a 1 um Step . . . . .	40
3.12	PEA: SMMRC Open Loop Position Control Plant Response for a 1 um Step . . . . .	40
3.13	PEA: Magnified Plant Position Error of SMMRC Open Loop Position Control for a 1 um Step . . . . .	41
3.14	PEA: SMMRC Open Loop Position Control Plant Response for a 5 nm Step . . . . .	41
3.15	PEA: SMMRC Open Loop Position Control Plant Response for a 1 nm Step . . . . .	42
3.16	PEA: SMMRC Open Loop Position Control Plant Response for a 0.5 nm Step . . . . .	42
3.17	First Kind of Adaptation Scheme on the Sliding Manifold Slope . . .	43
3.18	Second Kind of Adaptation Scheme on the Sliding Manifold Slope (a)Slope Has an Upper Bound for Large Errors and (b)Slope Grows without Bound . . . . .	44
3.19	Maxon RE-40: Position Control for One Increment Pulse Reference with Adaptive Sliding Manifold . . . . .	45
3.20	Maxon RE-40: Magnified Position Error of Position Control for One Increment Pulse Reference with Adaptive Sliding Manifold . . . . .	45
3.21	Maxon RE-40: Position Control for Sinusoidal Reference with Adap- tive Sliding Manifold . . . . .	46
4.1	Cascaded Force Controller . . . . .	47
4.2	PEA Cascaded Force Controller Results . . . . .	50
4.3	Estimated and Actual Position Errors on Both Sides . . . . .	51

4.4	Cascaded Hybrid Force/Position Controller . . . . .	52
4.5	Maxon RE-40: Position and Position Reference; Position Error Graphs	53
4.6	Maxon RE-40: Magnified Position Error for $10 < t < 12$ . . . . .	54
4.7	Maxon RE-40: Observed Torque and Torque References . . . . .	54
4.8	Maxon RE-40: Torque Error for Both Torque References . . . . .	55
4.9	PEA - Experiment 1: Position and Position Reference; Position Error Graphs . . . . .	55
4.10	PEA - Experiment 1: Magnified Position Error for $0 < t < 20$ . . . . .	56
4.11	PEA - Experiment 1: Measured Force and Force Reference; Force Error Graphs . . . . .	56
4.12	PEA - Experiment 1: Magnified Force Error for $30 < t < 55$ . . . . .	57
4.13	PEA - Experiment 1: Magnified Position at the Transition from Po- sition to Force Mode . . . . .	57
4.14	PEA - Experiment 1: Magnified Position at the Transition from Force to Position Mode . . . . .	58
4.15	PEA - Experiment 2: Position and Position Reference; Position Error Graphs . . . . .	58
4.16	PEA - Experiment 2: Magnified Position Error for $15 < t < 35$ . . . . .	59
4.17	PEA - Experiment 2: Measured Force and Force Reference; Force Error Graphs . . . . .	59
4.18	PEA - Experiment 2: Magnified Force Error for $45 < t < 70$ . . . . .	60
4.19	PEA - Experiment 2: Magnified Position at the Transition from Po- sition to Force Mode . . . . .	60
4.20	PEA - Experiment 2: Magnified Position at the Transition from Force to Position Mode . . . . .	61
4.21	PEA - Experiment 3: Position and Position Reference; Position Error Graphs . . . . .	61
4.22	PEA - Experiment 3: Magnified Position Error for $55 < t < 75$ . . . . .	62
4.23	PEA - Experiment 3: Measured Force and Force Reference; Force Error Graphs . . . . .	62
4.24	PEA - Experiment 3: Magnified Force Error for $20 < t < 50$ . . . . .	63

4.25	PEA - Experiment 3: Magnified Position at the Transition from Position to Force Mode . . . . .	63
4.26	PEA - Experiment 3: Magnified Position at the Transition from Force to Position Mode . . . . .	64
5.1	Visualisation of Bilateral Control for the 1D Rotational Case . . . . .	66
5.2	General Two-port Model of a Bilateral Teleoperation System . . . . .	67
5.3	Proposed Force-Hybrid Architecture of Bilateral Control . . . . .	69
5.4	Two RE-40's: Master and Slave Positions and Position Error Graphs	70
5.5	Two RE-40's: Magnified Position Error between Master and Slave Sides for $9 < t < 12$ . . . . .	70
5.6	Two RE-40's: Master and Slave Torques and Torque Error Graphs . .	71
5.7	Two RE-40's: Magnified Torque Error between Master and Slave Sides for $5 < t < 7$ . . . . .	71
5.8	Two RE-40's: Hybrid Controller Results on the Slave Side; Slave Torque, Positive and Negative Slave Torque References and Error Graphs with respect to Each Torque Reference . . . . .	72
5.9	Two RE-40's: Magnified Hybrid Torque Error with respect to Negative Torque Reference on the Slave Side for $5 < t < 7$ . . . . .	72
5.10	Two RE-40's: Magnified Hybrid Torque Error with respect to Positive Torque Reference on the Slave Side for $13 < t < 15$ . . . . .	73
5.11	Scaled Safe Teleoperation Ex 1: Master (Scaled) and Slave Positions and Position Error Graphs . . . . .	74
5.12	Scaled Safe Teleoperation Ex 1: Master and Slave (Scaled) External Torques and Torque Error Graphs . . . . .	74
5.13	Scaled Safe Teleoperation Ex 2: Master (Scaled) and Slave Positions and Position Error Graphs . . . . .	75
5.14	Scaled Safe Teleoperation Ex 2: Master and Slave (Scaled) External Torques and Torque Error Graphs . . . . .	76
5.15	Scaled Safe Teleoperation Ex 2: Slave External Force, Hybrid Force Reference and Hybrid Force Error Graphs . . . . .	76
5.16	The general structure of Task Based Control with a Transformation to Task Space . . . . .	78

5.17	Task Based Bilateral Control . . . . .	80
5.18	Task Based Bilateral Control Ex 1 (Two RE-40's): Master and Slave Positions and Position Error Graphs . . . . .	83
5.19	Task Based Bilateral Control Ex 1 (Two RE-40's): Magnified Position Error between Master and Slave Sides for $16 < t < 18$ . . . . .	83
5.20	Task Based Bilateral Control Ex 1 (Two RE-40's): Master and Slave Torques and Torque Error Graphs . . . . .	84
5.21	Task Based Bilateral Control Ex 2 (Scaled): Master (Scaled) and Slave Positions and Position Error Graphs . . . . .	85
5.22	Task Based Bilateral Control Ex 2 (Scaled): Master and Slave (Scaled) Torques and Torque Error Graphs . . . . .	85
A.1	Structure of the Maxon RE-40 Setup . . . . .	88
A.2	Piezostack Actuators Used in the PEA Experiments . . . . .	89
A.3	Structure of the PEA Setup . . . . .	90
A.4	Simplified Structure of the PEA Setup . . . . .	90
A.5	Electromechanical Model of PEA . . . . .	91
A.6	1 Hz Sinusoidal Voltage Input with Varying Amplitude for Hysteresis Analysis of PEA . . . . .	93
A.7	Position Output of PEA for 1 Hz Sinusoidal Voltage Input with Vary- ing Amplitude . . . . .	93
A.8	PEA Position Voltage (Hysteresis) Curve for 1 Hz Sinusoidal Voltage Input with Varying Amplitude . . . . .	94
A.9	The Experimental Setup for Unscaled Bilateral Control . . . . .	95
A.10	The Experimental Setup for Scaled Bilateral Control . . . . .	96

## List of Tables

A.1	Maxon RE-40 DC Motor Parameters . . . . .	89
A.2	Nominal Parameters of the PEA Model . . . . .	92

## List of Abbreviations

$nD$	:	$n$ -Dimensional
SISO	:	Single Input Single Output
PC	:	Position Controller
FC	:	Force Controller
VSS	:	Variable Structure System
VSC	:	Variable Structure Control
SMC	:	Sliding Mode Control
MEMS	:	Microelectromechanical Systems
NEMS	:	Nanoelectromechanical Systems
DOF	:	Degree of Freedom
SMPC	:	Sliding Mode Position Controller
SMFC	:	Sliding Mode Force Controller
FRF	:	Frequency Response Function
SMHC	:	Sliding Mode Hybrid Force/Position Controller
SMPEE	:	Sliding Mode Position Error Estimator
MRC	:	Model Reference Control
SMMRC	:	Sliding Mode Model Reference Controller
PZT	:	Lead Zirconium Titanate
PEA	:	Piezoelectric Actuator

# Chapter 1

## Introduction

There are many applications or tasks that cannot be done autonomously with robotic systems and/or directly by human operators. Bilateral control, which is typically used for teleoperation, offers a solution to these tasks since it enables the operator to work somewhere without actually being there. That is, if actual presence of an operator is not possible, inclusion of a bilateral control system between the operator and the task would simply give a possibility to the so called *telepresence* of the operator.

Some examples of these kinds of tasks involve

- delicate production or manipulation in scales human beings cannot operate on, mostly due to the limitations in the precision of motion and feeling of the forces (e.g. micro-component production),
- applications in hazardous working conditions, where human beings may not survive (e.g. chemical applications),
- applications in remote and probably many distinct environments and that can only be performed by qualified operators, who are unable to travel to each and every one of them (e.g. medical operations (surgeries) with a high probability of failure for the unexceptional operators).

As bilateral control enables skilled teleoperation on the tasks mentioned above, it offers better safety, lower cost and high accuracy, if carefully designed.

## 1.1 Objective

In robotic applications, high precision motion control is not necessarily enough for high system performance since automation, which generally mimicks human behaviour, has not been developed to maintain stability in their highly nonlinear, random or unknown nature. These applications require the presence of an operator due to the high adaptive capabilities of human beings for optimal performance if they can even work otherwise at all. Nevertheless, in these kind of applications, the environment or workspace make it hard and in many cases impossible for the operator to be able to interact with the system directly.

One kind of the applications mentioned above mainly suffers from the scale. Today, macro robotic automation has almost been excelled and extensive amount of research is being made on small scales that human beings cannot feel, let alone operate directly. Therefore, copying and developing human behaviour to create autonomous systems is not an option anymore. Also, in micro/nano scales it is a known fact that, surface forces become more effective and this creates an unfamiliar and unfriendly environment unabling researchers to apply the same methods as the macro scales. We should here note that manipulation under five nanometers might even suffer from chemical effects as well, adding to the complication of the problem.

Not to mention, there are some other tasks that should take place in hazardous environments for human beings such as some chemical experiments or that need extra effort, attention and/or financial investment to have direct interaction of a human being such as space explorations or medical operations. These tasks may have disastrous effects without the supervision of human operators, and therefore automation on them is yet an open problem.

The limitations in the actual presence of an operator can be solved with bilateral control creating a “telepresence” of the operator and therefore achieving skilled teleoperation. Bilateral control is defined as the control of two systems working together on an actual or virtual task. Typically, it is used for teleoperation, in which one system is called the “master” side and the other is called the “slave” side of bilateral action. Slave subsystem is tracking the positions of the master subsystem and master side provides the forces encountered by the slave side to the operator and hence, teleoperation is achieved.

However, more generally the two subsystems might be treated as “peers” creating a decentralised nature to the bilateral controller, in which case the controller may be further generalised to a “multilateral” structure. With this approach, all subsystems contribute to the requirements of the task, creating a possibility to solve the more general problem of cooperation and/or coordination.

The main objective of this thesis is to develop a model independent approach that addresses main problems of bilateral control in high precision motion control systems. To fulfill this objective, some additional solutions have been developed such as a sliding mode cascaded hybrid force/position controller to be used at the slave side of bilateral action, or a sliding mode model reference controller that essentially compensates for the nonlinearities in one of the experimental setups (PEA). The thesis focuses on theoretical development for fully actuated electromechanical systems affine with respect to control and simple SISO actual implementation of the ideas arised.

## 1.2 Bilateral Control

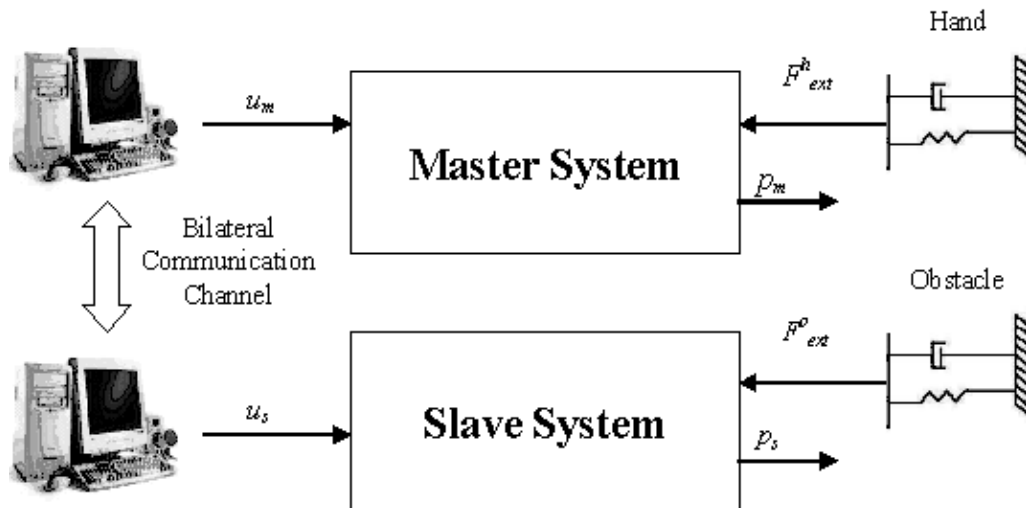


Figure 1.1: The general structure of the two subsystems of bilateral control

In some robotic applications there is a necessity of telepresence of an operator due to hazardous working conditions and/or inefficient autonomous ability of the manipulator as stated above. The method of using a master system handled by an operator to control a slave system and therefore achieving skilled teleoperation is

usually called bilateral control. More generally bilateral control is defined to be two (hence the prefix ‘bi’) systems working together to realize one virtual or actual task.

Even though simpler structures do exist [1], the most convenient structure for bilateral control is force-position architecture as shown in Fig. 1.2 such that the position of the master side is sent to the slave side as position reference while the additive inverse of the forces encountered by the slave side are fed back to the master side as force reference, therefore causing a “feeling” of the environment by the operator. The conformity of this feeling with the real forces is called the “transparency” of the controller. In many cases transparency is crucial to any bilateral controller as much as the stability of the overall system is.

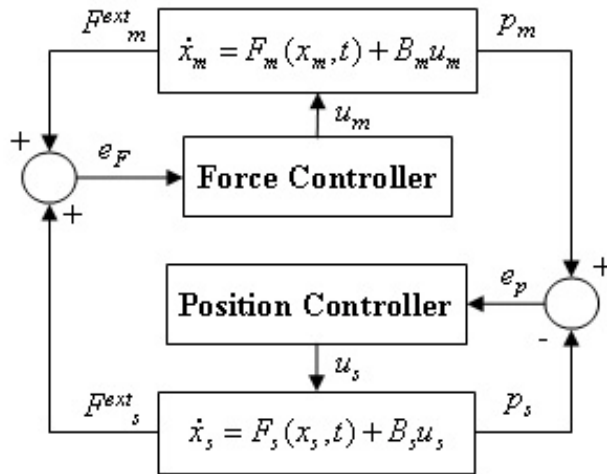


Figure 1.2: The general classical force-position architecture of bilateral control

One other issue of bilateral control is the possible time delays of the communication link between the master and slave sides of architecture. Due to these time delays it may be impossible for the operator to be able to react in time to an input. There are numerous attempts to attack this problem such as [2–4].

Of the above performance criteria, Yokokohji and Yoshikawa defined the ideal response of bilateral control systems in [5]. However, in practice, the system becomes unstable if ideal response is attempted to be realized. There are many methods of decoupling the control problem into several subproblems. Among them, Ohnishi et al.’s [6] approach seems to be the most promising one; since it considers the two sides of the operation to be essentially one combined system of connected sides with

different configurations. Then it defines “functions” of the tasks (force and position control) and transforms the inputs and outputs of the subsystems to the function space. Decoupled controllers are running the differential (force) and common (position) modes of the control.

### 1.3 Hybrid Force/Position Control

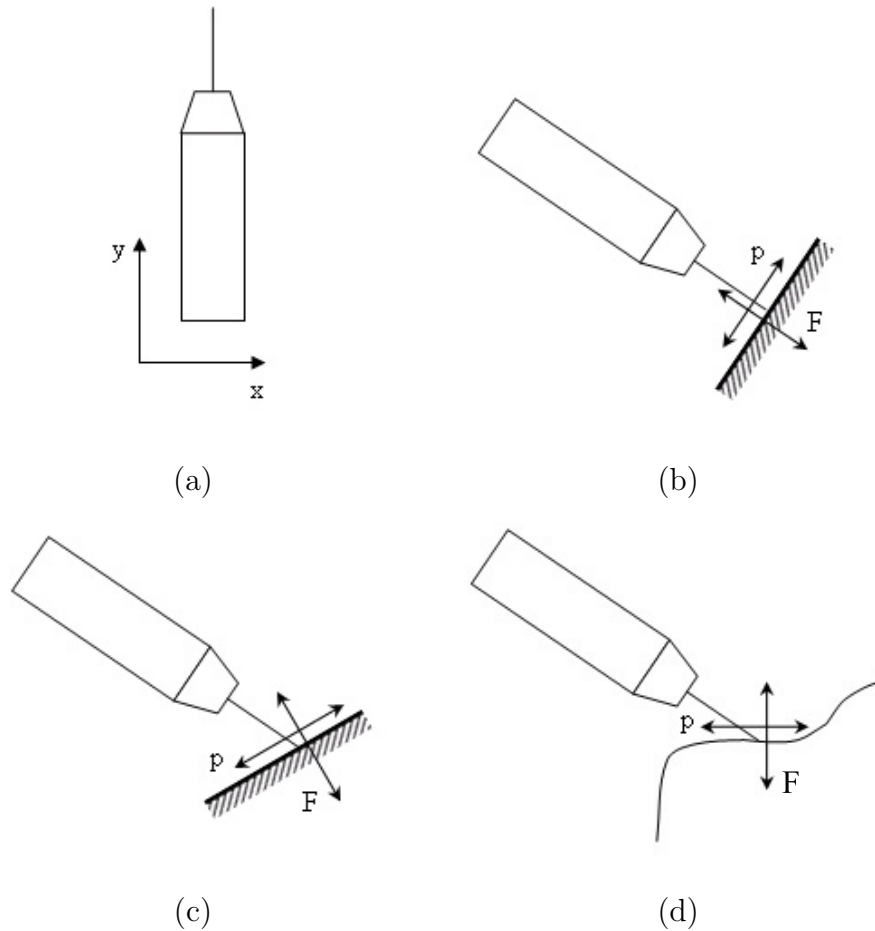


Figure 1.3: Hybrid Control in Two Degrees of Freedom (a)A 2D Manipulator (b)Case 1: Motion Coordinates Parallel to Position, Force Subspaces (c)Case 2: Motion Coordinates Making an Angle to Position, Force Subspaces (d)Case 3: Real-life Case

In many robotic applications, when the manipulator interacts with the external environment, controlling both the tip position and the external force on the contact surface is necessary, which is generally referred as hybrid control.

For Hybrid Control realization, Raibert and Craig [7, 8] developed a scheme

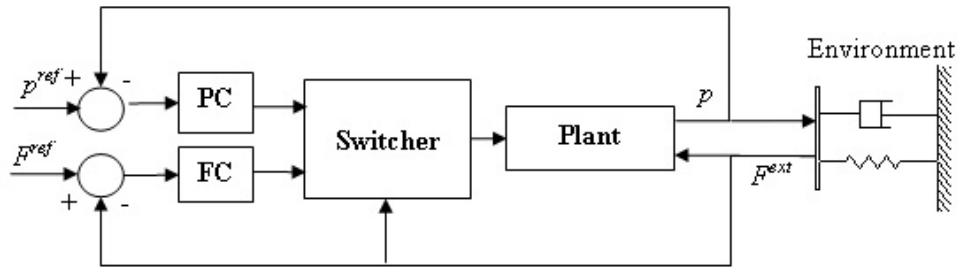


Figure 1.4: The classical approach to hybrid control

to decompose the task space into two orthogonal subspaces, namely position and force as shown in Fig. 1.3 for two degrees of freedom. Their approach has been the classical solution to the problem; however, it had flaws since they considered switching between the two modes when necessary as depicted in Fig. 1.4, which was problematic for two reasons. 1) Jumps occurred in the controller input (i.e. two distinct controllers) to the plant as switching occurs, which was one of the reasons of the kinematic instability problem [9] and so, a high frequency motion of the tip. 2) It is hard to determine and realize switching in practice due to disturbances and non-linearities. Some other researchers (e.g. [10,11]) worked on and some improved Raibert and Craigs idea and generated schemes, which decompose the redundant robot system into force, position and redundant joint subspaces. Hogan [12] used the impedance approach to solve hybrid control problem. Impedance controller was generated to establish a desired dynamical relationship (impedance) between the position of the tip and the force it exerts on the environment. The primary advantage of the impedance approach was in simplicity, since a single controller was running the plant in both the free and constrained motion of the tip. Therefore, there is no need for control mode switching, which removes the main problems with the discontinuous hybrid control approaches. He has experimentally demonstrated in [13] that impedance controllers can perform stable contact tasks.

Some other researchers have been applying adaptive control methods to overcome the kinematic instability problem as well as any nonlinearity such as parameter variations the system might encounter [14].

## 1.4 Motivation for using Sliding Mode Control

For high precision motion control problems, robustness of the control algorithm is the most crucial element even if the system model is linear. Furthermore, when the plant to be controlled has high nonlinearities such as internal hysteresis, which is the case for the piezoactuator used in many experiments throughout this thesis, or friction, the advantage of a robust controller, which is designed according to nominal plant parameters and which rejects parameter uncertainties, would be simply less effort on modeling the system and compensation methods. Moreover, it is a fact that using more complicated models may not always lead to better compensation results than just using a simple model (e.g. the model of Coulomb Friction), since the quality of the compensation depends not only on the model, but also on the implementation constraints.

Furthermore, using a model based controller could have disastrous effects since in that case, how accurately the states could be measured or estimated become a direct key factor in the performance of the control action. Such a controller requires special attention and effort to define the system with a complete and so, complicated model with assistive and preferably online identification methods, if possible. Not to mention that the model based controller designed for one plant would simply not fit other plants even for the same type of series manufactured machines due to parameter uncertainties and variations because of time-varying characteristics, operating condition changes, load changes, etc.

To avoid the difficulties mentioned above and concentrate on the main issues of the control problem, one needs to find a methodology that produces a robust controller designed according to the nominal parameters and has fine disturbance rejection, to realize high precision motion control with minimum effort.

The theory of variable structure systems (VSS) opened up a wide new area of development for control designers. Variable structure control (VSC) with sliding modes, which is frequently known as sliding mode control (SMC) is characterized by a discontinuous control action which changes structure upon reaching a set of predetermined switching surfaces. This kind of control may result in a very robust system with its built-in disturbance rejection, which in turn implicitly compensates for the unmodeled dynamics, and thus provides a possibility for achieving the pre-

viously stated goals. Interested reader may refer to Chapter 2 for a brief survey on Sliding Mode Variable Structure Control.

## 1.5 High Precision in Motion Control

For any measurement, precision means the fineness of the measured values, which becomes an issue of consideration in the discretization of analog signals, hence an analog measurement would have infinite precision. The fineness of some measured value implies the size of the unit measurement (i.e. the smallest measurable value), which is infinitely small for the analog case. Therefore, the smaller the size of the unit measurement, the higher the precision achieved, that is an instrument that measures parts per million is more precise than one which measures parts per hundred.

Precision and accuracy are two distinct concepts, however precision in effect defines the best accuracy any measurement can achieve. Also, for a motion controller, since the quantities are measured or observed from measured quantities, the smallest error one can respond to is directly related to the measurement device. Assuming that the measurement accuracy is defined as its precision, the smallest error (after zero) would be the precision of the measurement, hence using high precision devices would be beneficial to a motion controller to improve its error efficiency. Note that, the precision for motion control tasks is not only related to the sensory device, but also to the minimum amount of motion an actuator can provide. That is, even if the precision of the sensory device is high enough for motion control on small scales, the actuator might be unable to respond to the respective control action due to static friction (stiction), etc.

Traditionally, the angle measurement device for rotational actuators is the encoder. An encoder can typically be absolute or incremental. Absolute encoders produce a specifically coded value for each shaft position, while incremental encoders work by summing up electrical pulses (hence the name incremental) and deliver relative position values according to a reference point (the initial value) by means of a specific number of signals (pulses) per shaft rotation.

Focusing on the incremental encoder for precision analysis, the relation between the number of ticks on the encoder to the precision is straightforward. For instance, an incremental encoder with  $N$  ticks, produces  $4N$  pulses per revolution. Therefore

its precision is

$$\frac{2\pi}{4N} \text{ rad}, \quad (1.1)$$

which also demonstrates the minimum observable error by the motion controller.

Today, and it will be shown in Chapter 3 that the precision in (1.1) could be achieved. However, there are many applications such as micro/nanomanipulation, some MEMS, NEMS applications, applications in the optoelectronics area, medical robotics, etc. that need controlled motion in smaller scales and as a direct result, higher precision than traditional actuators can deliver. For these kinds of motion needs, many kinds of actuators have been and are being designed to transform energy into motion using many methods some of which are listed down [15].

- Electromagnetic
- Thermomechanical
- Piezoelectric
- Magnetostrictive
- Electrohydrodynamic
- Electrostatic
- Phase Change
- Shape Memory
- Electrorheological
- Diamagnetism

as well as magnetohydrodynamic, shape changing polymers, and biological methods (living tissues, muscle cells, etc.)

One of the most promising actuators that can deliver motion in micro/nanometer levels is the piezoelectric actuator (PEA) or piezoactuator for short. The main principle under its operation is the piezoelectric effect, further explained in the next section.

### 1.5.1 Piezoelectric Effect

Piezoelectric effect, discovered by Jacques and Pierre Curie in the 1880's during experiments on quartz, is a property of certain materials to produce an electrical charge when mechanically deformed. Conversely, to physically deform in the presence of an electric field is called "inverse piezoelectric effect". The amount of electrical charge produced under pressure (or mechanical deformation) is called "piezoelectricity".

The word piezo is Greek for “push”, hence the effect is summarized in the name. Note that, “piezoelectricity” could also be used in the literature for the “piezoelectric effect” and “piezoelectric effect” could also denote “inverse piezoelectric effect”, since typically the two exist together in piezoelectric materials.

There is a magnetic analogy to the effect where ferromagnetic materials respond mechanically to magnetic fields. This effect is called “magnetostriction”. However, unlike ferroelectric materials, piezoelectric materials do not store charge after the force is removed.

Many crystalline materials exhibit piezoelectric behavior. A few materials exhibit the phenomenon strongly enough to be used in applications that take advantage of their properties. These include quartz, Rochelle salt, lead titanate zirconate ceramics (e.g. PZT-4, PZT-5A, etc.), barium titanate, and polyvinylidene fluoride (a polymer film).

This effect is put to use in several ways, the most common of which is in quartz crystal oscillators. When these are incorporated into the proper circuitry, they resonate at precise frequencies, depending on their size and on the way in which they are cut. Every computer has at least one clock frequency which is generated by a quartz crystal. Also, many modern accelerometers and pressure sensors use piezoelectric crystals. More exotic compounds are used in ultrasonic technology; different compounds of barium titanate are common. When used for sonar, where long-distance transmission of sound is required, the crystals become large to generate low frequencies, and are usually driven with high voltages to produce higher-amplitude pulses. The same crystal is connected to appropriate circuitry to receive the weaker return pulses.

Also, piezoelectric ceramic materials have found use in producing motions on the order of nanometers (e.g. in the control of scanning tunneling microscopes or atomic force microscopes) and this application is the main concern of usage for PZT in this work, namely “piezoelectric actuation” and the PZT used as an actuator is typically called a “piezoelectric actuator(PEA)”.

In naturally occurring piezoelectric materials, such as quartz, the (inverse) piezoelectric effect is too small to be of practical use. Man-made piezoelectric polycrystalline ceramics are much more suitable for actuator purposes because the useful

properties, such as maximum elongation, can be influenced by the proper mixture of ingredients. A disadvantage of man-made piezoelectric ceramics is that a hysteresis effect is encountered between electrical voltage and electrical charge (or position in effect) as shown in Figure A.8. The piezoelectric effect (or the piezo effect for short) and the hysteresis effect play an important role in the dynamical behavior of these actuators.

The fundamental component of a PZT stack actuator is a wafer of piezoelectric material sandwiched between two electrodes. Prior to fabrication, the wafer is polarized uniaxially along its thickness, and thus exhibits significant piezoelectric effect in this direction only. A typical PZT stack actuator is formed by assembling several of the wafer elements in series mechanically and connecting the electrodes so that the wafers are parallel electrically, as illustrated in Figure 1.5. The nominal quasi-static behavior of a PZT stack actuator is a steady-state output displacement that is monotonically related to the voltage input.

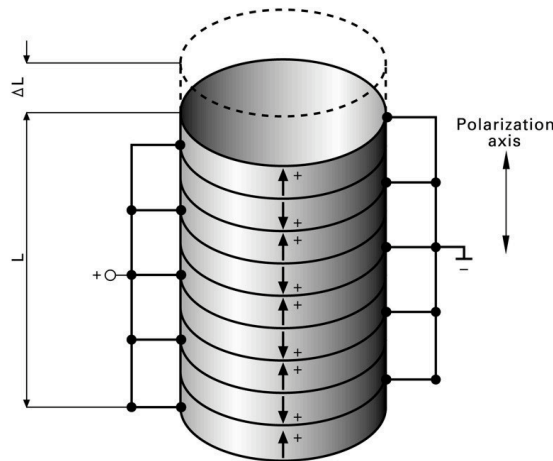


Figure 1.5: Illustration of a PZT Stack Actuator, Image Courtesy of PI GmbH

There are many manipulators based on PEA components following the novel trends in the mechatronics system technology in the development of standalone micromechatronic systems and/or controlled motion in small (e.g. micro, nano, sub-nano) scales for the aforementioned applications. Some examples of these manipulators are given in the following images. For instance, the system shown in Figure 1.6 provides motion in 3D cartesian coordinates with 1 nm resolution.



Figure 1.6: 3-Axis nanopositioning system (Nanocube), PI GmbH



Figure 1.7: Custom 3-Axis XYZ Stage, DSM



Figure 1.8: Microscope Turret NanoPositioner, PI GmbH



Figure 1.9: Microscope Objective NanoPositioners, PI GmbH

## Chapter 2

### Sliding Mode Variable Structure Control

#### 2.1 Introduction

Variable structure control (VSC) appeared in the Soviet Union in late fifties to solve control problems of second order systems initially. The idea of the pioneers of the field was to switch among two or more controls to obtain improved, mathematically stable control system performance [28, 29]. Switching among control inputs to the plant leads to a system defined with a differential equation with a discontinuous right-hand side, hence the name “Variable Structure System (VSS)”. Note that, in some fields such as power electronics, switching is a “way of life” and the systems treated there are discontinuous by themselves without any artificial introduction of switching, therefore it may be argued that they are the original VSS’s.

Typically, as developed in a second phase commenced in the sixties by Emelyanov [30–32], VSC is designed in such a way that it satisfies the existence conditions of the so-called “sliding mode”, in which case it gains some distinguished and advantageous features. VSC with sliding modes is simply called as Sliding Mode Variable Structure Control or Sliding Mode Control (SMC) for short. The basic idea of SMC is to define a “sliding manifold” (switching curve) on the state space phase plane and enforce the system to reach this manifold in finite time and confine it on the manifold afterwards. Therefore, the manifold should be designed in such a way that the motion on the manifold satisfies control objectives.

Note that, even though it is expressed as the plant motion is confined on the manifold, in reality it is confined in a boundary layer around the manifold due to the infamous “chattering” phenomenon of SMC. Many efforts have been given to reduce the effects of chattering since the first discovery of SMC until now, since

it remains to be the single obstacle for sliding mode to become one of the most significant discoveries of the modern control theory with its promising potential. The theory has since been continually developed and extended by Utkin and other researchers [19, 33, 34].

In a third development phase started in the seventies, VSC's based on a principle that precluded sliding modes were devised by the pioneering works of Kiendl [35] and Kiendl&Schneider [36]. After the development of SMC, VSC and SMC have been used interchangeably. However, VSC is a more general control methodology that also involves control approaches lacking sliding modes [37] as stated above. Therefore, since the controllers in this thesis are VSC's with sliding modes, they are simply called SMC to avoid confusion.

The most distinguished property of SMC is that the closed loop system is completely insensitive to parametric variations and external disturbances, therefore it has the ability to result in very robust and in many cases 'invariant' control systems. However, it wasn't until the survey paper in 1977 by Utkin [19], VSC and SMC have received wide acceptance and interest of the control research community worldwide. Until then, significant research and work have been done on the field by many researchers since robustness has been the most crucial feature for modern control problems especially for high precision motion control. In the last two decades, SMC has been applied to a wide variety of engineering systems such as nonlinear systems, multi input multi output (MIMO) systems, discrete time models, large scale and infinite dimensional systems, and stochastic systems.

## **2.2 Sliding Mode in Variable Structure Systems**

SMC is characterized by a discontinuous control action, which changes structure upon reaching a set of predetermined switching surfaces. This kind of control may result in a very robust system and thus provides a possibility for achieving the goals of high-precision and fast response. It has been stated in Section 2.1 that SMC has some advantageous features, these features are listed below:

- The order of the motion can be reduced
- The motion equation of the sliding mode can be designed linear and homoge-

nous, despite that the original system may be governed by nonlinear equations.

- The sliding mode does not depend on the process dynamics, but is determined by parameters selected by the designer.
- Once the sliding motion occurs, the system has invariant properties which make the motion independent of certain system parameter variations and disturbances. Thus the system performance can be completely determined by the dynamics of the sliding manifold.

Consider the system, affine with respect to control  $\mathbf{u} \in \mathfrak{R}^m$ :

$$\dot{\mathbf{x}} = F(\mathbf{x}, t) + B(\mathbf{x}, t)\mathbf{u} \quad (2.1)$$

where  $\mathbf{x} \in \mathfrak{R}^n$  is the state vector of the system, generally written in controllable canonical form

$F(\mathbf{x}, t) : \mathfrak{R}^n \times \mathfrak{R}^+ \rightarrow \mathfrak{R}^n$  is a continuous and bounded linear or nonlinear function defining the uncontrolled dynamics of the system

$B(\mathbf{x}, t) : \mathfrak{R}^n \times \mathfrak{R}^+ \rightarrow \mathfrak{R}^{n \times m}$  is a continuous and bounded matrix with  $\text{rank}(B) = m$  for every  $\mathbf{x}, t$  couple, yielding the system to be linear according to control input  $t \in \mathfrak{R}^+$  denotes the independent variable time.

SMC dictates a discontinuous control, which changes structure according to  $\sigma(\mathbf{x})$  such that

$$u_i = \begin{cases} u_i^+ & \text{for } \sigma_i(\mathbf{x}) > 0 \\ u_i^- & \text{for } \sigma_i(\mathbf{x}) < 0 \end{cases} \quad (2.2)$$

for  $i = 1, 2, \dots, m$ ,  $\sigma(\mathbf{x}) = G\mathbf{x}$ ,  $\sigma \in \mathfrak{R}^m$  whose components are  $m$  smooth functions and  $G \in \mathfrak{R}^{m \times n}$ , yielding

$$\sigma(\mathbf{x}) = \left[ \begin{array}{cccc} \sigma_1(\mathbf{x}) & \sigma_2(\mathbf{x}) & \cdots & \sigma_m(\mathbf{x}) \end{array} \right]^T \quad (2.3)$$

here  $u_i^+$ ,  $u_i^-$ , and  $\sigma_i(\mathbf{x})$  are continuous functions with  $u_i^+ \neq u_i^-$ . Sliding mode may appear on the manifold  $\sigma(\mathbf{x}) = 0$ , which is the intersection of  $m$  hyperplanes defined by the  $m$  components of  $\sigma(\mathbf{x})$  as  $\sigma_i(\mathbf{x}) = 0$ ,  $i = 1, 2, \dots, m$ . Sliding mode may or may not arise on the individual surfaces  $\sigma_i(\mathbf{x}) = 0$ . Both cases are shown in Figure 2.1. Note that  $\sigma(\mathbf{x})$  is called the “switching function” and if sliding mode exists,  $\sigma(\mathbf{x}) = 0$  is called the “sliding manifold” or “sliding hyperplane” of  $m$  dimensions,

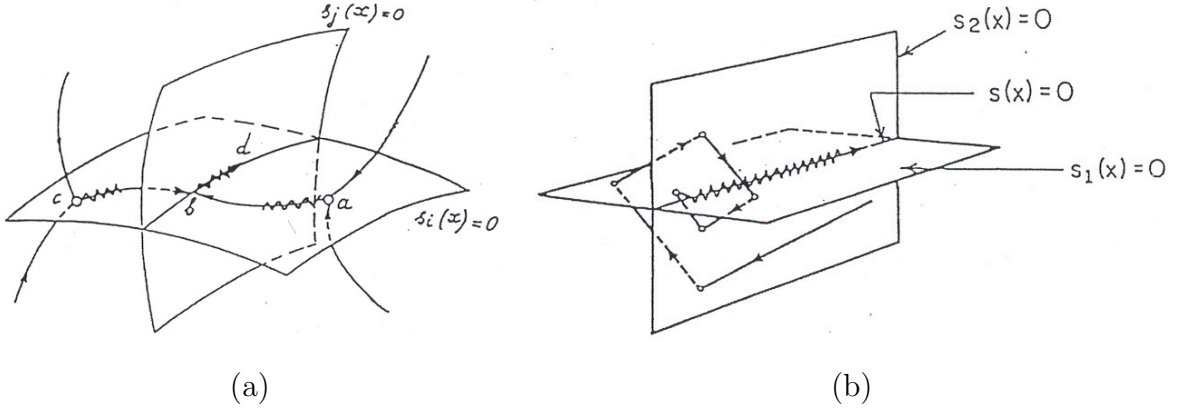


Figure 2.1: Sliding Mode Possibilities ( $s = \sigma$ ) (a) Sliding Mode in Discontinuity Surfaces and Their Intersection (b) Sliding Mode only in the Intersection of Discontinuity Surfaces

since  $i$ th control  $u_i$  faces discontinuities on the  $i$ th surface  $\sigma_i(\mathbf{x})$  in terms of switching according to (2.2),  $i = 1, 2, \dots, m$ .

If, for any initial condition  $\mathbf{x}_o$ , there exists a time  $t_o$  such that  $\mathbf{x}(t)$  is on the manifold  $\sigma(\mathbf{x}) = 0$  for  $t \geq t_o$ , then  $\mathbf{x}(t)$  is a “sliding mode” of the system, in which the motion is determined by the manifold equation only and therefore, note that motion order is reduced to the order of control inputs, namely  $m$ . The order reduction means that system model of the  $n$ th order is decomposed into two modes, one is the so-called “reaching mode” which is defined by a motion of  $(n-m)$ th order and the other is the sliding mode defined by the motion on the sliding manifold of  $m$ th order. Decoupled motion equations of the system could be written as

$$\dot{\mathbf{x}}_1 = f_1(\mathbf{x}_1, \sigma_1(\mathbf{x}_1)) \quad (2.4)$$

$$\mathbf{x}_2 = \sigma_1(\mathbf{x}_1) \quad (2.5)$$

for  $\mathbf{x}_1, f_1 \in \mathfrak{R}^{n-m}$  and  $\mathbf{x}_2 \in \mathfrak{R}^m$ . If  $\sigma(\mathbf{x}) = \mathbf{x}_2 - \sigma_1(\mathbf{x}_1) = 0$  is smartly designed in such a way that it satisfies the control objectives (e.g.  $\mathbf{x}$  follows  $\mathbf{x}^{ref}$ ), then SMC is realized.

An SMC implementation basically consists of two phases; “reaching phase” where system is forced to move towards the sliding manifold and which occurs for  $t < t_o$  and “sliding phase” where system motion is governed by the sliding manifold equation. According to this discussion, stability could be guaranteed only if there exists a reaching phase, which is also called the “reaching condition”, where state

trajectory points towards the sliding manifold and system motion approaches the manifold at least asymptotically for a set of points around the manifold, which is called the “region of attraction” of the controller. From geometrical considerations, if the deviation from the switching surface  $\sigma$  and its time derivative have opposite signs (i.e.  $\sigma(\mathbf{x})\dot{\sigma}(\mathbf{x}) < 0$ ) in the region of attraction of the controller, existence of sliding mode is enforced in that region. Note that, if the region of attraction is infinite, the closed loop system becomes globally stable if (2.4,2.5) are stable.

In the above discussion, the sliding mode is defined to be the part of the VSC, where the system motion is confined to a manifold in the state space. However, this definition is incomplete since this method of system order reduction without problem may be only realized with discontinuous control switching at infinite frequency. In real life implementations, since infinite frequency switching is not possible, this effect could not be optimally realized. Modern control systems are based on discrete-time microprocessor implementation with a sampling time, which happens to define the maximum switching frequency and this limited frequency in the control switching results in oscillations at finite frequency around the manifold  $\sigma(\mathbf{x}) = 0$  referred to as “chattering”. In addition, in the case of neglected small time constants in plant models, sensors and actuators, discrepancy occurs in the dynamics. In discontinuous control systems, the switching of the control excites these unmodelled dynamics, which leads to oscillations in the state vector at a high frequency, usually referred to as “chattering”. Chattering is known to result in low control accuracy, high heat losses, and high wear of mechanically moving parts.

There are some attempts to remove or decrease the effect of chattering. One of the attempts to remove chattering caused by unmodelled dynamics involve the usage of asymptotic (Luenberger) observers, which serves as a bypass to the high frequency component of the control input, therefore the unmodeled dynamics of the system are not excited, and ideal sliding arises. One other way implies replacing the discontinuous control with its continuous approximation in a boundary layer [38]. If the gain in the boundary layer is reduced such that the unmodelled dynamics are not excited chattering-free motion could be achieved. However, as a direct result, the disturbance rejection properties of discontinuous (or high gain) control are not utilised to the full extent, which means controller robustness degradation. The

discrete-time implementations of sliding-mode involves control to be a continuous function of the state, which eliminates the chattering phenomenon in effect. Since all the work in this thesis has been done with a dSpace 1103 card on a digital computer, next section elaborates on the discrete-time implementation of SMC.

### 2.3 Sliding Mode Control in Discrete Time

SMC theory was originally developed from a continuous time perspective. It has been realized that directly applying the continuous-time SMC algorithms to discrete-time systems will lead to some unconquerable problems, such as the limited sampling frequency, sample/hold effects and discretization errors. Since the switching frequency in sampled-data systems can not exceed the sampling frequency, a discontinuous control does not enable generation of motion in an arbitrary manifold in discrete-time systems. This leads to chattering at the sampling frequency along the designed sliding surface, or even instability in case of a too large switching gain.

The discontinuous sliding-mode controller involves a continuous plant model with a discontinuous right-hand-side due to the switching control function as mentioned above. Due to the problems with the discrete implementation of this discontinuous approach, Drakunov and Utkin [39] introduced a continuous approach to SMC for an arbitrary finite dimensional discrete-time system. This approach implies that for a sampled-data controller, as the system becomes discrete, the controller should be continuous to overcome the sampling frequency limitations of the discontinuous approach. For such continuous implementation of SMC, plant motion is proven to reach the sliding manifold of predefined state trajectory in finite time.

Derivation of the control law starts with the selection of a positive definite Lyapunov function candidate,  $\nu(\sigma)$  to satisfy Lyapunov stability criterion as the reaching condition, namely

$$\dot{\nu}(\sigma)\nu(\sigma) < 0. \quad (2.6)$$

For a Lyapunov function of the form

$$\nu(\sigma) = \frac{\sigma^T \sigma}{2}, \quad (2.7)$$

the derivative of the function is

$$\dot{\nu}(\sigma) = \sigma^T \dot{\sigma}. \quad (2.8)$$

If the control function is designed such that

$$\dot{\sigma} + D\sigma = 0, \quad (2.9)$$

Lyapunov function derivative becomes a negative-definite function as

$$\dot{\nu}(\sigma) = -\sigma^T D\sigma, \quad (2.10)$$

which satisfies the Lyapunov stability criterion, for  $D \in \mathfrak{R}^{m \times m}$  being a positive-definite symmetric matrix. For simplicity and without loss of generality,  $D$  could be taken as a diagonal matrix with positive elements in the form,

$$D = \begin{bmatrix} D_{11} & 0 & \dots & 0 \\ 0 & D_{22} & 0 & \vdots \\ \vdots & 0 & \ddots & 0 \\ 0 & \dots & 0 & D_{mm} \end{bmatrix} \quad (2.11)$$

which essentially defines the slope of the sliding-manifold at each dimension, therefore providing some sort of a control decoupling of the  $m$  dimensions. Note that, the Lyapunov function and its derivative having opposite signs with the aid of control enforces the system to move to  $\dot{\nu}(\sigma) = \nu(\sigma) = 0$  and hence, ensures stability.

For the discrete-time sliding mode development, the continuous motion equation in (2.1) should be replaced by its discrete-time equivalent

$$\mathbf{x}_{k+1} = F_k(\mathbf{x}_k) + B_k(\mathbf{x}_k)\mathbf{u}_k, \quad (2.12)$$

for  $\mathbf{x}_i = \mathbf{x}(i\Delta t)$  and  $\mathbf{x}_i \in \mathfrak{R}^n$ ;  $F_i = \Delta t F(\mathbf{x}_i, i\Delta t) + \mathbf{x}_i$  and  $F_i : \mathfrak{R}^n \rightarrow \mathfrak{R}^n$ ;  $B_i = \Delta t B(\mathbf{x}_i, i\Delta t)$  and  $B_i : \mathfrak{R}^n \rightarrow \mathfrak{R}^{n \times m}$ ;  $\mathbf{u}_i = \mathbf{u}(i\Delta t)$  and  $\mathbf{u}_i \in \mathfrak{R}^m$ ;  $i \in Z^+$  and  $\Delta t$  is the sample time.

For a state tracking error  $\mathbf{e}_x = \mathbf{x}^{ref} - \mathbf{x}$ ,  $\sigma$  is selected as  $\sigma(\mathbf{x}) = G\mathbf{e}_x$  for  $G \in \mathfrak{R}^{m \times n}$  such that  $\det(GB_k) \neq 0$  to satisfy control objectives on the sliding manifold  $\sigma(\mathbf{x}) = 0$ . Also (2.9) should be converted to its discrete time equivalent for further development of the controller as

$$\frac{\sigma_{k+1} - \sigma_k}{\Delta t} + D\sigma_k = 0, \quad (2.13)$$

which becomes

$$\sigma_{k+1} + \underbrace{(D\Delta t - I^{m \times m})}_{D_d} \sigma_k = 0 \quad (2.14)$$

after simple manipulations, where  $\Delta t$  is the sample time,  $I^{m \times m}$  is the identity matrix of dimensions  $m \times m$  and  $D_d \in \mathfrak{R}^{m \times m}$ . As  $\sigma_{k+1} = G(\mathbf{x}_{k+1}^{ref} - \mathbf{x}_{k+1})$ , putting (2.12) in yields

$$\sigma_{k+1} = G(\mathbf{x}_{k+1}^{ref} - F_k - B_k \mathbf{u}_k). \quad (2.15)$$

Defining equivalent control,  $\mathbf{u}_{eq}$  as the amount of control that puts the motion of the plant on the sliding manifold i.e.  $\sigma_{k+1} = \sigma_k = 0$  [19], (2.15) above could be written as

$$\sigma_{k+1} = GB_k(\mathbf{u}_{eq_k} - \mathbf{u}_k). \quad (2.16)$$

Solving for  $\mathbf{u}_{eq_k}$  in (2.16) gives

$$\mathbf{u}_{eq_k} = \mathbf{u}_k + [GB_k]^{-1} \sigma_{k+1}. \quad (2.17)$$

Putting (2.16) in (2.14) gives

$$GB_k(\mathbf{u}_{eq_k} - \mathbf{u}_k) + D_d \sigma_k = 0. \quad (2.18)$$

The only unknown here is  $\mathbf{u}_{eq_k}$ , however it may be approximated with a low-pass filter on the control  $\mathbf{u}$  since it happens to be the low frequency component of the control or in this implementation, as  $\mathbf{u}_{eq}$  is a smooth function, an approximation could be made using (2.17) and replacing  $\mathbf{u}_k$  with  $\mathbf{u}_{k-1}$  such that

$$\widehat{\mathbf{u}}_{eq_k} \approx \mathbf{u}_{k-1} + [GB_k]^{-1} \sigma_{k+1}. \quad (2.19)$$

Putting (2.19) in (2.18) and solving for  $\mathbf{u}_k$  gives

$$\mathbf{u}_k = \mathbf{u}_{k-1} + [GB_k]^{-1}(\sigma_{k+1} + D_d \sigma_k), \quad (2.20)$$

which could be written like

$$\mathbf{u}_k = \mathbf{u}_{k-1} + [GB]^{-1}(\dot{\sigma} + D\sigma)|_{t-\Delta t} \quad (2.21)$$

as well.

For a discrete-time system, the discrete sliding mode can be interpreted as that the states are only required to be kept on the sliding surface at each sampling instant. Between the samples, the states are allowed to deviate from the surface within a boundary layer.

Note that the control defined by (2.21) is continuous unlike the case for continuous-time. Thus chattering is no longer a matter of concern. This is the most striking contrast between discrete-time sliding mode and continuous-time sliding mode. Furthermore, in continuous-time systems with continuous control, the sliding manifold of state trajectories can be reached only asymptotically, while in discrete time systems with continuous control, sliding motion with state trajectories in some manifold may be reached within a finite time interval, [19].

## 2.4 Disturbance Compensation based on Sliding Mode Control

When the motion control problem suffers from nonlinearities such as:

- Hysteresis, dead zone, saturation, backlash, etc of the actuators and/or sensing devices
- High parameter variations and drifts according to different conditions of operation
- Time delay

it might be possible to combine all the effects of these different kind of disturbances on the plant response (i.e. observe their force/torque equivalent) and provide a compensation for them as an addition to the controller output and use this sum as the plant input. This kind of compensation is called “disturbance compensation” and the observer used is called “disturbance observer”.

As electromechanical motion systems could be described by a second order differential equation, consider the following model:

$$m\ddot{\mathbf{p}} + g(\dot{\mathbf{p}}, \mathbf{p}, t) = K_f \mathbf{u} + \mathbf{F}_{ext}, \quad (2.22)$$

where  $\mathbf{p} \in \mathfrak{R}^l$  is the displacement (position) output of the system,

$\mathbf{u} \in \mathfrak{R}^m$  is the current/voltage (control) input to the system,

$m \in \mathfrak{R}^{l \times l}$  is the mass/inertia matrix of the system,

$g : \mathfrak{R}^l \times \mathfrak{R}^l \times \mathfrak{R}^+ \rightarrow \mathfrak{R}^l$  is a nonlinear function defining the dynamics of the system,

$K_f \in \mathfrak{R}^{l \times m}$  is the force/torque constant matrix of the input to the plant.

This plant model has the aforementioned nonlinearities in  $g$  with uncertainties in

the parameters  $m$  and  $K_f$ . Focusing on the fully actuated (i.e.  $m = l$ ) mechanical systems affine with respect to control, which is an interconnection of  $l$  SISO systems,  $K_f$  matrix has a diagonal structure, each component being the force/torque constant of each dimension.

For disturbance compensation, first the linear model of the same system is written, which defines the ideal response of the actual plant.  $m_n$ ,  $b_n$  and  $k_n \in \mathfrak{R}^{l \times l}$  are the nominal parameter matrices for mass, damper, spring coefficients respectively and  $K_{f_n}$  is the nominal force/torque constant for estimation of  $\hat{p}$ ,  $\dot{\hat{p}}$ , and  $\ddot{\hat{p}}$ ,

$$m_n \ddot{\hat{\mathbf{p}}} + b_n \dot{\hat{\mathbf{p}}} + k_n \hat{\mathbf{p}} = K_{f_n} \mathbf{u} + \mathbf{F}_{ext}. \quad (2.23)$$

All the changes of the parameters from this model in the actual plant being considered as disturbances and adding an additional disturbance function  $\mathbf{d} \in \mathfrak{R}^l$  as well as the compensation in the plant input  $\mathbf{u}_{dis} \in \mathfrak{R}^m$ , (2.22) becomes

$$m_n \ddot{\mathbf{p}} + b_n \dot{\mathbf{p}} + k_n \mathbf{p} = K_{f_n} (\mathbf{u} - \mathbf{u}_{dis}) + \mathbf{F}_{ext} + \underbrace{\mathbf{d}(\ddot{\mathbf{p}}, \dot{\mathbf{p}}, \mathbf{p}, t) + \Delta m \ddot{\mathbf{p}} + \Delta b \dot{\mathbf{p}} + \Delta k \mathbf{p}}_{\mathbf{F}_d}. \quad (2.24)$$

For fully actuated electromechanical systems, combination of all sources of disturbances could be denoted as  $\mathbf{F}_d \in \mathfrak{R}^l$  and if  $K_{f_n} \mathbf{u}_{dis} = \mathbf{F}_d$  the plant would behave like the linear model. Therefore, if the errors from the plant output to the linear model output could be diminished the system could be enforced to behave like a linear model.

Calculating the position estimation errors  $\hat{\mathbf{e}} \in \mathfrak{R}^l$  and so, the disturbance estimation error  $\mathbf{e}_{dis} \in \mathfrak{R}^l$  by subtracting (2.23) from (2.24), one gets,

$$m_n \ddot{\hat{\mathbf{e}}} + b_n \dot{\hat{\mathbf{e}}} + k_n \hat{\mathbf{e}} = \mathbf{F}_d - K_{f_n} \mathbf{u}_{dis} = \mathbf{e}_{dis} \quad (2.25)$$

for  $\hat{\mathbf{e}} = \mathbf{p} - \hat{\mathbf{p}}$ .

To find the necessary  $\mathbf{u}_{dis}$ , two approaches could be brought in the selection of the sliding mode variable  $\sigma_{dis}$ :

1.  $\sigma_{dis} = G_{dis}(m_n \ddot{\hat{\mathbf{e}}} + b_n \dot{\hat{\mathbf{e}}} + k_n \hat{\mathbf{e}}) = G_{dis} \mathbf{e}_{dis}$
2.  $\sigma_{dis} = G_{dis}(\dot{\hat{\mathbf{e}}} + C_{dis} \hat{\mathbf{e}})$ ,

for positive definite  $G_{dis} \in \mathfrak{R}^{m \times l}$ . First approach tries to diminish the disturbance error  $\mathbf{e}_{dis} = \mathbf{F}_d - K_{f_n} \mathbf{u}_{dis}$  directly, while the second one tries to diminish  $\hat{\mathbf{e}}$  for

positive definite  $C_{dis} \in \mathfrak{R}^{l \times l}$ , which in consequence diminishes the disturbance error  $e_{dis}$ . After the selection of  $\sigma_{dis}$ , stability is ensured for

$$\dot{\sigma}_{dis} + D_{dis}\sigma_{dis} = 0 \quad (2.26)$$

according to Lyapunov Stability Criterion for positive definite  $D_{dis} \in \mathfrak{R}^{m \times m}$  as mentioned above.

Using the first  $\sigma_{dis}$  above, the iterative sliding mode disturbance compensator is derived as follows, the same scheme could be applied to the second  $\sigma_{dis}$  definition as well. Note that the external force should be measured or observed to use in the linear model of estimation (2.23).

$$\sigma_{dis} = \underbrace{G_{dis}\mathbf{F}_d}_{G_{dis}K_{fn}\mathbf{u}_{dis_{eq}}} - G_{dis}K_{fn}\mathbf{u}_{dis} \quad (2.27)$$

$$\sigma_{dis} = G_{dis}K_{fn}(\mathbf{u}_{dis_{eq}} - \mathbf{u}_{dis}) \quad (2.28)$$

solving for equivalent control,  $\mathbf{u}_{dis_{eq}}$  in (2.28)

$$\mathbf{u}_{dis_{eq}}(t) = [G_{dis}K_{fn}]^{-1}\sigma_{dis} + \mathbf{u}_{dis}(t), \quad (2.29)$$

putting (2.28) into (2.26), we achieve

$$\dot{\sigma}_{dis} + D_{dis}G_{dis}K_{fn}(\mathbf{u}_{dis_{eq}}(t) - \mathbf{u}_{dis}(t)) = 0. \quad (2.30)$$

In this equation, one needs to know  $\mathbf{u}_{dis_{eq}}$  to calculate the control input of the current time step  $\mathbf{u}_{dis_k}$ , however it is difficult to calculate  $\mathbf{u}_{dis_{eq}}$ . One possibility is to use an approximation of  $\mathbf{u}_{dis_{eq}}$  such that in (2.29),  $\mathbf{u}_{dis}(t)$  is replaced by  $\mathbf{u}_{dis}(t - \Delta t)$  i.e.

$$\mathbf{u}_{dis_{eq}}(t) \approx [G_{dis}K_{fn}]^{-1}\sigma_{dis} + \mathbf{u}_{dis}(t - \Delta t), \quad (2.31)$$

wher  $\Delta t$  is the sample time of the controller. Note that this approach would yield efficient results since  $\mathbf{u}_{dis_{eq}}$  is a continuous function and if the step time is sufficiently small. Putting the approximated  $\mathbf{u}_{dis_{eq}}(t)$  shown in (2.31) into (2.30) and solving for  $\mathbf{u}_{dis}(t)$ , the iteration scheme for the disturbance compensation is found as

$$\mathbf{u}_{dis}(t) = \mathbf{u}_{dis}(t - \Delta t) + [D_{dis}G_{dis}K_{fn}]^{-1}(\dot{\sigma}_{dis} + D_{dis}\sigma_{dis})|_{t-\Delta t}, \quad (2.32)$$

or in discrete-time

$$u_{dis_k} = u_{dis_{k-1}} + [D_{dis}G_{dis}K_{fn}]^{-1}(\dot{\sigma}_{dis} + D_{dis}\sigma_{dis})|_{k-1}. \quad (2.33)$$

On the disturbance observer sliding manifold (i.e.  $\dot{\sigma}_{dis} = \sigma_{dis} = 0$ ),

$$\mathbf{u}_{dis} = \mathbf{u}_{dis_{eq}} = [G_{dis}K_{f_n}]^{-1}G_{dis}\mathbf{F}_d. \quad (2.34)$$

Putting (2.34) in (2.24) and rearranging yields,

$$m_n\ddot{\mathbf{p}} + b_n\dot{\mathbf{p}} + k_n\mathbf{p} = K_{f_n}\mathbf{u} + \mathbf{F}_{ext} + \mathbf{F}_d - K_{f_n}[G_{dis}K_{f_n}]^{-1}G_{dis}\mathbf{F}_d. \quad (2.35)$$

As  $K_{f_n}[G_{dis}K_{f_n}]^{-1}G_{dis} = I$ , on the sliding mode the system behaves as the nominal model

$$m_n\ddot{\mathbf{p}} + b_n\dot{\mathbf{p}} + k_n\mathbf{p} = K_{f_n}\mathbf{u} + \mathbf{F}_{ext}. \quad (2.36)$$

## Chapter 3

### Implementation of a Discrete Sliding Mode Approach to High Precision Motion Control

In Section 2.3, a general system affine with control input  $\mathbf{u}$  was considered in (2.1) to derive an iterative discrete SMC scheme. Here, the implementation of that discussion on various control objectives for real-life mechanical systems affine with respect to control will be shown.

Most generally,  $l$  DOF mechanical systems could be described by a second order nonlinear equation as follows:

$$\ddot{\mathbf{p}} = \mathbf{h}(\dot{\mathbf{p}}, \mathbf{p}, \mathbf{u}, t), \quad (3.1)$$

where  $\mathbf{p} \in \mathfrak{R}^l$  is the displacement, output of the system,

$\mathbf{h}(\dot{\mathbf{p}}, \mathbf{p}, \mathbf{u}, t) : \mathfrak{R}^l \times \mathfrak{R}^l \times \mathfrak{R}^m \times \mathfrak{R}^+ \rightarrow \mathfrak{R}^l$  is a continuous and bounded linear or nonlinear function defining the dynamics of the system,

$\mathbf{u} \in \mathfrak{R}^m$  is the control input to the system, generally taken as force/torque or current/voltage, with a simple linear relation to force/torque like  $\mathbf{F}_{in} = K_F \mathbf{u}$ ,  $K_F$  being the so-called force/torque constant,

$t \in \mathfrak{R}$  denotes the independent variable time.

If the system in (3.1) is affine with respect to control, which is a specific (but broad in terms of physical relevance) class of all systems, the function  $\mathbf{h}$  could be decomposed into two parts as:

$$\ddot{\mathbf{p}} = \mathbf{f}(\dot{\mathbf{p}}, \mathbf{p}, t) + \mathbf{b}(\dot{\mathbf{p}}, \mathbf{p}, t)\mathbf{u}(\mathbf{p}, t), \quad (3.2)$$

for  $\mathbf{f} : \mathfrak{R}^l \times \mathfrak{R}^l \times \mathfrak{R}^+ \rightarrow \mathfrak{R}^l$  is the linear or nonlinear bounded function defining the dynamics of the system and  $\mathbf{b} : \mathfrak{R}^l \times \mathfrak{R}^l \times \mathfrak{R}^+ \rightarrow \mathfrak{R}^{l \times m}$  is the control related function such that  $\text{rank}(\mathbf{b}) = m$  for all  $\mathbf{p}, t$  pairs. This work focuses on fully actuated

electromechanical systems (i.e.  $m = l$ ), which is essentially an interconnection of  $l$  SISO systems, and hence  $b$  matrix has a diagonal structure with full rank.

Defining the state vector  $\mathbf{x} = [\mathbf{p} \ \dot{\mathbf{p}}]^T$ , the model given in (3.2) could be rewritten as:

$$\dot{\mathbf{x}} = F(\mathbf{x}, t) + B(\mathbf{x}, t)\mathbf{u}, \quad (3.3)$$

such that  $x \in \mathfrak{R}^{2l}$ ,  $F: \mathfrak{R}^{2l} \times \mathfrak{R}^+ \rightarrow \mathfrak{R}^{2l}$  and  $B: \mathfrak{R}^{2l} \times \mathfrak{R}^+ \rightarrow \mathfrak{R}^{2l \times m}$  with  $\text{rank}(B) = m$ . Therefore, for  $n = 2l$ , the equation given in (2.1) has been achieved and the same kind of control designation could be applied to the mechanical systems linear with control.

Next, a similar form of the environmental external force model will be derived. The general model for the external force when the system is in contact with the environment can be written by the following spring damper equation:

$$\mathbf{F}_{ext} = K_{ext}\Delta\mathbf{p} + b_{ext}\dot{\Delta\mathbf{p}}, \quad (3.4)$$

$$\Delta\mathbf{p} = \mathbf{p} - \mathbf{p}_{env} \quad (3.5)$$

where  $\mathbf{F}_{ext} \in \mathfrak{R}^l$  is the external force on all  $l$  dimensions,  $\Delta\mathbf{p} \in \mathfrak{R}^l$  is the amount of deflection of the tip into the environment (hand or obstacle),  $\mathbf{p}$  is the position of the tip and  $\mathbf{p}_{env}$  is the position of the obstacle in  $l$  dimensions,  $K_{ext}, b_{ext} \in \mathfrak{R}^{l \times l}$  are the environmental spring and damper matrices, essentially defining the stiffness and damping elements of each dimension.

Plant state vector was defined as  $\mathbf{x} = [\mathbf{p} \ \dot{\mathbf{p}}]^T$ , defining an environment state vector likewise gives  $\mathbf{x}_{env} = [\mathbf{p}_{env} \ \dot{\mathbf{p}}_{env}]^T$ . For an environmental matrix  $A_{ext} = [K_{ext} \ b_{ext}]$ , (3.4) could be converted to:

$$\mathbf{F}_{ext} = A_{ext}(\mathbf{x} - \mathbf{x}_{env}), \quad (3.6)$$

with  $A_{ext} \in \mathfrak{R}^{l \times 2l}$  and  $\mathbf{x}_{env} \in \mathfrak{R}^{2l}$ .

### 3.1 Position Control

In Section 2.3, a continuous SMC scheme was derived based on the discrete-time model (2.12) for a state trajectory reference tracking problem. This section will elaborate on the same problem, since it implies controlling position for mechanical

systems, however based on the continuous model shown in (3.3), directly. Taking the system written in (3.3) into consideration, assume a control problem for the system state vector  $\mathbf{x}$  to track some reference  $\mathbf{x}_{ref}$ . Then the state error  $\mathbf{e}_x \in \mathfrak{R}^n$  becomes

$$\mathbf{e}_x = \mathbf{x}_{ref} - \mathbf{x}. \quad (3.7)$$

For the given error,  $\sigma_x \in \mathfrak{R}^n$  is selected as

$$\sigma_x = G_x \mathbf{e}_x, \quad (3.8)$$

for  $G_x \in \mathfrak{R}^{m \times n}$  is a positive definite matrix with  $\text{rank}(G_x) = m$ , such that  $\det(G_x B) \neq 0$  to satisfy control objectives on the sliding manifold  $\sigma(\mathbf{x}) = 0$ . Therefore, for  $\sigma_x = 0$  state error is forced to diminish according to the elements of  $G_x$ . Note that for a 1-dof fully actuated system (i.e.  $l = m = 1$ ),  $G_x$  is a row vector of two positive elements like:

$$G_x = K_x \begin{bmatrix} C_x & 1 \end{bmatrix} \quad (3.9)$$

with  $K_x$  considered as a tuning factor. For a positive definite Lyapunov function of the form

$$\nu_x(\sigma_x) = \frac{\sigma_x^T \sigma_x}{2}, \quad (3.10)$$

the derivative of the function is

$$\dot{\nu}_x(\sigma_x) = \sigma_x^T \dot{\sigma}_x. \quad (3.11)$$

If the control function is designed such that

$$\dot{\sigma}_x + D_x \sigma_x = 0, \quad (3.12)$$

for positive-definite symmetric matrix  $D_x$ . Note that,  $D_x$  could be considered as a diagonal matrix with elements defining the slope of the sliding manifold for each dimension of  $\sigma_x$ , Lyapunov function derivative becomes a negative-definite function as

$$\dot{\nu}_x(\sigma_x) = -\sigma_x^T D \sigma_x, \quad (3.13)$$

which satisfies the Lyapunov stability criterion, for  $D_x \in \mathfrak{R}^{m \times m}$ . Using (3.3) and (3.7), projection of system motion onto the sliding manifold is

$$\dot{\sigma}_x = G_x \underbrace{(\mathbf{x}_{ref} - F - B\mathbf{u}^p)}_{B\mathbf{u}_{eq}^p} \quad (3.14)$$

$$\dot{\sigma}_x = G_x B(\mathbf{u}_{eq}^p - \mathbf{u}^p). \quad (3.15)$$

Here the superscript  $p$  denotes that the designed  $\mathbf{u}^p$  is a position control input. As defined in Section 2.3, equivalent position control is the amount of control input that makes  $\dot{\sigma}_x = \sigma_x = 0$  [19]. Solving for the equivalent control in (3.15) yields:

$$\mathbf{u}_{eq}^p = \mathbf{u}^p + [G_x B]^{-1} \dot{\sigma}_x. \quad (3.16)$$

If (3.15) is put in (3.12),

$$G_x B(\mathbf{u}_{eq}^p - \mathbf{u}^p) + D_x \sigma_x = 0 \quad (3.17)$$

is achieved. In this equation, the only obstacle to calculate  $\mathbf{u}^p$  is that  $\mathbf{u}_{eq}^p$  is unknown, however, since it is a smooth function, an approximation could be made by replacing  $\mathbf{u}^p$  in (3.16) with its value in the previous time step. Putting that approximation in (3.17) and solving for the current control input  $\mathbf{u}^p(t)$  gives:

$$\mathbf{u}^p(t) = \mathbf{u}^p(t - \Delta t) + [G_x B]^{-1}(\dot{\sigma}_x + D_x \sigma_x)|_{t-\Delta t}, \quad (3.18)$$

where  $\Delta t$  is the step time. Here, since the controller will be implemented in discrete time, subscripts are added to the control input like

$$\mathbf{u}_k^p = \mathbf{u}_{k-1}^p + [G_x B]^{-1}(\dot{\sigma}_x + D_x \sigma_x)|_{k-1}. \quad (3.19)$$

The resulting position controller has been tested on a PEA with a sinusoidal position reference. The results are given in Figure 3.1.

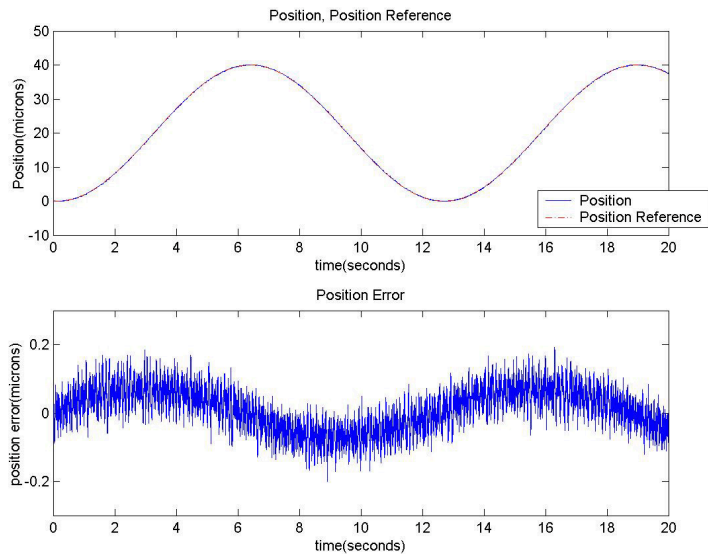


Figure 3.1: PEA Position Controller Results

## 3.2 Force Control

Let the external force to the system be modeled by (3.6), where  $A_{ext}$  matrix consists of the environmental parameters for spring and damping coefficients;  $\mathbf{x}$  is the state vector,  $\mathbf{x}_{env}$  is the obstacle (environment) state vector and  $\mathbf{F}_{ext}$  is the external force exerted on the system. For a reference  $\mathbf{F}_{ref} \in \mathfrak{R}^l$  for the external force to be controlled according to, the force error  $\mathbf{e}_f \in \mathfrak{R}^l$  is simply

$$\mathbf{e}_f = \mathbf{F}_{ref} - \mathbf{F}_{ext}. \quad (3.20)$$

The sliding mode variable  $\sigma_f \in \mathfrak{R}^m$  should be chosen such that force control is realized on  $\sigma_f = 0$ , hence taking

$$\sigma_f = G_f \mathbf{e}_f, \quad (3.21)$$

would satisfy this condition for the positive definite  $G_f \in \mathfrak{R}^{m \times l}$ . For stability, a positive definite Lyapunov function of the form

$$\nu_f(\sigma_f) = \frac{\sigma_f^T \sigma_f}{2}, \quad (3.22)$$

is used, and the derivative of the function is

$$\dot{\nu}_f(\sigma_f) = \sigma_f^T \dot{\sigma}_f. \quad (3.23)$$

If the control function is designed such that

$$\dot{\sigma}_f + D_f \sigma_f = 0, \quad (3.24)$$

for positive definite symmetric matrix  $D_f \in \mathfrak{R}^{m \times m}$ , Lyapunov function derivative becomes a negative-definite function as

$$\dot{\nu}_f(\sigma_f) = -\sigma_f^T D_f \sigma_f, \quad (3.25)$$

which satisfies the Lyapunov stability criterion. Using (3.6) and (3.3), sliding mode variable derivative becomes

$$\dot{\sigma}_f = \underbrace{G_f(\dot{\mathbf{F}}_{ref} + A_{ext}\dot{\mathbf{x}}_{env} - A_{ext}F)}_{G_f A_{ext} B \mathbf{u}_{eq}^f} - G_f A_{ext} B \mathbf{u}^f \quad (3.26)$$

$$\dot{\sigma}_f = G_f A_{ext} B (\mathbf{u}_{eq}^f - \mathbf{u}^f) \quad (3.27)$$

where  $\mathbf{u}^f$  is the output of the force controller, (hence the superscript  $f$ ) and aforementioned equivalent control  $\mathbf{u}_{eq}^f(t)$  can be stated as:

$$\mathbf{u}_{eq}^f(t) = \mathbf{u}^f(t) + [G_f A_{ext} B]^{-1} \dot{\sigma}_f. \quad (3.28)$$

Putting (3.27) in (3.24), one achieves

$$G_f A_{ext} B (\mathbf{u}_{eq}^f(t) - \mathbf{u}^f(t)) + D_f \sigma_f = 0. \quad (3.29)$$

In this equation, the only unknown is the so-called equivalent control,  $\mathbf{u}_{eq}^f$ , which is difficult to calculate. There are many methods to estimate its value such as using a low pass filter on the control function  $\mathbf{u}(t)$ . However, approximating it using (3.28), by replacing the unknown  $\mathbf{u}^f(t)$  with  $\mathbf{u}^f(t - \Delta t)$  such that

$$\mathbf{u}_{eq}^f(t) \approx \mathbf{u}^f(t - \Delta t) + [G_f A_{ext} B]^{-1} \dot{\sigma}_f. \quad (3.30)$$

Putting this approximation in (3.29) and solving for the current control input yields:

$$\mathbf{u}^f(t) = \mathbf{u}^f(t - \Delta t) + [G_f A_{ext} B]^{-1} (\dot{\sigma}_f + D_f \sigma_f)|_{t-\Delta t}, \quad (3.31)$$

where  $\Delta t$  is the step time. Here, since the controller will be implemented in discrete time, subscripts are added to the control input like

$$\mathbf{u}_k^f = \mathbf{u}_{k-1}^f + [G_f A_{ext} B]^{-1} (\dot{\sigma}_f + D_f \sigma_f)|_{k-1}. \quad (3.32)$$

The performance of the derived controller is demonstrated on experiments with both measured (by load cell) and observed external forces/torques as shown in Figures 3.2, 3.3, 3.4 for measured data on the PEA setup and Figures 3.5 and 3.6 for observed data on the Maxon RE-40 setup.

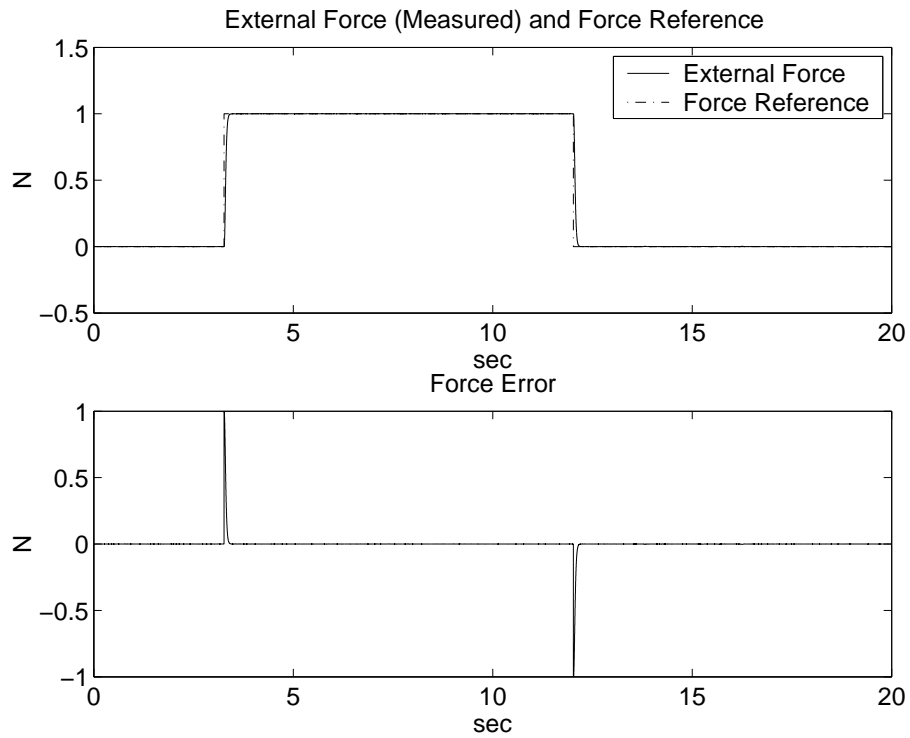


Figure 3.2: PEA: External Force (measured by load cell) Control for a Step Reference

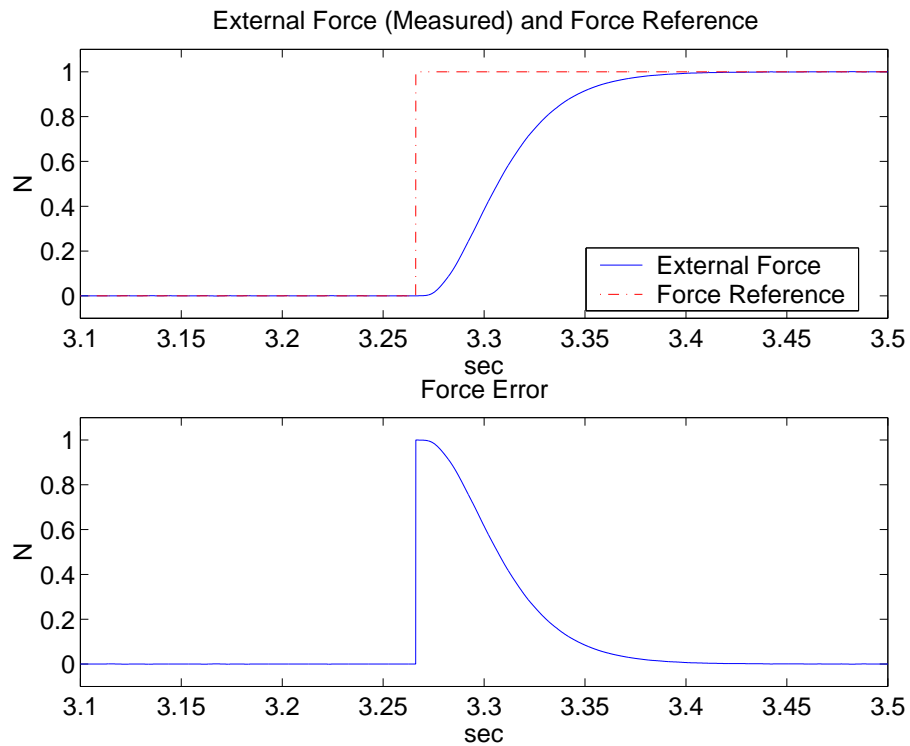


Figure 3.3: PEA: External Force Control for a Step Reference Magnified for  $3.1 < t < 3.5$

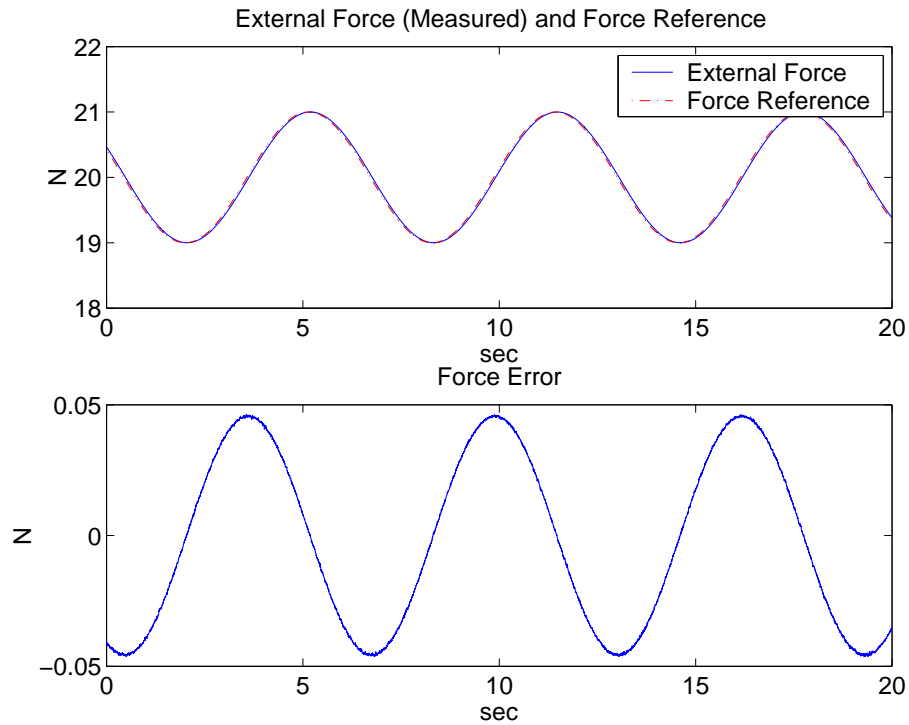


Figure 3.4: PEA: External Force (measured by load cell) Control for a Sinusoidal Reference

### 3.3 External Force Observer

In most cases, the structure of the setup makes it difficult to attach a force sensor, therefore measuring the external force becomes nearly impossible. However, a possibility is to make use of a disturbance observer based external force observer to estimate these values instead of directly measuring them. Pros of using this observer could be:

- low cost
- avoidance from the noise of sensing devices
- possibility to estimate all the external forces unlike the sensors, which have a frequency bandwidth for accurate sensing,

while cons are:

- the noise in the state readings and system input (current/voltage) measurements

- the fact that an accurate model of the system is crucial to be able to estimate the external forces accurately.

Considering the effect of external forces in the model (3.2) with a minor change converting all the elements of the equation to forces,

$$m\ddot{\mathbf{p}} + g(\dot{\mathbf{p}}, \mathbf{p}, t) = K_f \mathbf{u} + \mathbf{F}_{ext}, \quad (3.33)$$

where  $m \in \mathfrak{R}^{l \times l}$  is the mass/inertia matrix of the system,  $g : \mathfrak{R}^l \times \mathfrak{R}^l \times \mathfrak{R}^+ \rightarrow \mathfrak{R}^l$  is a linear or nonlinear function defining the model of the system,  $K_f \in \mathfrak{R}^{l \times m}$  is the force/torque constant matrix of the input to the plant,  $\mathbf{u}$  is the current/voltage input and  $\mathbf{F}_{ext} \in \mathfrak{R}^l$  is the external force/torque vector to be estimated on all  $l$  dimensions. Using accurate values for all the parameters in the model (3.33), theoretically all one needs to do is solve for the external force vector and use it as the force to be controlled, i.e.

$$\mathbf{F}_{ext} = m\ddot{\mathbf{p}} + g(\dot{\mathbf{p}}, \mathbf{p}, t) - K_f \mathbf{u}. \quad (3.34)$$

for the  $\mathbf{p}$ ,  $\dot{\mathbf{p}}$ ,  $\ddot{\mathbf{p}}$  values coming from the sensor and the control input  $\mathbf{u}$  to the plant.

However, in reality the above equation yields noisy data since it involves derivatives of the state readings, which include sensor noises amplified with derivation. As Ohnishi points [40], this noise could be reduced with the addition of a low-pass filter to the estimation such that:

$$\widehat{\mathbf{F}}_{ext} = \mathbf{F}_{ext} \frac{d}{s + d}. \quad (3.35)$$

Therefore, the estimation would be less sensitive to noise (with higher frequency than  $d$ ) and provide more reliable results. In the thesis work, this estimation was used for the external forces for Maxon RE-40 motor experiments since it has a linear model and the structure of the setup makes it hard to attach a torque sensor on the motor shaft. The external force control results using the observer discussed in this section are given in Figures 3.5 and 3.6, for stationary and mobile obstacles, respectively.

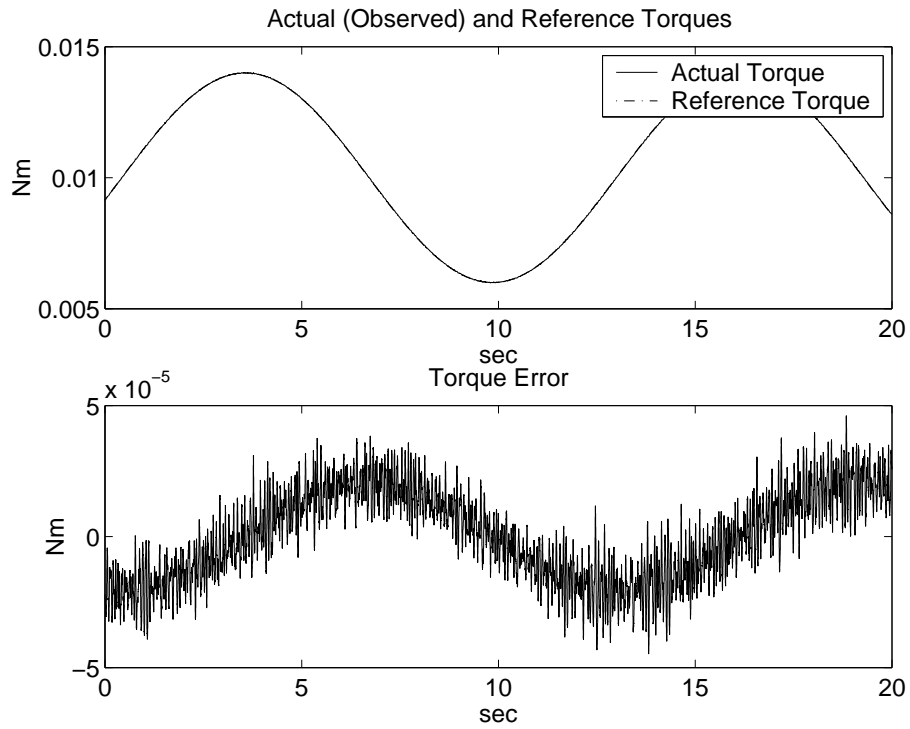


Figure 3.5: Maxon RE-40: External Torque Control based on Observed Data with Stationary Obstacle

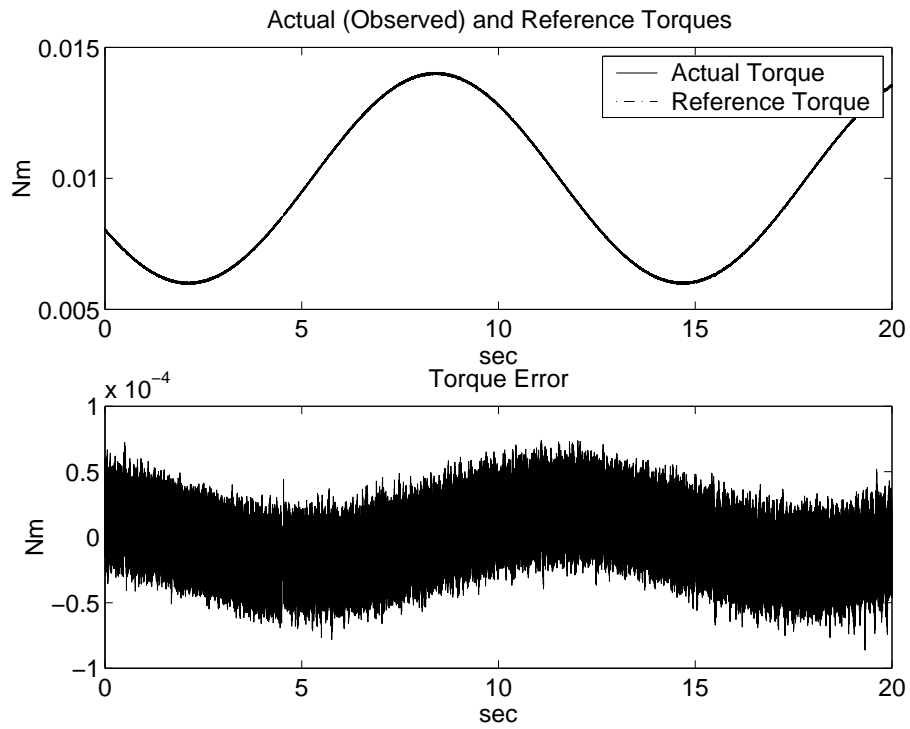


Figure 3.6: Maxon RE-40: External Torque Control based on Observed Data with Moving Obstacle

### 3.4 Disturbance Compensation and Plant Behaviour Dictation using a Sliding Mode Model Reference Controller(SMMRC)

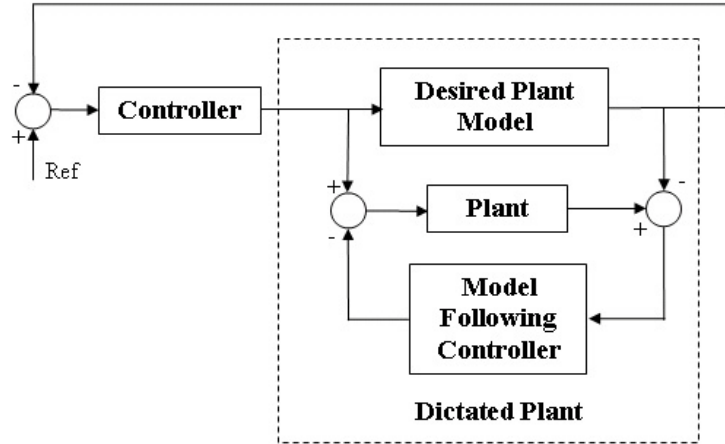


Figure 3.7: Traditional Model Reference Controller

Model Reference Control (MRC), or sometimes referred as Model Following Control, is a strong tool to compensate for the effect of disturbances due to the aforementioned nonlinearities in Section 2.4. The traditional approach to MRC is to use the output of the desired plant model (generally the linearized model of the plant with nominal parameters) as a reference for the control on the actual plant, which serves as a dictation on the plant motion equation essentially. This approach is shown in Figure 3.7.

In this section, a different approach is brought to MRC, exploiting the features of SMC. SMC, as mentioned in Chapter 2, works by constraining the motion equation of the plant in a predefined manifold  $\sigma = 0$ . The gist of SMC is selecting a manifold such that control objectives are realized on or with the help of it and using a reaching condition such as Lyapunov Stability Criterion to confine the motion on the manifold.

From the above discussion, it is obvious that any SMC for systems affine with respect to control and represented in controllable canonical form (which is the case for fully actuated mechanical systems this thesis focuses on) is actually an MRC. Therefore, if one selects the manifold in such a way that, the motion on the manifold is the desired plant model, the objectives of MRC would be fulfilled. The resultant

controller shown in Figure 3.8 is called SMMRC in this thesis. Note that, the desired model doesn't need to be the one with the nominal parameters, but any model within the reachability of the plant is possible with the proposed method. Hereafter, the experiments on PEA will be made using this dictated plant.

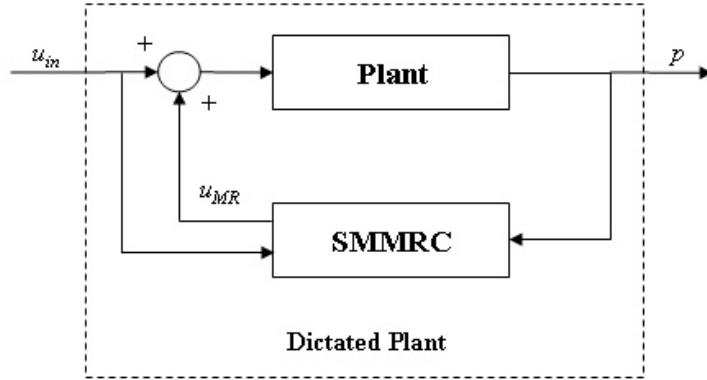


Figure 3.8: Sliding Mode Model Reference Controller

The compensation designed will be in terms of an additional  $\mathbf{u}_{mr} \in \mathfrak{R}^m$  to the plant input  $\mathbf{u}_{in} \in \mathfrak{R}^m$  such that  $\mathbf{u}$  in (3.3) is

$$\mathbf{u} = \mathbf{u}_{in} + \mathbf{u}_{mr} \quad (3.36)$$

as seen in the Figure 3.8.

Derivation of the controller typically starts with the proper model reference error function  $\mathbf{e}_{mr} \in \mathfrak{R}^n$  definition:

$$\mathbf{e}_{mr} = \dot{\mathbf{x}} - A_d \mathbf{x} - B_d \mathbf{u}_{in} \quad (3.37)$$

such that, for  $\mathbf{e}_{mr} = 0$ , the plant moves with the desired motion equation i.e.

$$\dot{\mathbf{x}} = A_d \mathbf{x} + B_d \mathbf{u}_{in}, \quad (3.38)$$

where  $A_d \in \mathfrak{R}^{n \times n}$  and  $B_d \in \mathfrak{R}^{n \times m}$  are the desired linear plant model parameters.

$\sigma_{mr} \in \mathfrak{R}^m$  is chosen to be

$$\sigma_{mr} = G_{mr} \mathbf{e}_{mr}, \quad (3.39)$$

for positive definite  $G_{mr} \in \mathfrak{R}^{m \times m}$  and  $\det G_{mr} B_d \neq 0$ . For stability, a positive definite Lyapunov function of the form

$$\nu_{mr}(\sigma_{mr}) = \frac{\sigma_{mr}^T \sigma_{mr}}{2}, \quad (3.40)$$

is used, and the derivative of the function is

$$\dot{\nu}_{mr}(\sigma_{mr}) = \sigma_{mr}^T \dot{\sigma}_{mr}. \quad (3.41)$$

If the control function is designed such that

$$\dot{\sigma}_{mr} + D_{mr}\sigma_{mr} = 0, \quad (3.42)$$

for positive definite symmetric matrix  $D_{mr} \in \mathfrak{R}^{m \times m}$ , Lyapunov function derivative becomes a negative-definite function as

$$\dot{\nu}_{mr}(\sigma_{mr}) = -\sigma_{mr}^T D_{mr} \sigma_{mr}, \quad (3.43)$$

which satisfies the Lyapunov stability criterion.

Using (3.39), (3.37) and (3.3), the sliding mode variable becomes

$$\sigma_{mr} = G_{mr}(F + B\mathbf{u} - A_d\mathbf{x} - B_d\mathbf{u}_{in}), \quad (3.44)$$

which can be written more clearly as

$$\sigma_{mr} = G_{mr} \underbrace{(F + \Delta B\mathbf{u}_{in} - A_d\mathbf{x} + B\mathbf{u}_{mr})}_{-B\mathbf{u}_{mr_{eq}}} \quad (3.45)$$

$$\sigma_{mr} = G_{mr}B(-\mathbf{u}_{mr_{eq}} + \mathbf{u}_{mr}). \quad (3.46)$$

Here  $\mathbf{u}_{mr_{eq}} \in \mathfrak{R}^m$  is the equivalent control defined in Section 2.3, which makes  $\sigma_{mr} = 0$  and  $\Delta B = B - B_d$ . Solving (3.46) for  $\mathbf{u}_{mr_{eq}}$  yields

$$\mathbf{u}_{mr_{eq}}(t) = \mathbf{u}_{mr}(t) - [G_{mr}B]^{-1}\sigma_{mr}. \quad (3.47)$$

Putting (3.46) in (3.42),

$$\dot{\sigma}_{mr} + D_{mr}G_{mr}B(\mathbf{u}_{mr}(t) - \mathbf{u}_{mr_{eq}}(t)) = 0, \quad (3.48)$$

the only unknown that prevents the calculation of  $\mathbf{u}_{mr}$  is  $\mathbf{u}_{mr_{eq}}$ , which is hard to calculate. However, since it is a smooth function, an approximation could be made by using the previous time step value of the  $\mathbf{u}_{mr}$  in (3.47) such that

$$\mathbf{u}_{mr_{eq}}(t) \approx \mathbf{u}_{mr}(t - \Delta t) + [G_{mr}B]^{-1}\sigma_{mr}. \quad (3.49)$$

Using this approximation in (3.48) and solving for current  $\mathbf{u}_{mr}$  gives

$$\mathbf{u}_{mr}(t) = \mathbf{u}_{mr}(t - \Delta t) + [D_{mr}G_{mr}B]^{-1}(\dot{\sigma}_{mr} + D_{mr}\sigma_{mr})|_{t-\Delta t}, \quad (3.50)$$

or in discrete-time

$$u_{mrk} = u_{mrk-1} + [D_{mr}G_{mr}B]^{-1}(\dot{\sigma}_{mr} + D_{mr}\sigma_{mr})|_{k-1}. \quad (3.51)$$

For analysis of the effect of the SMMRC on plant behaviour consider (3.45). From the selection of  $\sigma_{mr}$ , it is clear that  $\mathbf{e}_{mr} \rightarrow 0$  on sliding mode, where

$$\mathbf{u}_{mr} = \mathbf{u}_{mr_{eq}} = [G_{mr}B]^{-1}G_{mr}(F + \Delta B\mathbf{u}_{in} - A_d\mathbf{x}). \quad (3.52)$$

Using this control input and (3.36) in (3.3),

$$\dot{\mathbf{x}} = F(\mathbf{x}, t) + B\mathbf{x}, t)(\mathbf{u}_{in} + B[G_{mr}B]^{-1}G_{mr}(F + \Delta B\mathbf{u}_{in} - A_d\mathbf{x})). \quad (3.53)$$

As  $B[G_{mr}B]^{-1}G_{mr} = I$ , on the sliding mode the system behaves as the desired motion equation in (3.38)

Below, open loop position control results of a PEA are given using the SMMRC designed above to demonstrate the performance of plant behaviour dictation. The open loop control input is given with an inverse desired plant model as shown in Figure 3.9.

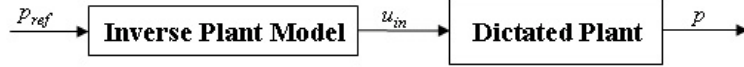


Figure 3.9: Open Loop Control using SMMRC

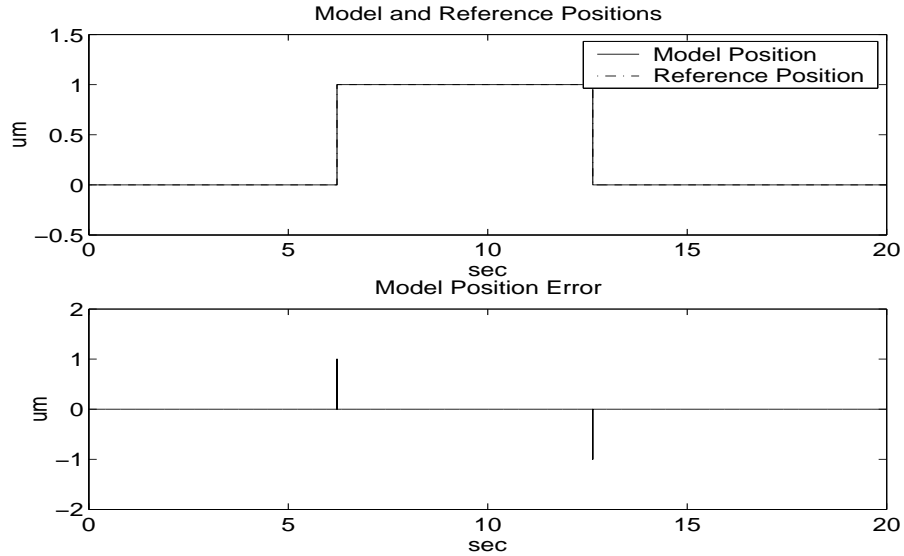


Figure 3.10: PEA: SMMRC Open Loop Position Control Model Response for a 1  $\mu\text{m}$  Step

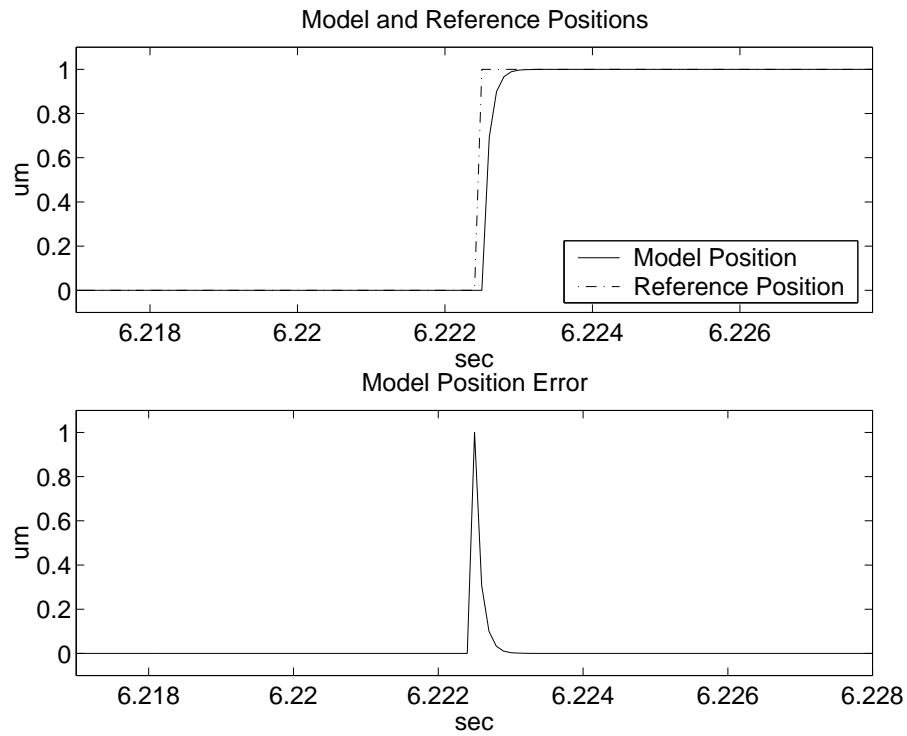


Figure 3.11: PEA: Magnified Model Position Error of SMMRC Open Loop Position Control for a 1 um Step

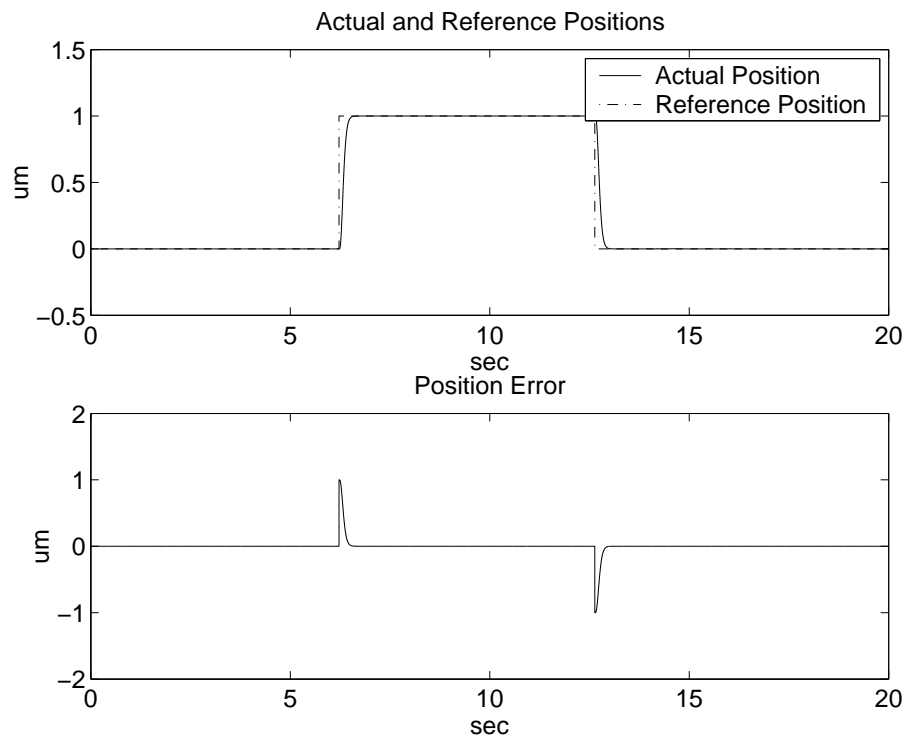


Figure 3.12: PEA: SMMRC Open Loop Position Control Plant Response for a 1 um Step

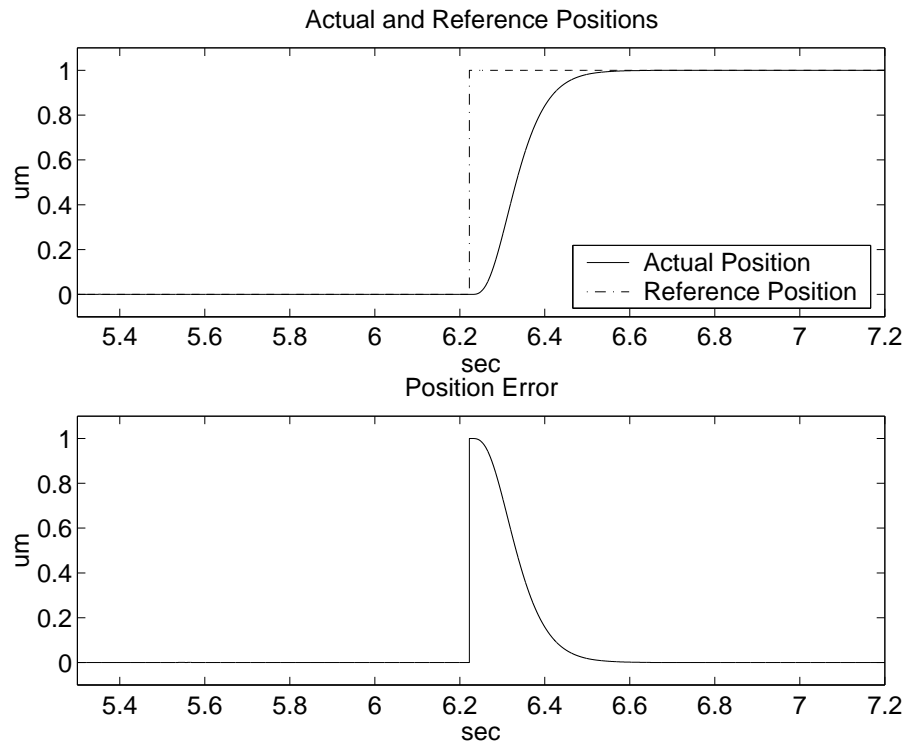


Figure 3.13: PEA: Magnified Plant Position Error of SMMRC Open Loop Position Control for a 1  $\mu\text{m}$  Step

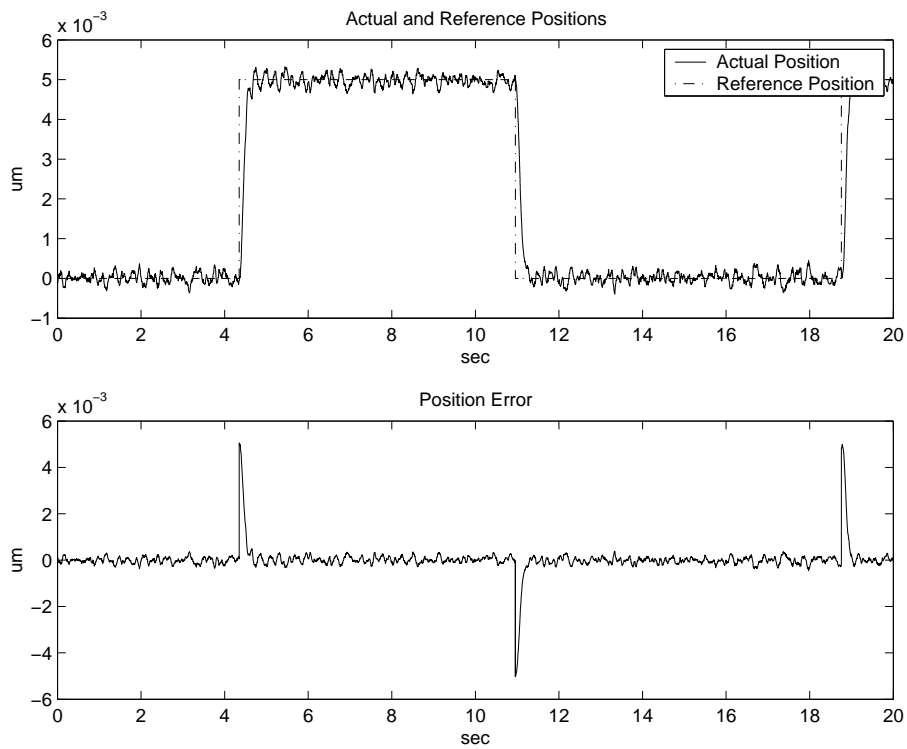


Figure 3.14: PEA: SMMRC Open Loop Position Control Plant Response for a 5 nm Step

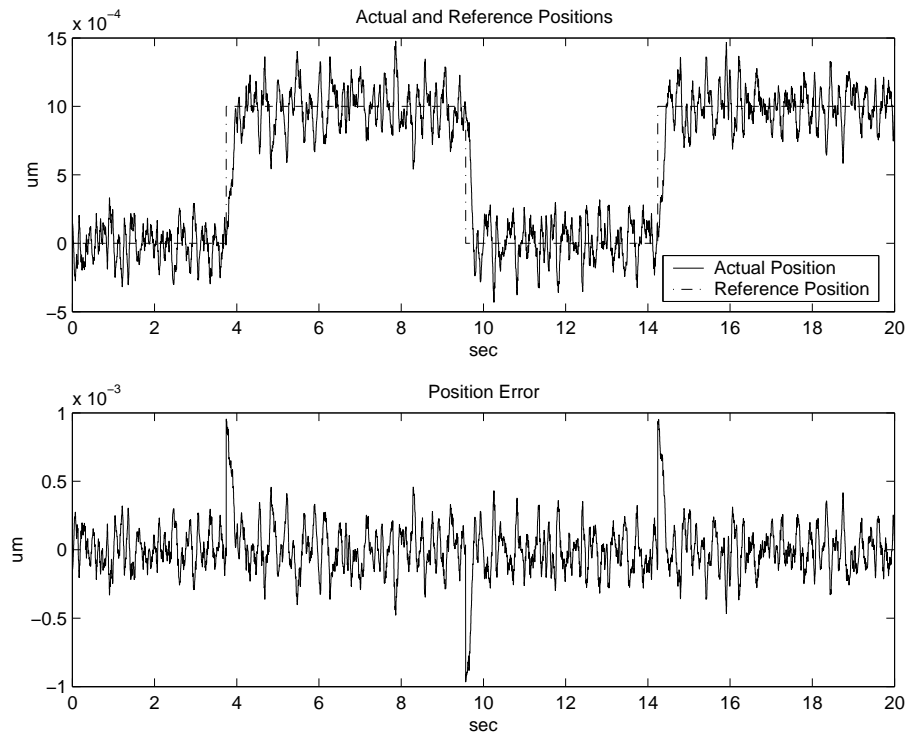


Figure 3.15: PEA: SMMRC Open Loop Position Control Plant Response for a 1 nm Step

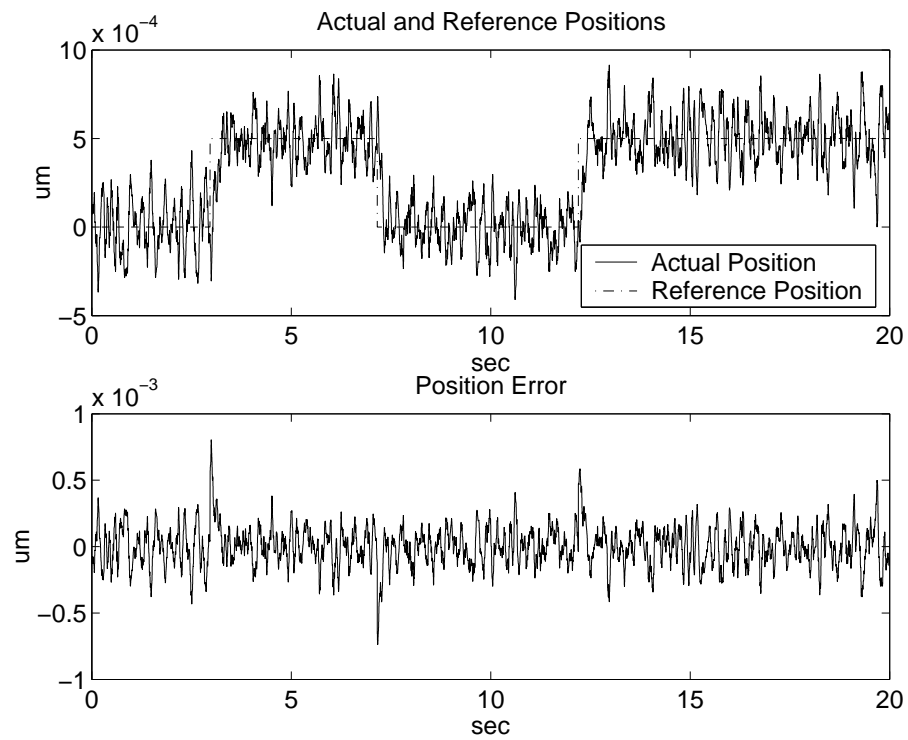


Figure 3.16: PEA: SMMRC Open Loop Position Control Plant Response for a 0.5 nm Step

### 3.5 Controller Parameter Adaptation

As mentioned before in Chapter 2, Sliding Mode is a robust control technique. However, since it doesn't have an adaptation scheme, it may not yield sufficient dynamics for different magnitudes of errors. In this section, an adaptation to the sliding manifold is described according to the error magnitude.

For the sliding manifold in the form

$$\dot{\sigma} + D\sigma = 0 \quad (3.54)$$

since  $D$  is the only parameter one can manipulate, there are generally two kinds of adaptations possible, where  $D_{ii}$  is one of the diagonal elements of the diagonal matrix  $D$ :

1. When the plant has high mass/inertia, the manifold should be steeper for small errors to overcome stiction and should have a lower slope for larger errors to overcome overshoot like  $D_{ii} = D_0 + \frac{D_1}{1+D_2|e|}$  as shown in Fig 3.17.

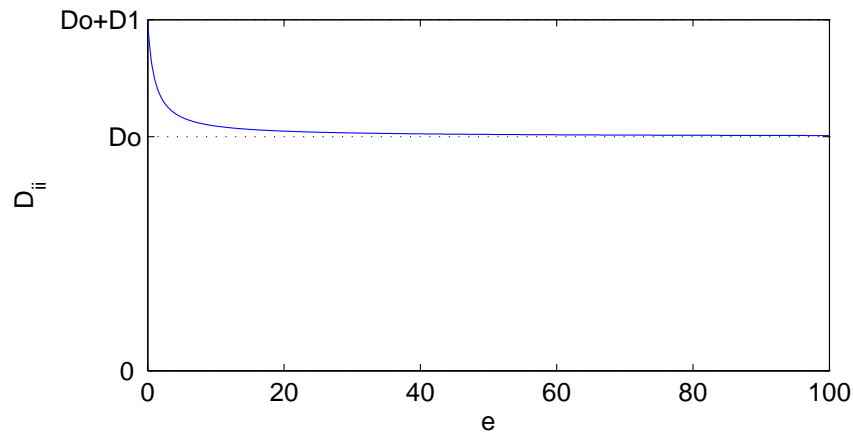
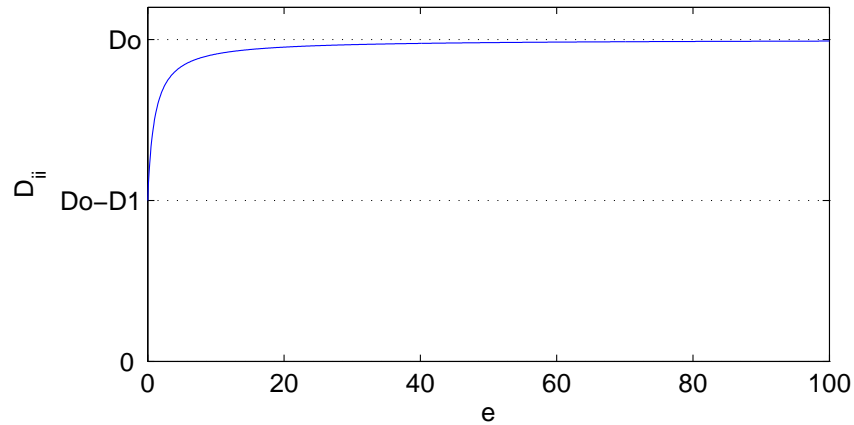
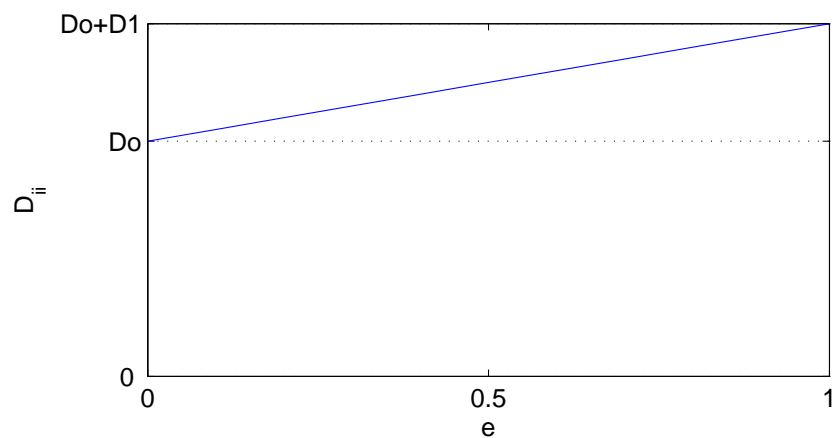


Figure 3.17: First Kind of Adaptation Scheme on the Sliding Manifold Slope

2. When the plant has low mass/inertia, the vice versa should be applied (i.e. steeper manifold for larger errors to overcome the underdamped dynamics and should have a lower slope for small errors) like  $D_{ii} = D_0 - \frac{D_1}{1+D_2|e|}$  or  $D_{ii} = D_0 + D_1 |e|$  as shown in Fig 3.18.



(a)



(b)

Figure 3.18: Second Kind of Adaptation Scheme on the Sliding Manifold Slope  
 (a) Slope Has an Upper Bound for Large Errors and (b) Slope Grows without Bound

Following figures are results of position control experiments on the Maxon RE-40 DC motor setup, with the second kind of adaptation scheme shown in Figure 3.18b. Figures 3.19, 3.20 are showing the results of a square wave trajectory with magnitude of a single step of the incremental encoder attached to the motor, namely  $\frac{2\pi}{2000} = 0.0031416$ . Note that there is about 7.5 msec delay on the response of the actuator to the reference in Figure 3.20, which stems from the fact that the incremental encoder is blind until one increment motion is finalized and hence the actual response and rise time of tracking can not be seen. Figure 3.21 shows the result of the adaptive sliding mode position control with a sinusoidal position reference. As shown in this figure, the errors never exceed one increment of the incremental encoder, therefore the control has achieved the best precision possible, for both small and large errors.

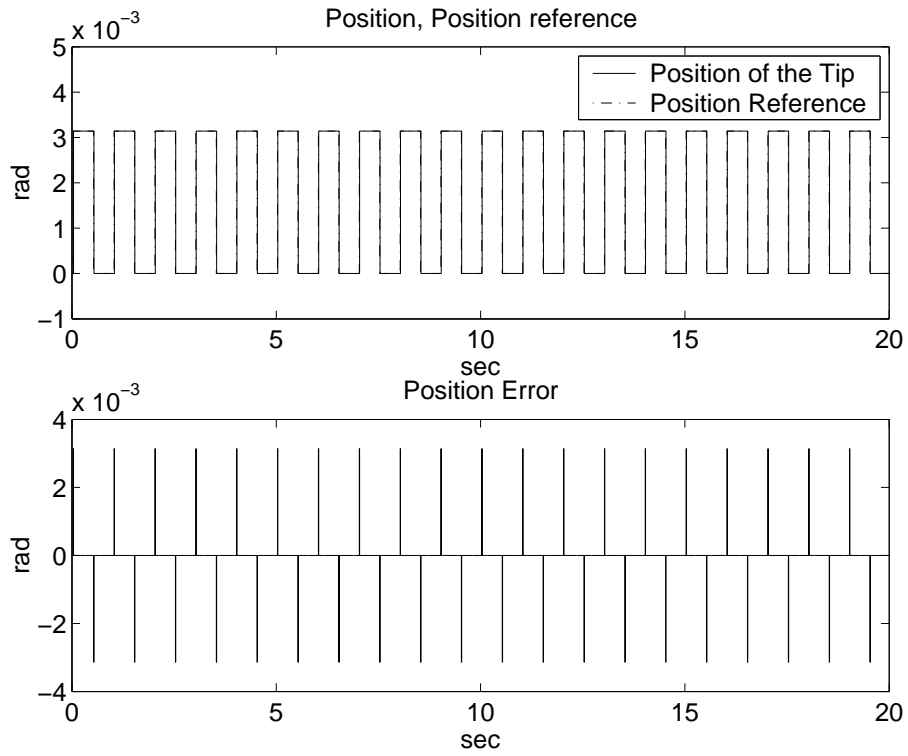


Figure 3.19: Maxon RE-40: Position Control for One Increment Pulse Reference with Adaptive Sliding Manifold

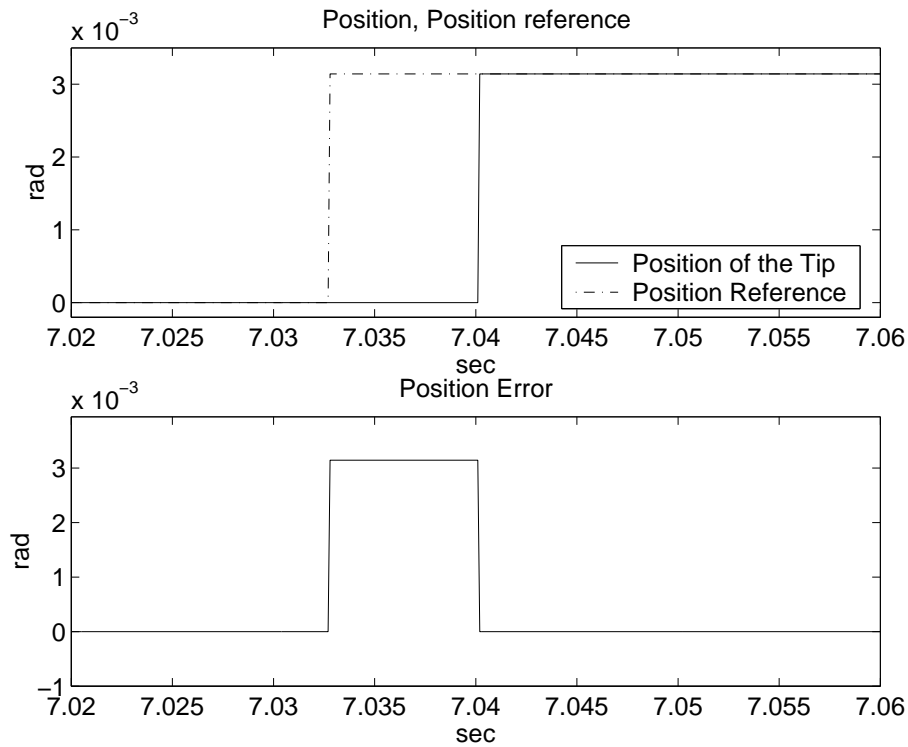


Figure 3.20: Maxon RE-40: Magnified Position Error of Position Control for One Increment Pulse Reference with Adaptive Sliding Manifold

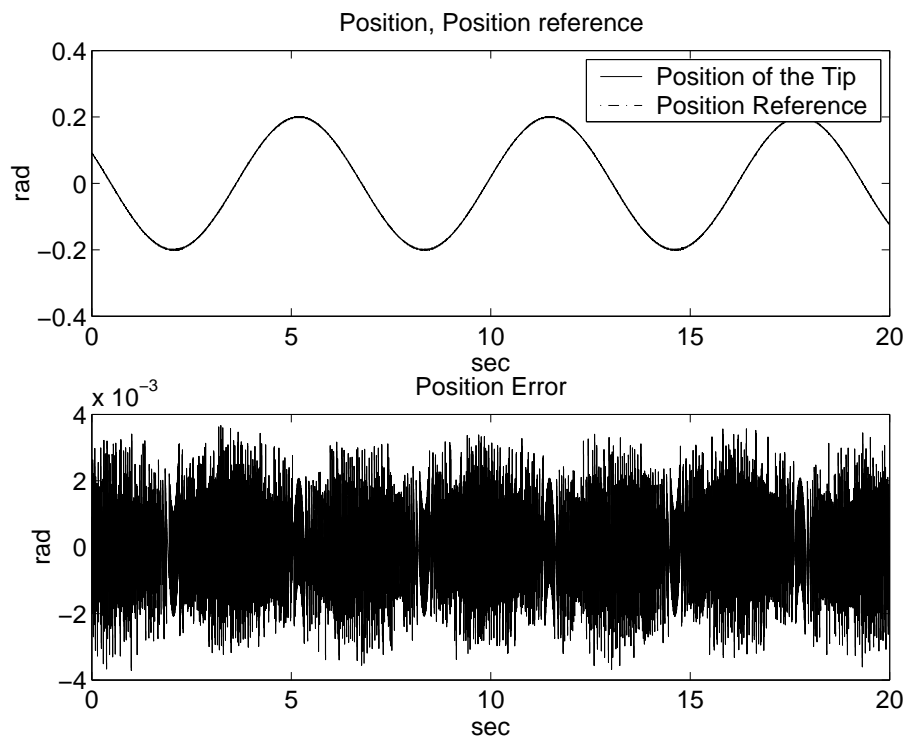


Figure 3.21: Maxon RE-40: Position Control for Sinusoidal Reference with Adaptive Sliding Manifold

## Chapter 4

### A Cascaded Sliding Mode Hybrid Force/Position Controller

As stated in Section 1.3, the objective of a hybrid controller is to control position of the tip and external force for unconstrained and constrained motions of the plant, respectively. Traditional approach and its predecessors mainly suffer from the kinematic instability problem due to the jump of control input at the switching of modes. Also, first contact forces are relatively high, causing a possible damage to the plant or the environment at this first (blind) contact.

Proposed in this thesis is to solve both problems at the core of any hybrid force/position control task by using a single position controller (SMPC) to run the plant, whose input (state error  $e_x$ ) is altered by means of a sliding mode position error estimator (SMPEE) -further explained in the next section- with respect to the external force error as shown in Figure 4.1. The cascaded force controller achieved provides good force tracking as shown for PEA in Figure 4.2.

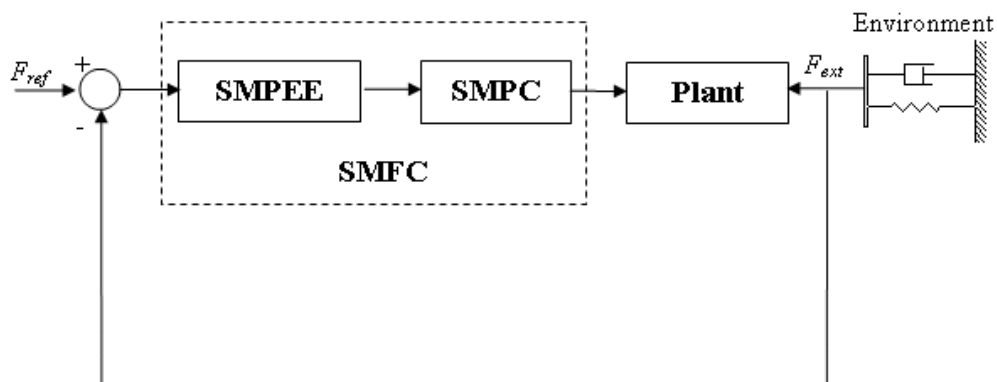


Figure 4.1: Cascaded Force Controller

## 4.1 Position Error Estimator with respect to External Force Error

Now that, a Sliding Mode Position Controller (SMPC) formulated in Section 3.1 runs the plant, the combined system (of SMPC and the plant) could be considered to be running in position control mode. Given the necessary  $\mathbf{x}_{ref}$  or  $\mathbf{e}_x$ , one can be certain that the controller will force the plant to track that reference or reduce that error.

This gives an opportunity to combine the hybrid motion controller (consisting of position tracking and the force control) with sliding mode technique. For this, the corresponding state error ( $\mathbf{e}_x$ ) should be determined, such that the desired force as a result of the interaction with unknown environment is achieved. In the following lines of equations, the same scheme for position control is followed, for this objective.

Consider the general environmental model (3.6), for which control of force will be designed. Let a relationship between the force reference and state reference vector be defined as:

$$\mathbf{F}_{ref} = \widehat{A}_{ext}(\mathbf{x}_{ref} - \mathbf{x}_{env}), \quad (4.1)$$

where  $\mathbf{F}_{ref} \in \mathfrak{R}^l$  is the reference external force in all  $l$  dimensions,  $\widehat{A}_{ext} \in R^{l \times n}$ , for  $n = 2l$ , is the estimate environmental matrix of the system consisting of estimate spring and damping coefficients such that  $\widehat{A}_{ext} = [\widehat{K}_{ext} \ \widehat{b}_{ext}]$ .  $\mathbf{x}_{ref} \in \mathfrak{R}^n$  is the reference state vector and  $\mathbf{x}_{env} \in \mathfrak{R}^n$  is the environment (obstacle) state vector.

Subtracting (3.6) from (4.1), force error is obtained as

$$\mathbf{e}_f = \widehat{A}_{ext}\mathbf{e}_x + \Delta A_{ext}\Delta\mathbf{x}, \quad (4.2)$$

for  $\Delta\mathbf{x} = \mathbf{x} - \mathbf{x}_{env}$  and  $\Delta A_{ext} = \widehat{A}_{ext} - A_{ext}$ . Defining the sliding mode variable as

$$\sigma_f = G_f\mathbf{e}_f = G_f(\mathbf{F}_{ref} - \mathbf{F}_{ext}), \quad (4.3)$$

for positive definite  $G_f \in \mathfrak{R}^{m \times l}$ . For stability, a positive definite Lyapunov function of the form

$$\nu_f(\sigma_f) = \frac{\sigma_f^T \sigma_f}{2}, \quad (4.4)$$

is used, and the derivative of the function is

$$\dot{\nu}_f(\sigma_f) = \sigma_f^T \dot{\sigma}_f. \quad (4.5)$$

If the position error is used as the control and designed such that

$$\dot{\sigma}_f + D_f \sigma_f = 0, \quad (4.6)$$

for positive definite symmetric matrix  $D_f \in \mathfrak{R}^{m \times m}$ , Lyapunov function derivative becomes a negative-definite function as

$$\dot{v}_f(\sigma_f) = -\sigma_f^T D_f \sigma_f, \quad (4.7)$$

which satisfies the Lyapunov stability criterion.

Putting (4.1) and (3.6) for the plant into (4.3), sliding mode variable becomes

$$\sigma_f = G_f \widehat{A}_{ext} \mathbf{e}_x - G_f \underbrace{[\Delta K_{ext} \quad \Delta b_{ext}]}_{\widehat{A}_{ext} \mathbf{e}_{x_{eq}}} (\mathbf{x} - \mathbf{x}_{env}) \quad (4.8)$$

$$\sigma_f = G_f \widehat{A}_{ext} (\mathbf{e}_x - \mathbf{e}_{x_{eq}}) \quad (4.9)$$

where  $\Delta K_{ext}$  and  $\Delta b_{ext}$  are the differences between the real and estimate values for environmental coefficients. Here, note that  $\mathbf{e}_x$  is used as the control input to the combined system of position controller and plant. From here, equivalent state error becomes

$$\mathbf{e}_{x_{eq}} = \mathbf{e}_x - [G_f \widehat{A}_{ext}]^{-1} \sigma_f. \quad (4.10)$$

Putting (4.9) in (4.6), one gets

$$\dot{\sigma}_f + D_f G_f \widehat{A}_{ext} (\mathbf{e}_x - \mathbf{e}_{x_{eq}}) = 0. \quad (4.11)$$

To calculate  $\mathbf{e}_x$ ,  $\mathbf{e}_{x_{eq}}$  is necessary, but difficult to find. However, it may be approximated by using the  $\mathbf{e}_x$  of the previous time step in (4.10). Putting the approximation in (4.11) and solving for the current  $\mathbf{e}_x$  yields,

$$\mathbf{e}_{x_k} = \mathbf{e}_{x_{k-1}} - [D_f G_f \widehat{A}_{ext}]^{-1} (\dot{\sigma}_f + D_f \sigma_f) \quad (4.12)$$

The performance of the resultant cascaded force controller is demonstrated with an experiment on the PEA as shown in Figure 4.2.

## 4.2 Force Controller Stability Analysis

The force controller is constructed in terms of a position error estimator with respect to force error keeping in mind that the system is controlled using the SMPC. At this

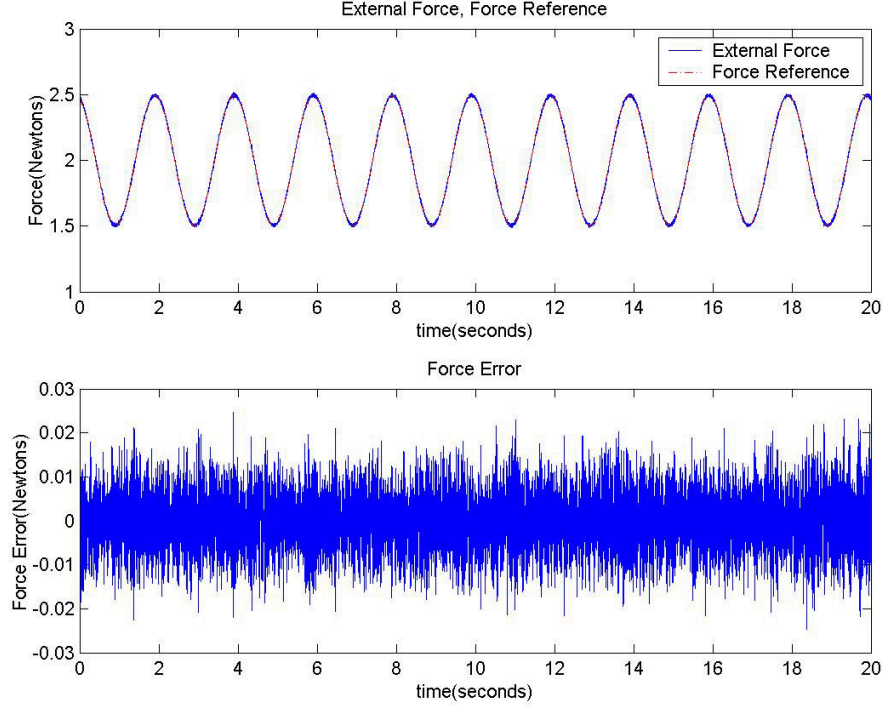


Figure 4.2: PEA Cascaded Force Controller Results

point, the estimated position error's capability to remove the force error should be investigated. In section 4.1, it is shown that, the error estimates reduce force error to zero, in this section, the direct effect of the control input  $\mathbf{u}$  to the plant on force error is examined.

In (4.2), a relationship between force error and state error is shown. Using (4.9), and solving for state error:

$$\mathbf{e}_x = \mathbf{e}_{x_{eq}} + [G_f \widehat{A}_{ext}]^{-1}(\sigma_f) \quad (4.13)$$

and its derivative:

$$\dot{\mathbf{e}}_x = \dot{\mathbf{e}}_{x_{eq}} + [G_f \widehat{A}_{ext}]^{-1}(\dot{\sigma}_f). \quad (4.14)$$

Remember from (3.12) that  $G_x \dot{\mathbf{e}}_x + D_x G_x \mathbf{e}_x = 0$ , so derivative of the state error becomes

$$G_x \dot{\mathbf{e}}_x = -D_x G_x \left[ \mathbf{e}_{x_{eq}} + [G_f \widehat{A}_{ext}]^{-1}(\sigma_f) \right]. \quad (4.15)$$

Equating  $G_x$  times (4.14) and (4.15),

$$G_x \dot{\mathbf{e}}_{x_{eq}} + G_x [G_f \widehat{A}_{ext}]^{-1}(\dot{\sigma}_f) + D_x G_x \left[ \mathbf{e}_{x_{eq}} + [G_f \widehat{A}_{ext}]^{-1}(\sigma_f) \right] = 0. \quad (4.16)$$

Rearranging (4.16) and putting (4.3) in

$$\underbrace{G_x \dot{\mathbf{e}}_{x_{eq}} + D_x G_x \mathbf{e}_{x_{eq}}}_0 + \underbrace{G_x [G_f \widehat{A}_{ext}]^{-1} G_f \dot{\mathbf{e}}_f + D_x G_x [G_f \widehat{A}_{ext}]^{-1} G_f \mathbf{e}_f}_0 = 0. \quad (4.17)$$

Therefore, supplying the position error estimate for force error, to the SMPC, a dynamical relationship  $K_f \dot{\mathbf{e}}_f + D_x K_f \mathbf{e}_f = 0$ , between force error and its derivative is enforced, which is the sliding manifold for force error and satisfies Lyapunov Stability Criterion. Here  $K_f$  is a matrix used to clear up the view to the forced dynamical relationship.

### 4.3 Error Selection for Hybrid Control

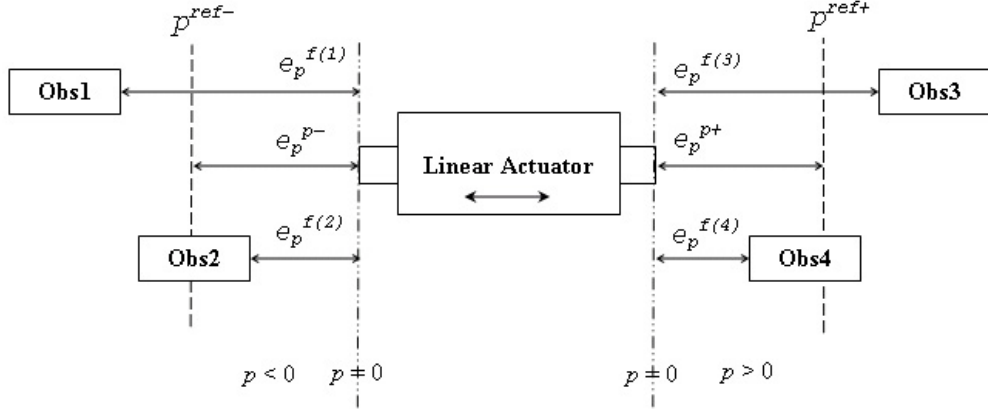


Figure 4.3: Estimated and Actual Position Errors on Both Sides

Now that two position errors are found for force and position control, respectively. Calling the two as the actual position error  $\mathbf{e}_p^p$  and the estimated position error  $\mathbf{e}_p^f$ , what one needs to do is feed the most reasonable one to the position controller at each time step for ideal hybrid control. This switching between the position errors differs from controller switching since it doesn't cause a jump in the control input to the plant (output of the position controller) and so, doesn't cause the classical kinematic instability problem [9], controller switching may cause.

Reasonable position error would be the one that wouldn't position the tip such that the external force exceeds the force reference in magnitude. Since force can be applied from both sides of the tip, positive and negative reference values are used to cover each possibility. So, for positive external force, the positive force reference and

for negative external force, the negative force reference is used and the corresponding position error for that force error is estimated. Then the estimated position error that causes the force error is compared with the actual position error and the one minimum in magnitude between the two is fed to the position controller.

A visual representation of the mentioned position errors could be found in Figure 4.3. Note that this figure is a simplified drawing to provide a visual understanding of the ideas behind position error estimation with respect to force error and position error selection. To make a clear representation of the errors, it is actually unrealistic since it assumes that the position errors with respect to the force errors could be estimated even when the plant is not in contact with the obstacles, which is not the case if no visual feedback is available. However, as it will be shown on experimental results, the force controller (position error estimator) is fast enough to converge to the respective position error as soon as there is a contact with an obstacle and could therefore remove the large forces encountered at the first blind contact with the obstacle.

The resulting sliding mode hybrid controller (SMHC) is shown in Fig. 4.4.

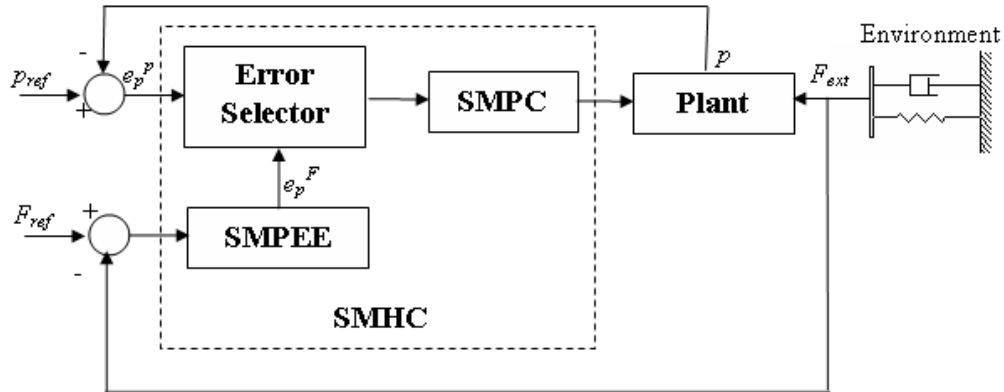


Figure 4.4: Cascaded Hybrid Force/Position Controller

## 4.4 Experimental Results

The experiment on Maxon RE-40 DC motor involves a sinusoidal position reference with constant positive and negative force references with the same magnitude, which can be considered as the maximum amount of force the actuator is allowed to exert on the environment due to the nature of the controller that doesn't create any

overshoot (i.e. first contact force mentioned above).

First experiment on PEA had both sinusoidal references for position and force, in the second experiment force reference is a square wave and in the third experiment force reference is changed to a triangular wave. As shown in the respective figures, hybrid control performs well in all the mentioned scenarios. For the triangular force reference, the position errors at the transition of modes look large in Figures 4.25 and 4.26. However this is because the magnification in these figures is larger than that of the previous experiments. The position errors in the position mode never exceeds  $0.05 \mu\text{m}$ . Note that the PEA plant is dictated to behave with its nominal values under SMMRC mentioned in Section 3.4.

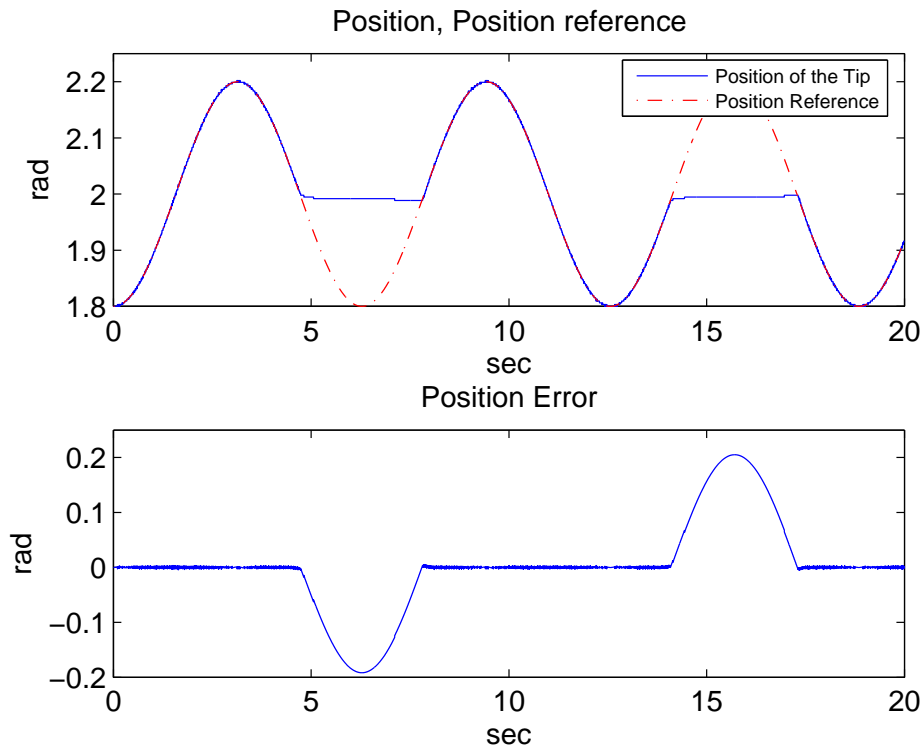


Figure 4.5: Maxon RE-40: Position and Position Reference; Position Error Graphs

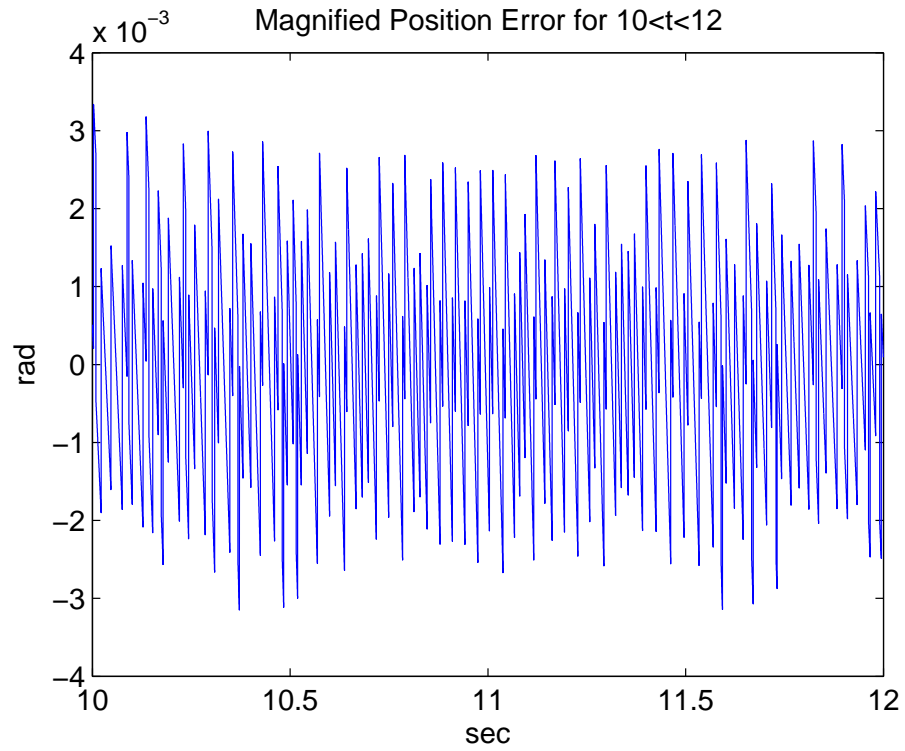


Figure 4.6: Maxon RE-40: Magnified Position Error for  $10 < t < 12$

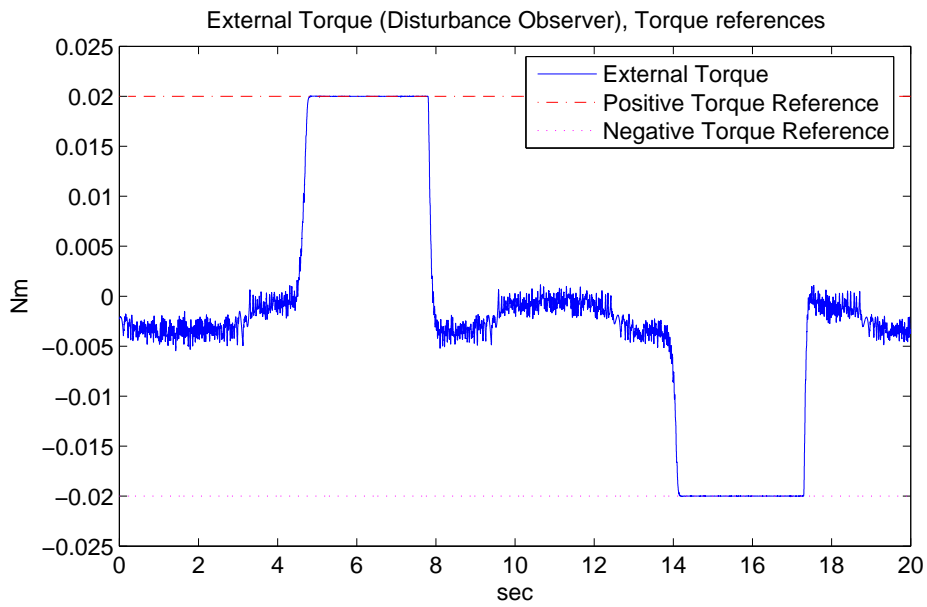


Figure 4.7: Maxon RE-40: Observed Torque and Torque References

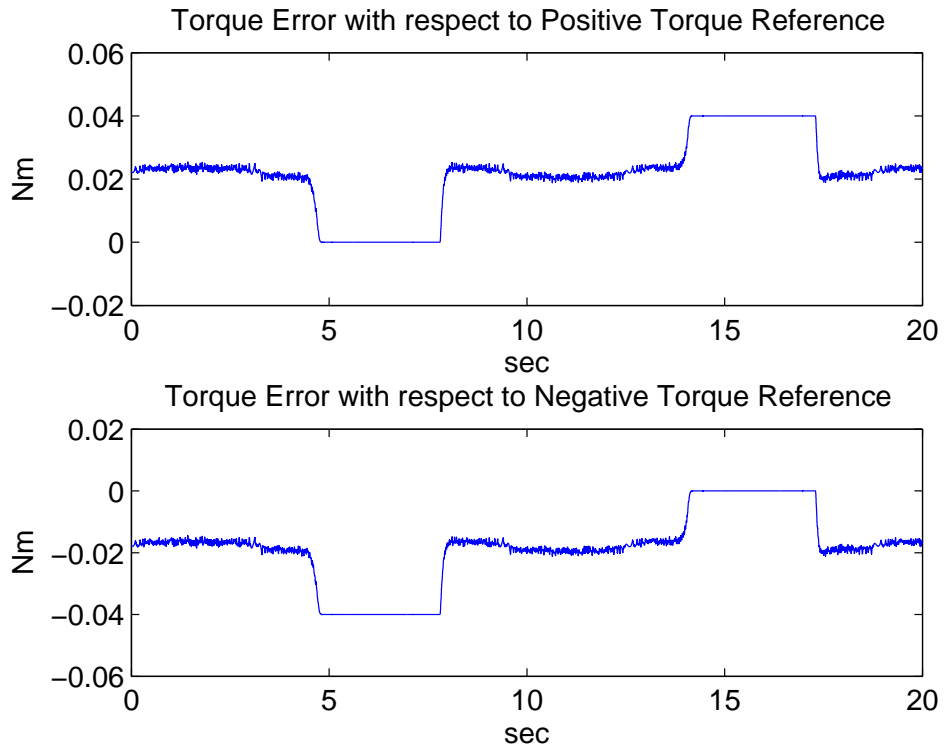


Figure 4.8: Maxon RE-40: Torque Error for Both Torque References

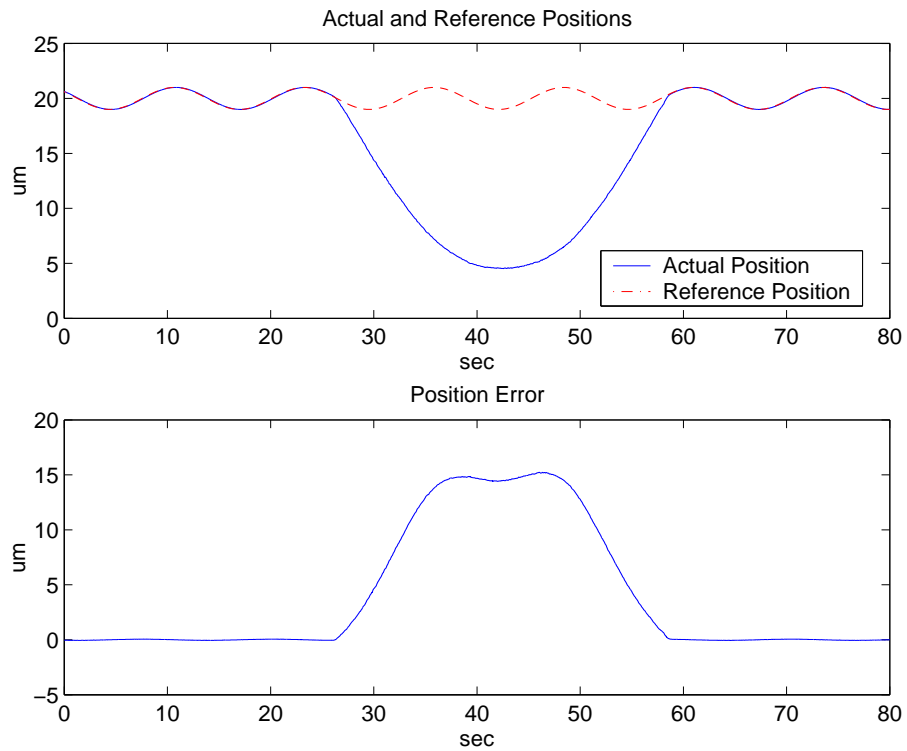


Figure 4.9: PEA - Experiment 1: Position and Position Reference; Position Error Graphs

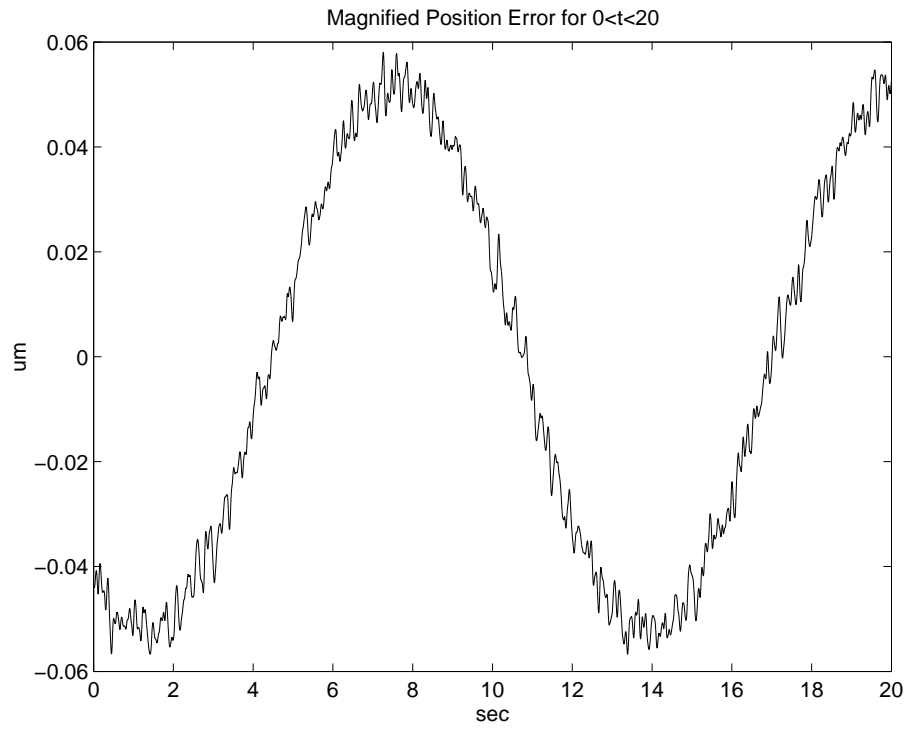


Figure 4.10: PEA - Experiment 1: Magnified Position Error for  $0 < t < 20$

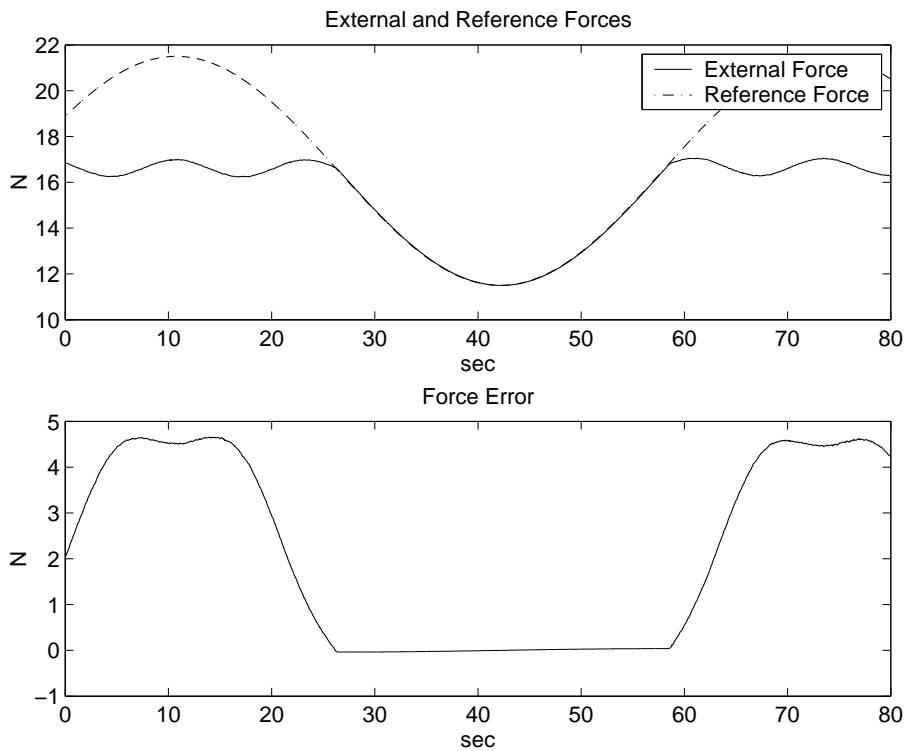


Figure 4.11: PEA - Experiment 1: Measured Force and Force Reference; Force Error Graphs

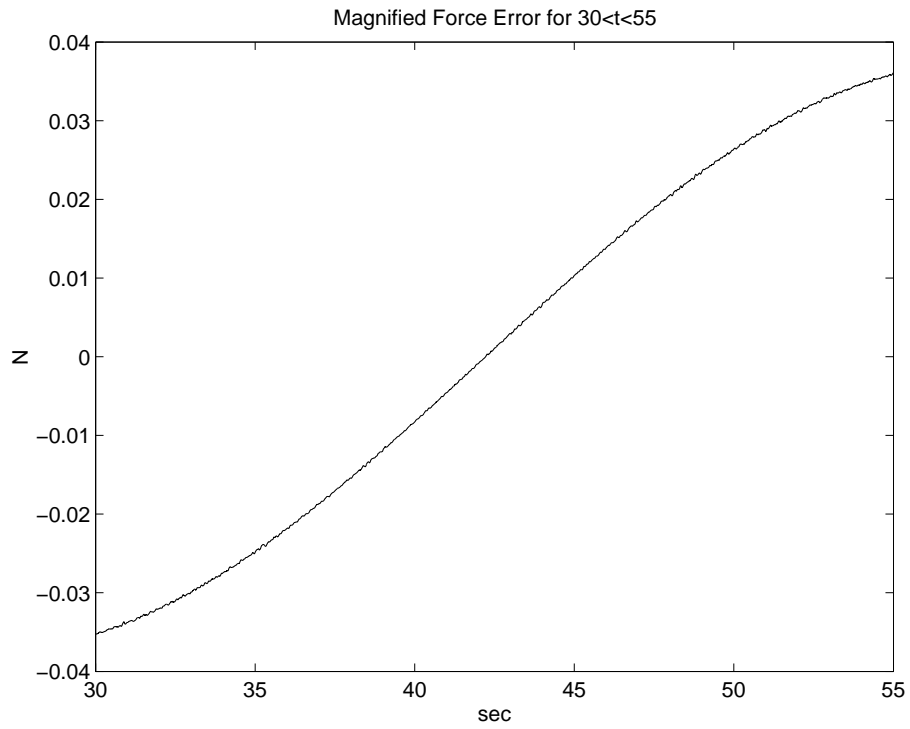


Figure 4.12: PEA - Experiment 1: Magnified Force Error for  $30 < t < 55$

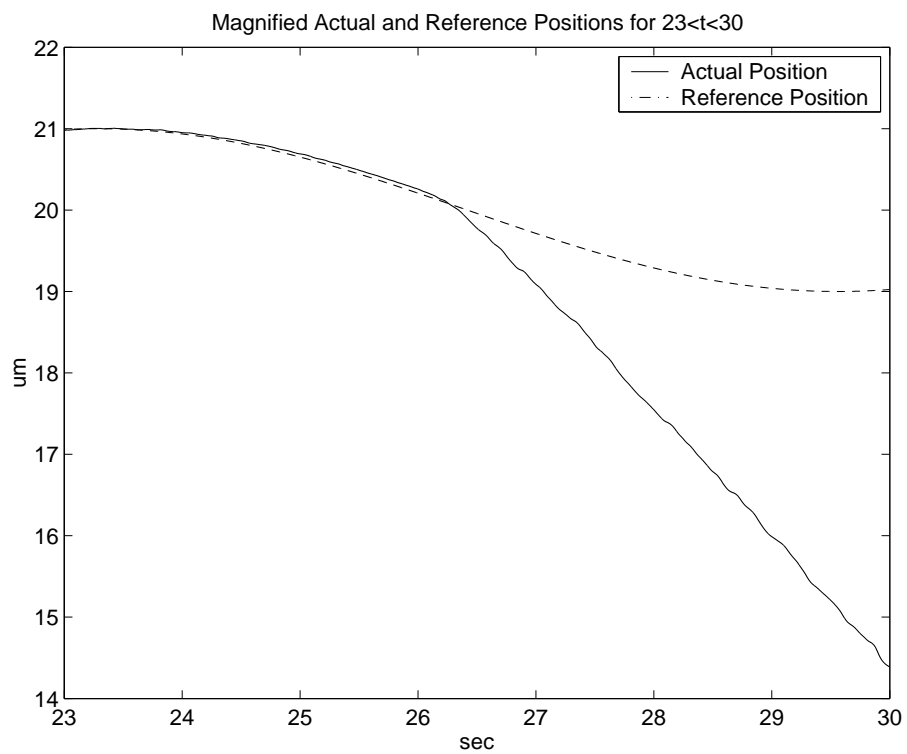


Figure 4.13: PEA - Experiment 1: Magnified Position at the Transition from Position to Force Mode

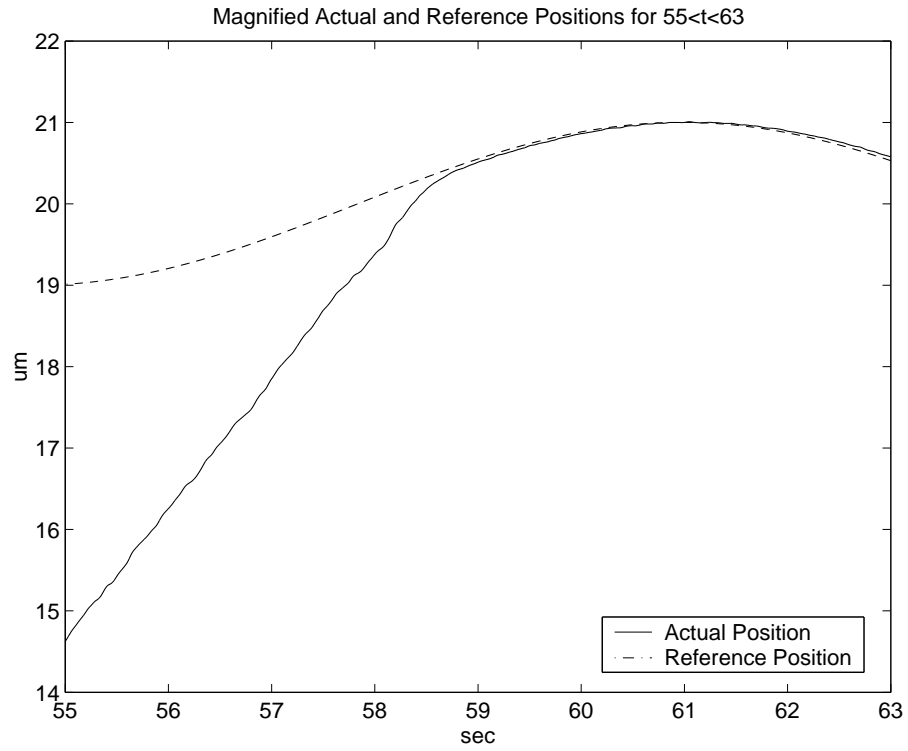


Figure 4.14: PEA - Experiment 1: Magnified Position at the Transition from Force to Position Mode

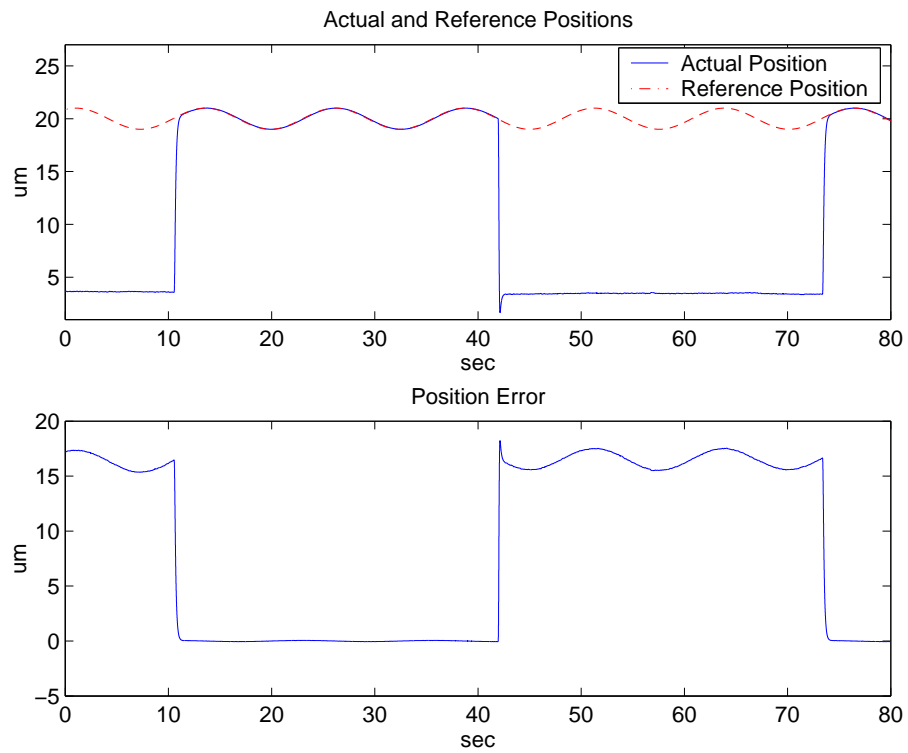


Figure 4.15: PEA - Experiment 2: Position and Position Reference; Position Error Graphs

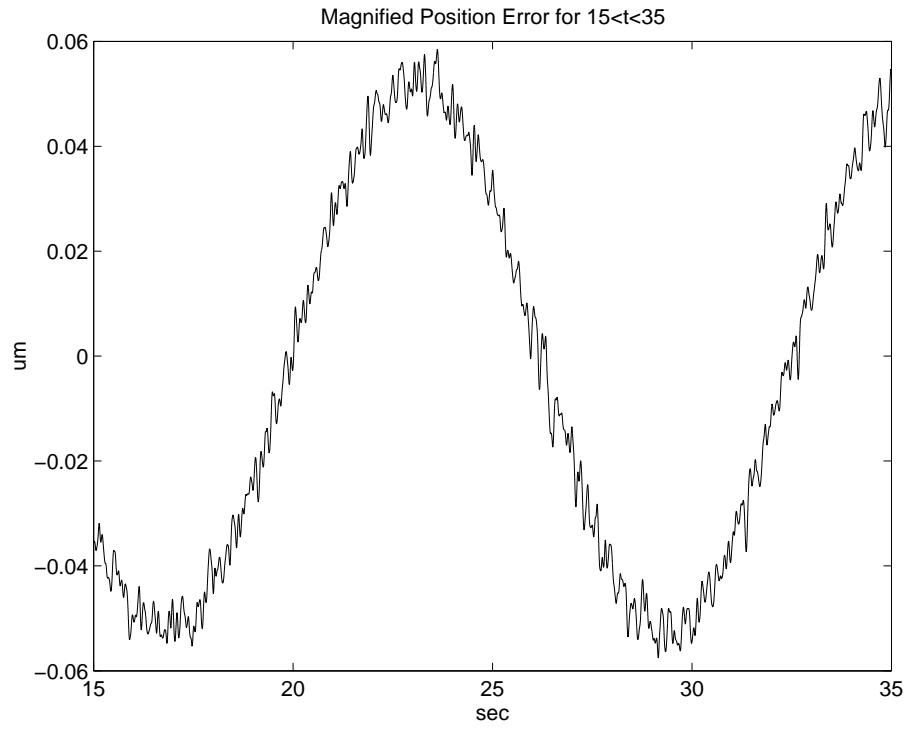


Figure 4.16: PEA - Experiment 2: Magnified Position Error for  $15 < t < 35$

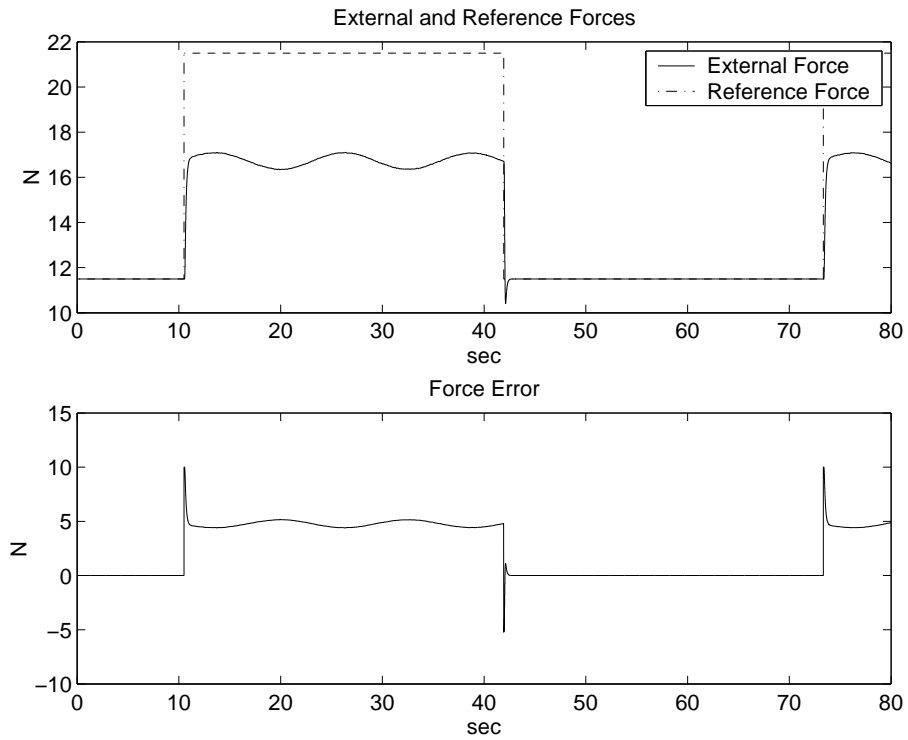


Figure 4.17: PEA - Experiment 2: Measured Force and Force Reference; Force Error Graphs

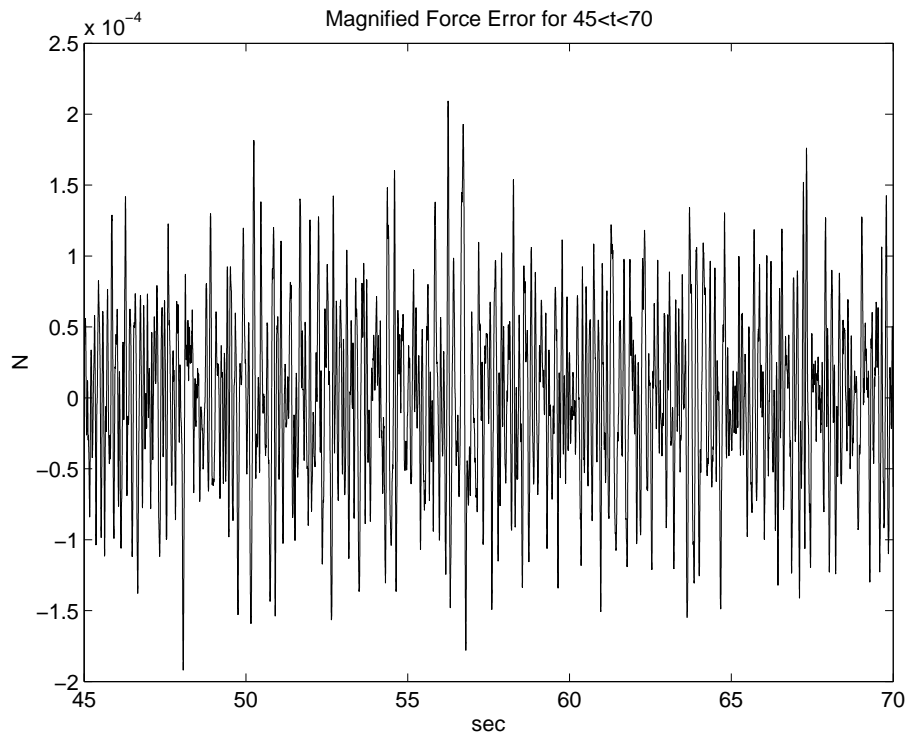


Figure 4.18: PEA - Experiment 2: Magnified Force Error for  $45 < t < 70$

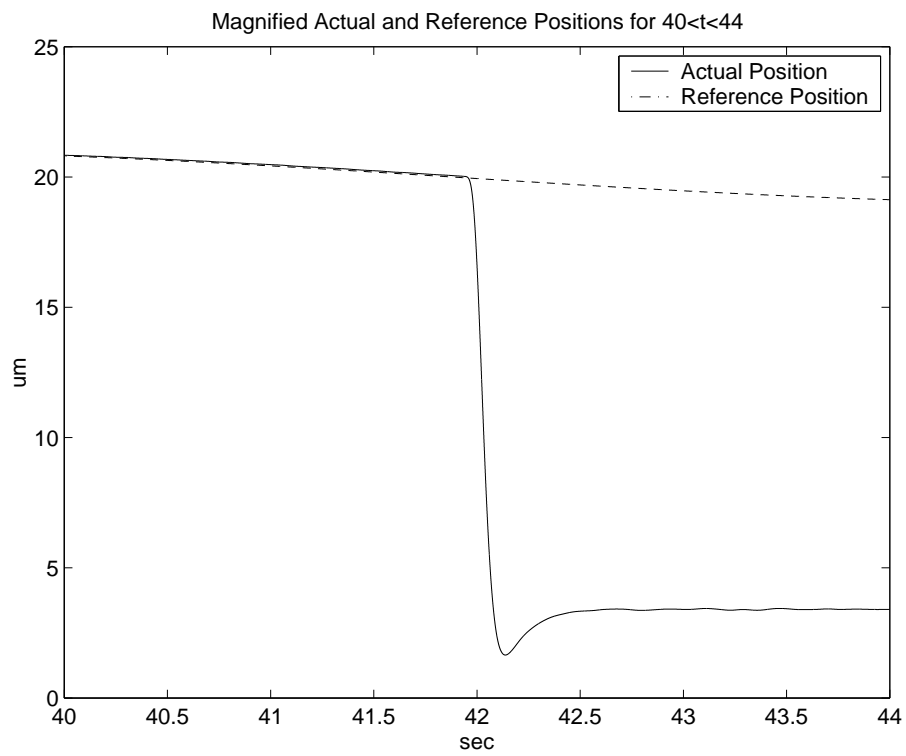


Figure 4.19: PEA - Experiment 2: Magnified Position at the Transition from Position to Force Mode

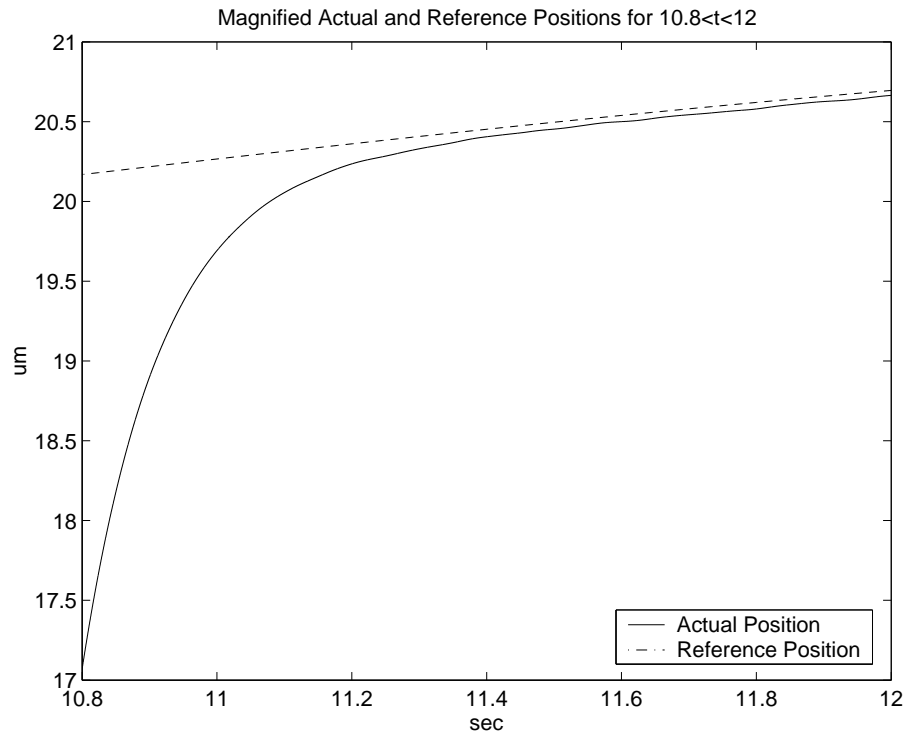


Figure 4.20: PEA - Experiment 2: Magnified Position at the Transition from Force to Position Mode

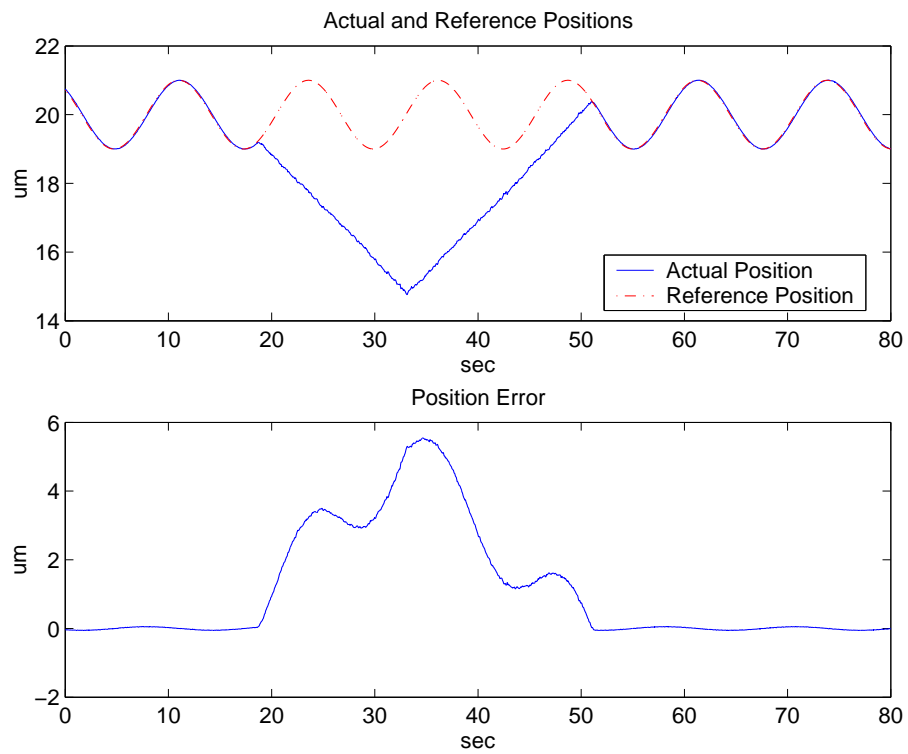


Figure 4.21: PEA - Experiment 3: Position and Position Reference; Position Error Graphs

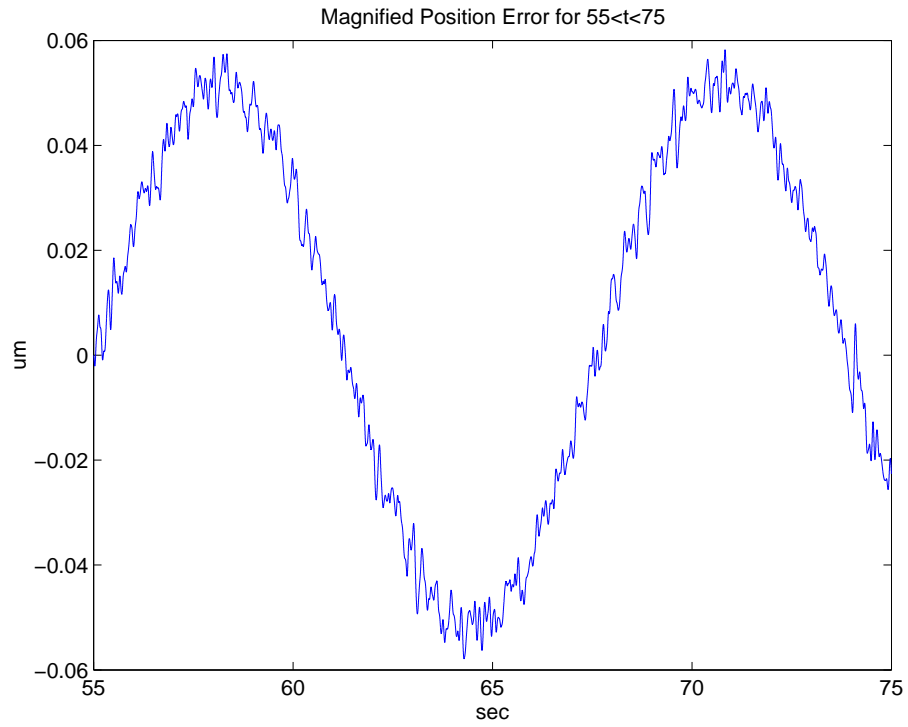


Figure 4.22: PEA - Experiment 3: Magnified Position Error for  $55 < t < 75$

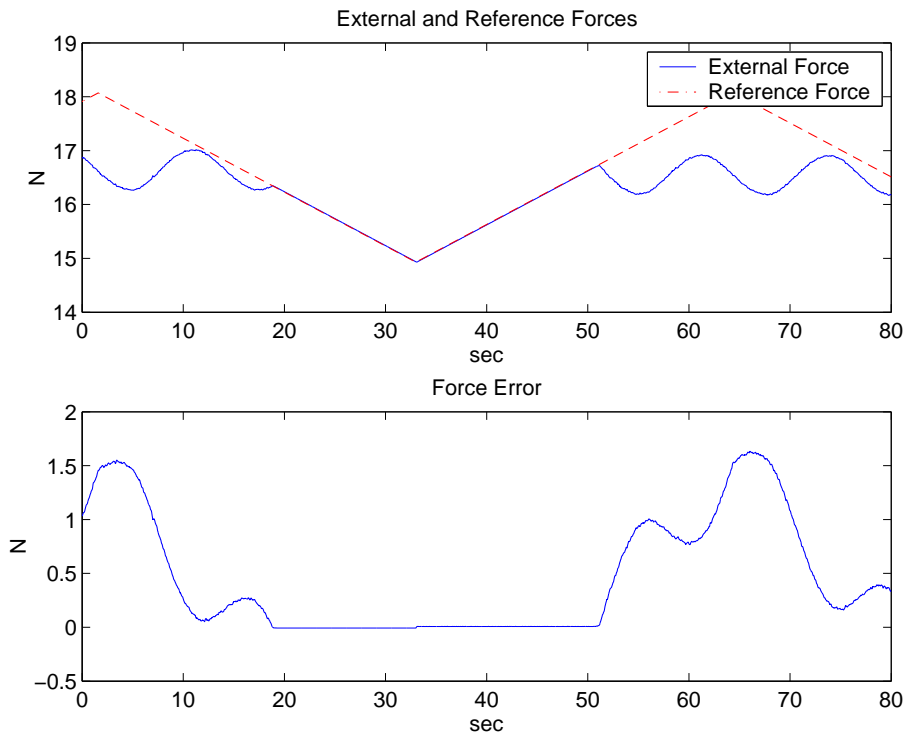


Figure 4.23: PEA - Experiment 3: Measured Force and Force Reference; Force Error Graphs

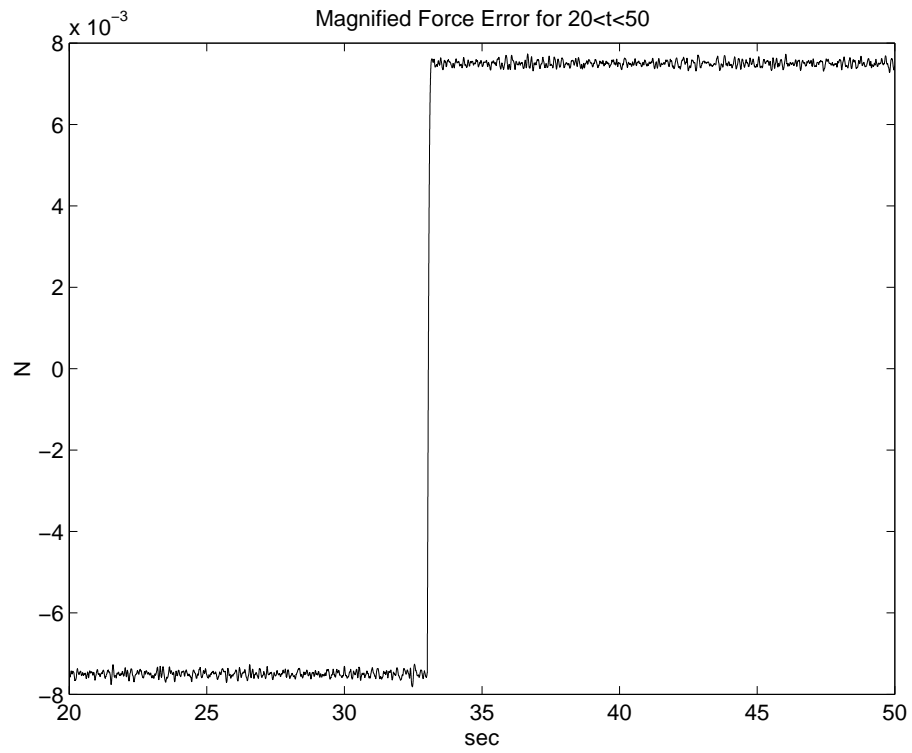


Figure 4.24: PEA - Experiment 3: Magnified Force Error for  $20 < t < 50$

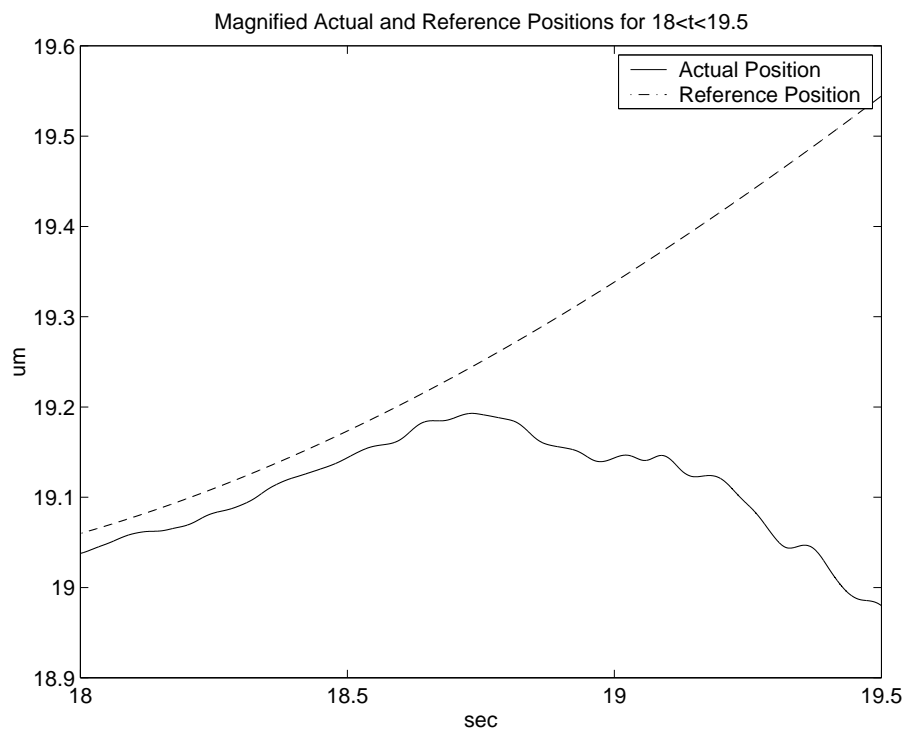


Figure 4.25: PEA - Experiment 3: Magnified Position at the Transition from Position to Force Mode

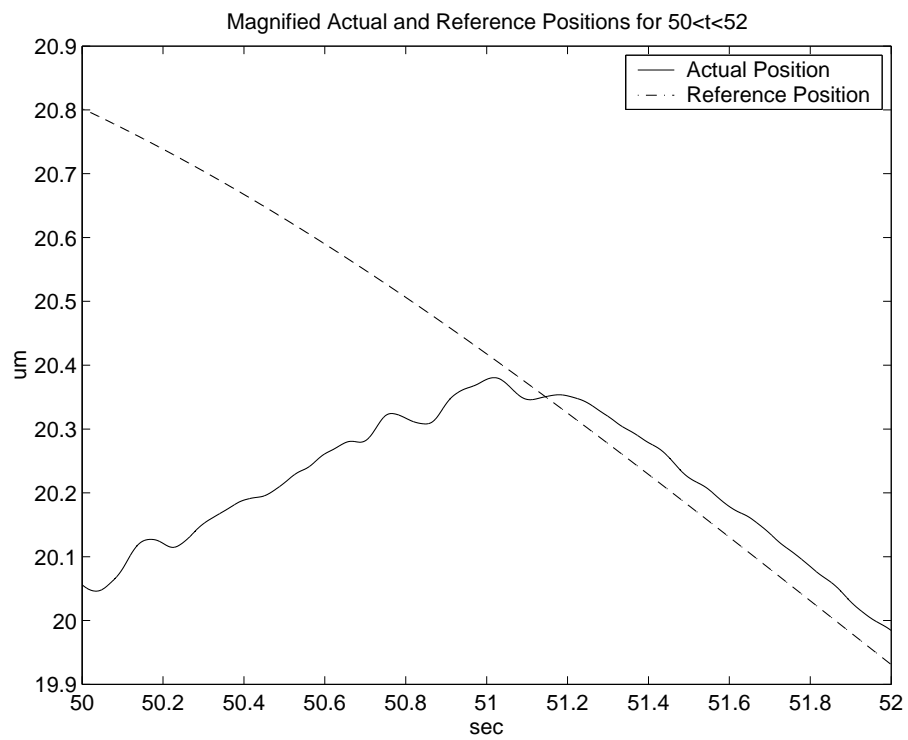


Figure 4.26: PEA - Experiment 3: Magnified Position at the Transition from Force to Position Mode

# Chapter 5

## Bilateral Control

Bilateral control is bi-directional control of force and position between two systems connected by a communication link, as shown in Figure 1.1. Conventionally these (sub)systems constitute the master and slave sides of the overall bilateral action. Master subsystem is the system controlled by the operator to teleoperate the slave system. Therefore, bilateral control is generally used interchangeably with teleoperation. However, this is a bit incomplete since teleoperation is one (large) subset of bilateral control, which may be generalized with a decentralized approach by treating the subsystems as peers and defining bilateral control as a coordination between the peers to perform an actual or virtual task.

The necessity of bilateral control and teleoperation has been discussed with examples in Section 1.2. In this chapter, first, traditional bilateral control will be addressed and an approach will be brought to maximize *transparency* using high precision controllers and methods discussed in Chapter 4, as well as to reduce the dangerous effect of time-delay by means of a reflex mechanism (hybrid force/position controller) discussed in Chapter 5 on the slave subsystem. In section 5.5, the decentralized structure will be further explained. Note that, the necessary conditions for bilateral control remain unchanged between the two approaches and the reason to bring the decentralized approach is the possibility to generalize it for some coordination of more than two systems, sometimes referred to as *multilateral control*.

To realize bilateral control without scaling, the operator on the master side should feel the forces encountered by the slave side, while the slave side should follow the positions of the master side i.e.

$$\mathbf{x}_s = \mathbf{x}_m, \tag{5.1}$$

$$\mathbf{F}_m^{ext} = -\mathbf{F}_s^{ext}. \quad (5.2)$$

Error of force tracking is defined as the sum of two external forces since the external forces encountered by the slave side (the additive inverse of the force slave side exerts on the environment) should be transferred to the operator by the master side. Therefore, if no scaling is present, a perfect bilateral controller could be visualized as a rigid coupling between the two subsystems as shown in Figure 5.1.

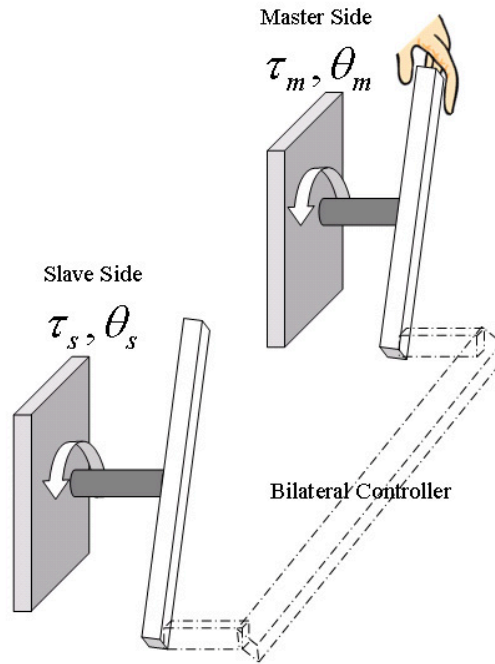


Figure 5.1: Visualisation of Bilateral Control for the 1D Rotational Case

Below, the main issues to be kept in mind for the bilateral controller designation are discussed.

## 5.1 Transparency

Shortly, transparency, as the name implies, is defined as the ability of the bilateral controller to be invisible to the operator. That is, the more accurately the objectives of bilateral action given in (5.1) and (5.2) are realized, the better transparency is achieved. This can be stated more clearly with the impedance point of view, looking at the two-port model of the bilateral controller [23] shown in Figure 5.2. When in contact with the task, the slave velocities  $V_e$  and forces  $F_e$  are dependent, related

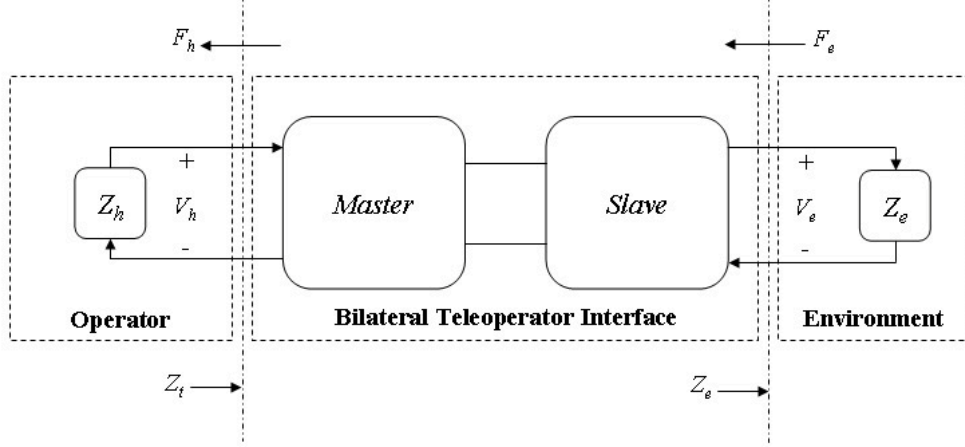


Figure 5.2: General Two-port Model of a Bilateral Teleoperation System

with the slave environment impedance  $Z_e$  such as

$$F_e = Z_e(V_e). \quad (5.3)$$

If the operator should feel as if s/he is directly touching the task, then the operator's force on the master side  $F_h$  and the master's velocity  $V_h$  (which are the forces and velocities of the operator hand, hence the subscript  $h$ ) should have the same values i.e.  $F_h = F_e$ ,  $V_h = V_e$ . This requires that the transmitted impedance to the operator  $Z_t$  such that

$$F_h = Z_t(V_h), \quad (5.4)$$

should be equal to the environmental impedance on the slave side  $Z_e$ .

This result winds the discussion back to the fact that a perfect bilateral controller is a virtual rigid coupling between the two subsystems. The transparency is generally shown with the  $H$  matrices such as

$$\begin{bmatrix} \mathbf{F}_m \\ \dot{\mathbf{p}}_m \end{bmatrix} = \begin{bmatrix} H_{11} & H_{12} \\ H_{21} & H_{22} \end{bmatrix} \begin{bmatrix} \dot{\mathbf{p}}_s \\ \mathbf{F}_s \end{bmatrix}. \quad (5.5)$$

Many works related to bilateral control use the  $H$  matrix representation of transparency to check the amount of transparency achieved with the proposed controller. However, in this work, the perfect transparency condition i.e.

$$H = \begin{bmatrix} 0 & -1 \\ 1 & 0 \end{bmatrix}, \quad (5.6)$$

is used as a means for the derivation of controller, shown in the respective sections.

## 5.2 Time Delay

Since bilateral control maintains a communication link between the two sides, it inherently has an unavoidable time-delay. There are many attempts to resolve the problems time delay brings to the overall structure such as [41–43]. One approach brought in the derivation of bilateral control explained in section 5.4 is to reduce the dangerous effects of time delay for a safe teleoperation with a reflex mechanism (*spinal cord*) on the slave side, which tries to control the external forces, the master side (*brain*) cannot react to in time.

Note that, with this approach, even though time-delay is not compensated with a predictive scheme as some researchers apply [44–46], the most dangerous effect of it is removed, which enables implementations in many fields such as medical robotics to become much safer and applicable.

## 5.3 Scaling

Generally, bilateral control is used for teleoperation on environments not reachable by human beings otherwise as discussed in section 1.2 before. One of these applications is on small scales. Therefore, a general bilateral controller should be able to scale the motions and forces between the two sides for extensive applicability.

With scaling in mind, the objectives of bilateral control are altered a bit such as:

$$\mathbf{x}_s = \alpha \mathbf{x}_m, \quad (5.7)$$

$$\mathbf{F}_m^{ext} = -\beta \mathbf{F}_s^{ext}. \quad (5.8)$$

and the respective  $H$  matrix becomes:

$$H = \begin{bmatrix} 0 & -\beta \\ \alpha & 0 \end{bmatrix}. \quad (5.9)$$

## 5.4 Safe Teleoperation with a Reflex Mechanism on the Slave Side

The conventional approach to bilateral control is the so-called *force-position* architecture shown in Figure 1.2, which essentially decomposes the task into two subtasks such as the slave side is under position control tracking the positions (or states) of

the master side (i.e.  $\mathbf{x}_s^{ref} = \mathbf{x}_m$ ) and similarly master side is under force control tracking the additive inverse of the forces slave side exerts on the environment (i.e.  $\mathbf{F}_m^{ref} = -\mathbf{F}_s^{ext}$ ).

Even though this approach seems to be the most reasonable one, it implicitly assumes no or small time delay for stability and/or for safety of the slave subsystem and its environment, which is as crucial as stability for some applications such as medical robotics. Since the reaction time of the operator on the master side to a motion creating large forces is at least  $2T_d^{min}$  (for  $T_d^{min}$  being the minimum time delay in the communication link), it might be difficult if not impossible to protect the slave system and its environment.

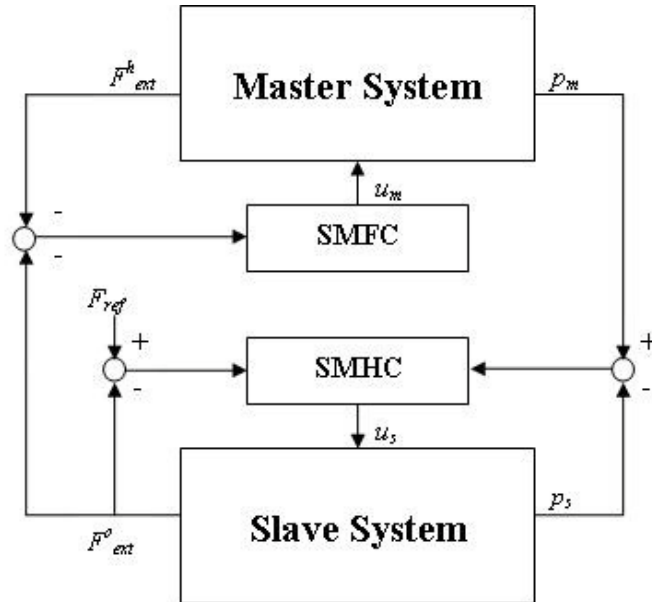


Figure 5.3: Proposed Force-Hybrid Architecture of Bilateral Control

Proposed in this thesis is an approach to add a reflex mechanism on the slave side, which would react directly on location without time delay as the spinal cord does in biological organisms. Note that the operator could be referred to as the *brain* with the same analogy. This reflex mechanism is consisting of the cascaded hybrid force/position controller designed in Chapter 4, which has the ability to control external forces and positions when necessary and could be able to remove the large forces at the first contact with the environment, which is a crucial property for safety since most of the damage occurs in this first blind contact. Furthermore, with the aid of this property a limit value could be defined as the force reference

on the slave side that ensures safe teleoperation in effect. Note that more generally, any force reference could be given to the hybrid controller as shown on experiments in Chapter 4, however for safety, a limit value would often be enough. The block diagram of the proposed *force-hybrid* architecture is given in Figure 5.3.

### 5.4.1 Experimental Results

#### Two Maxon RE-40 DC Motors

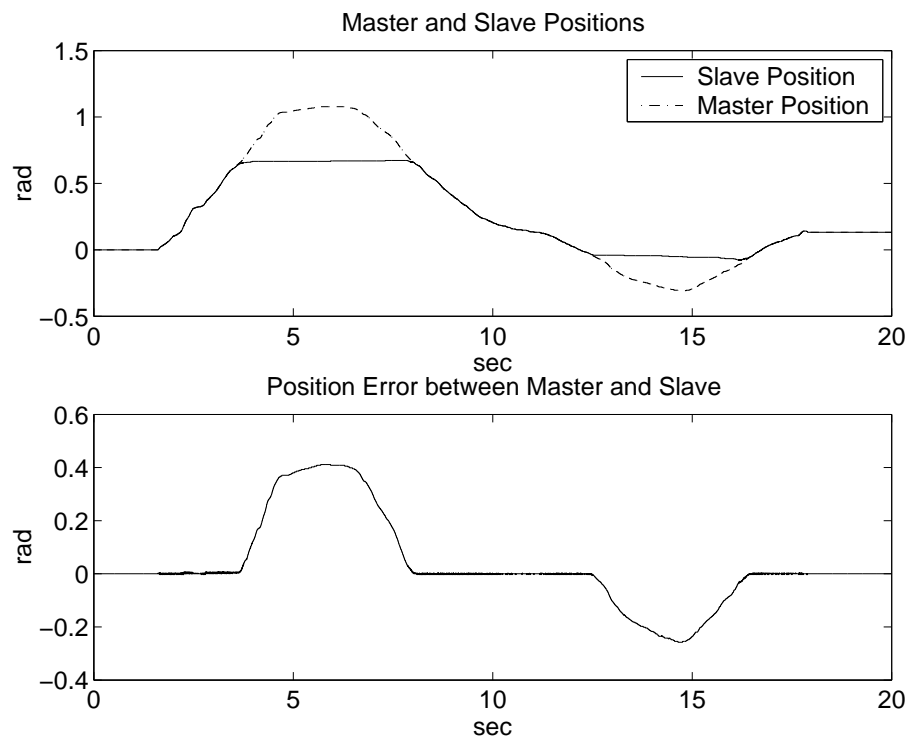


Figure 5.4: Two RE-40's: Master and Slave Positions and Position Error Graphs

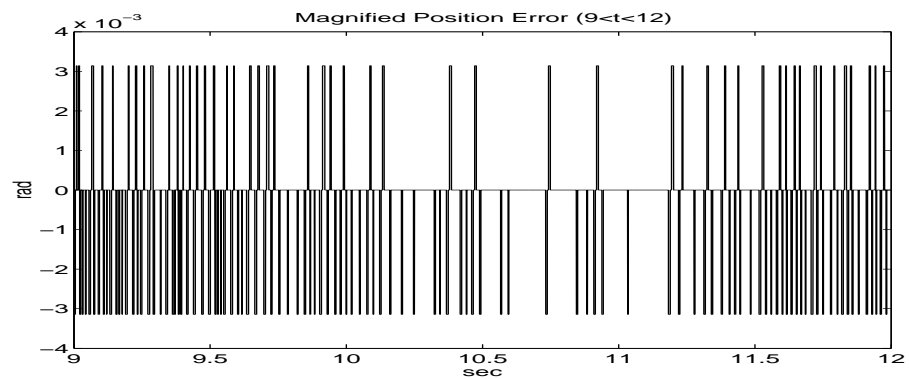


Figure 5.5: Two RE-40's: Magnified Position Error between Master and Slave Sides for  $9 < t < 12$

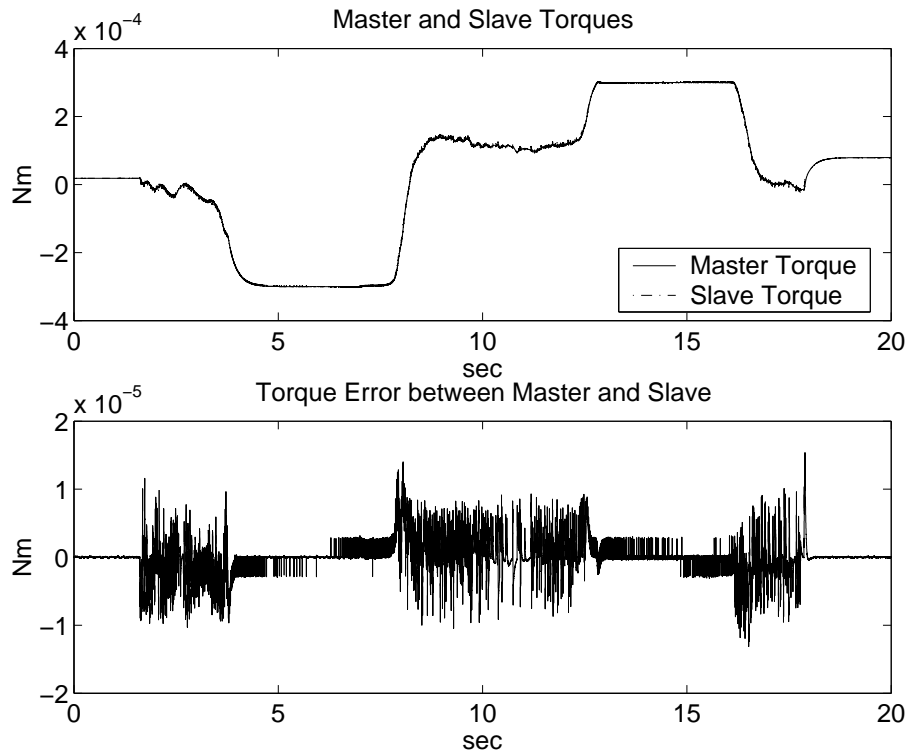


Figure 5.6: Two RE-40's: Master and Slave Torques and Torque Error Graphs

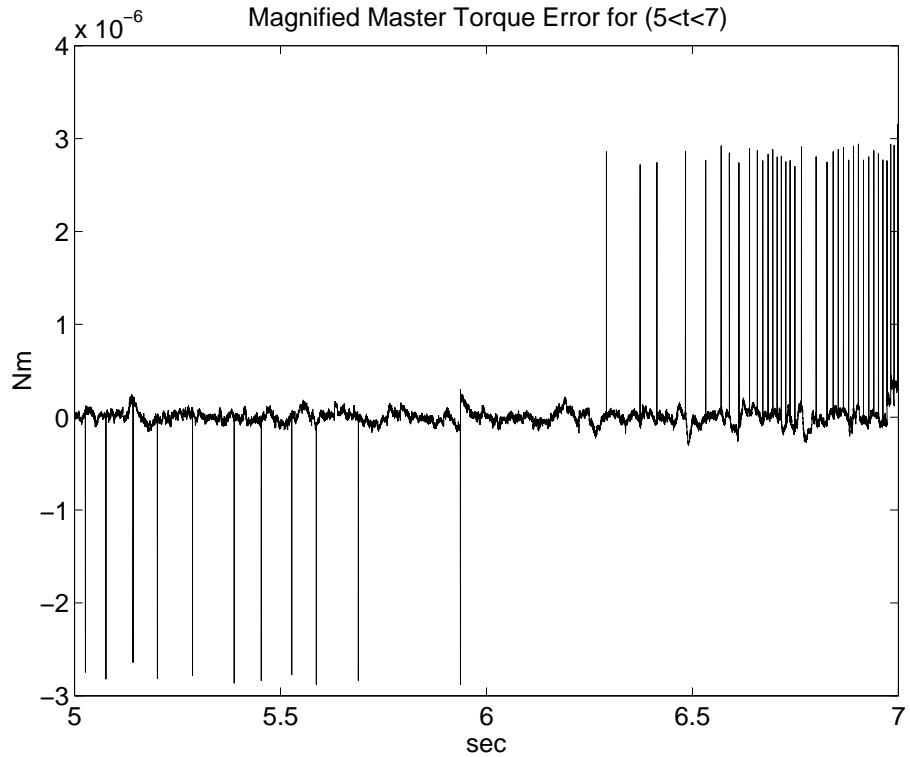


Figure 5.7: Two RE-40's: Magnified Torque Error between Master and Slave Sides for  $5 < t < 7$

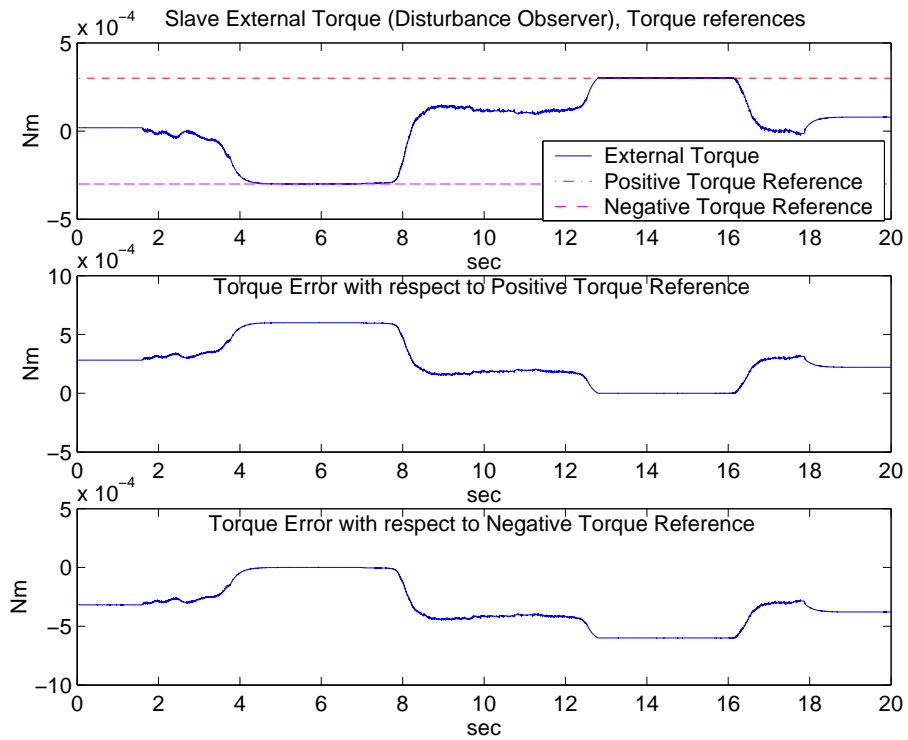


Figure 5.8: Two RE-40's: Hybrid Controller Results on the Slave Side; Slave Torque, Positive and Negative Slave Torque References and Error Graphs with respect to Each Torque Reference

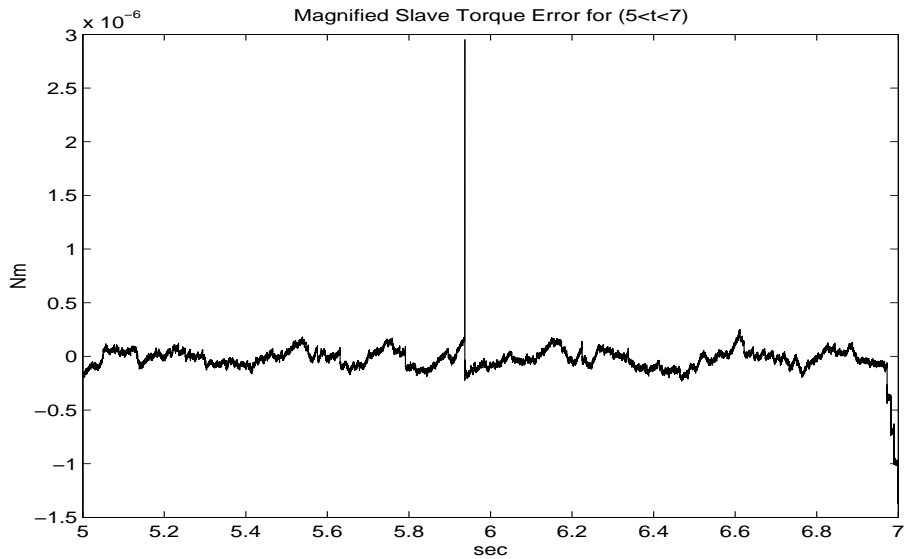


Figure 5.9: Two RE-40's: Magnified Hybrid Torque Error with respect to Negative Torque Reference on the Slave Side for  $5 < t < 7$

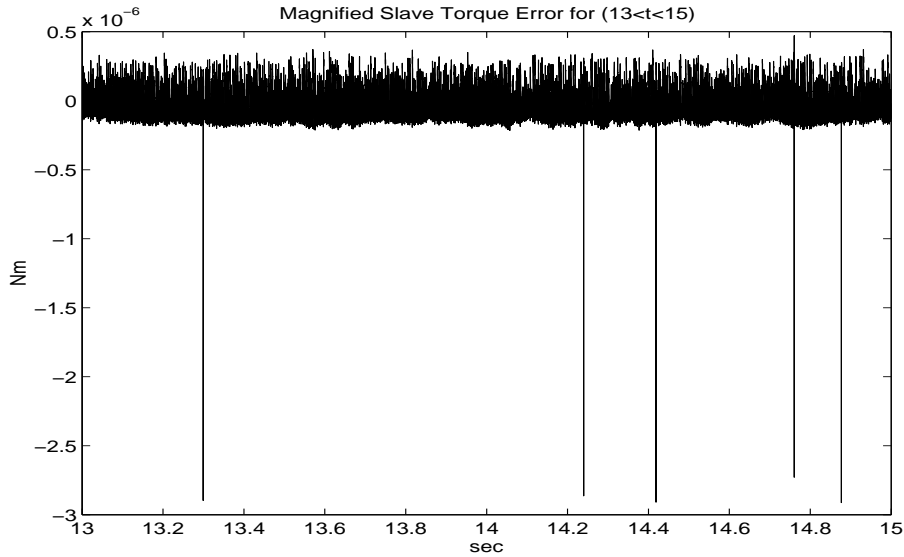


Figure 5.10: Two RE-40's: Magnified Hybrid Torque Error with respect to Positive Torque Reference on the Slave Side for  $13 < t < 15$

### Scaled Teleoperation with a Maxon RE-40 DC Motor as the Master and a Piezoactuator as the Slave

In the first and second experiments, scaling factors of  $\alpha = 1 \times 10^{-3} \frac{\mu\text{m}}{\text{rad}}$  and  $\beta = 1 \times 10^{-4} \frac{\text{Nm}}{\text{N}}$  are used, that is an angular displacement of 1 rad on the master side corresponds to a linear displacement of 1 nm on the slave side and a force of 1 N on the slave side corresponds to a torque of  $1 \times 10^{-4}$ . The objective of these experiments is to provide very fine motion on the slave side for a relatively larger displacement on the master side, hence  $\alpha$  is selected according to this objective. Then the corresponding forces/torques for each amount of displacement were compared for the selection of  $\beta$ , keeping in mind that the DC motor on the master side has low torques as mentioned in Section A.1.

First experiment is for the unconstrained case where force mode of hybrid control on the slave side doesn't interfere and therefore the controller reduces to the simpler force-position architecture mentioned above. The results for position and force tracking are shown in Figures 5.11 and 5.12 respectively.

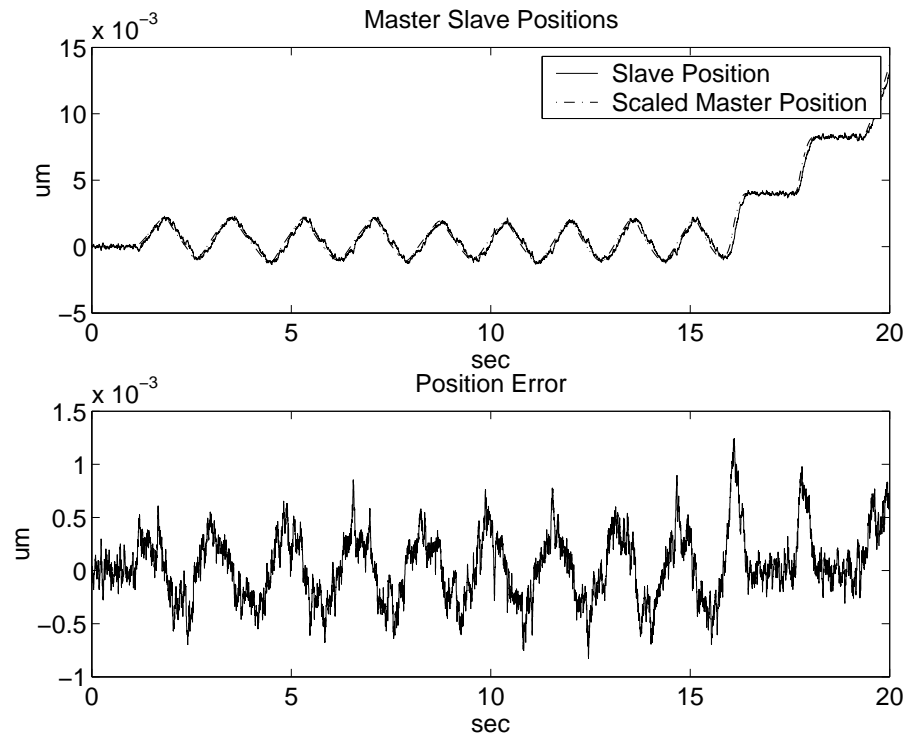


Figure 5.11: Scaled Safe Teleoperation Ex 1: Master (Scaled) and Slave Positions and Position Error Graphs

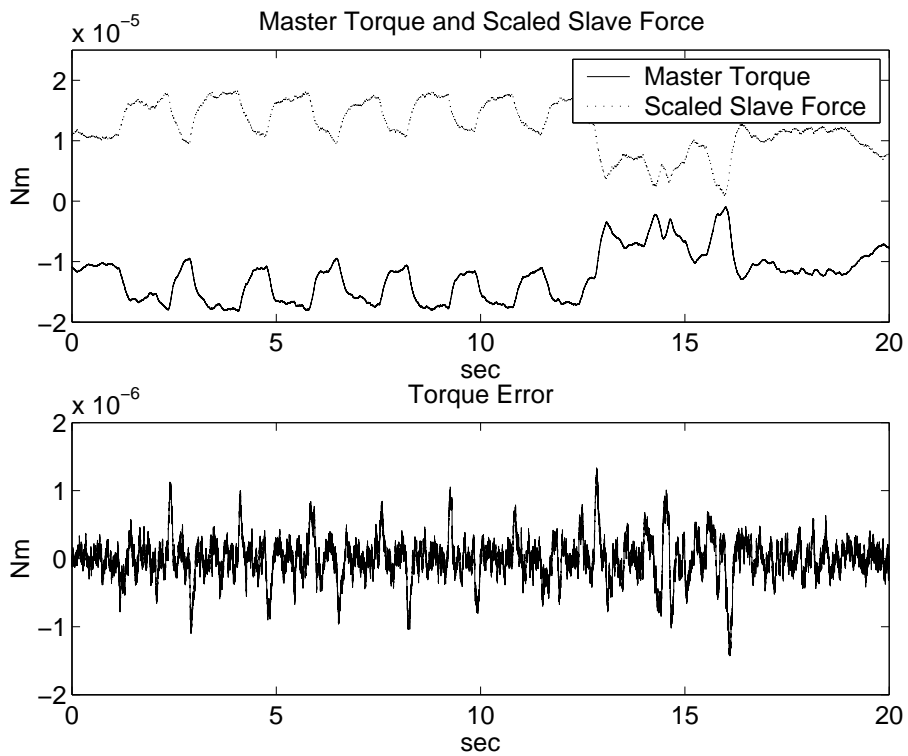


Figure 5.12: Scaled Safe Teleoperation Ex 1: Master and Slave (Scaled) External Torques and Torque Error Graphs

Second experiment is for demonstration of the effect of hybrid control. Note that, large position errors occur in this experiment due to two reasons. First, the motor on the master side has low torques such that the operator could easily overcome and move further. Second, and more importantly, when the external force curve touches the reference force curve on the slave side, hybrid controller switches to force mode and tries to track the force reference as long as position reference implies larger external forces. This second effect is the main reason the proposed controller could be used as a safety mechanism for the slave side. That is, even for larger motors with higher torques, if the scaling factors are designed such that the scaled torques on the master side are not higher than the operator can handle and force reference on the slave side is given such that the task could be accomplished while no dangerous force is exerted on the environment, both the slave subsystem, its environment and the operator are protected from large external forces. The results for position and force tracking are shown in Figures 5.13 and 5.14 respectively and the results for the force control of SMHC on the slave side is shown in Figure 5.15.

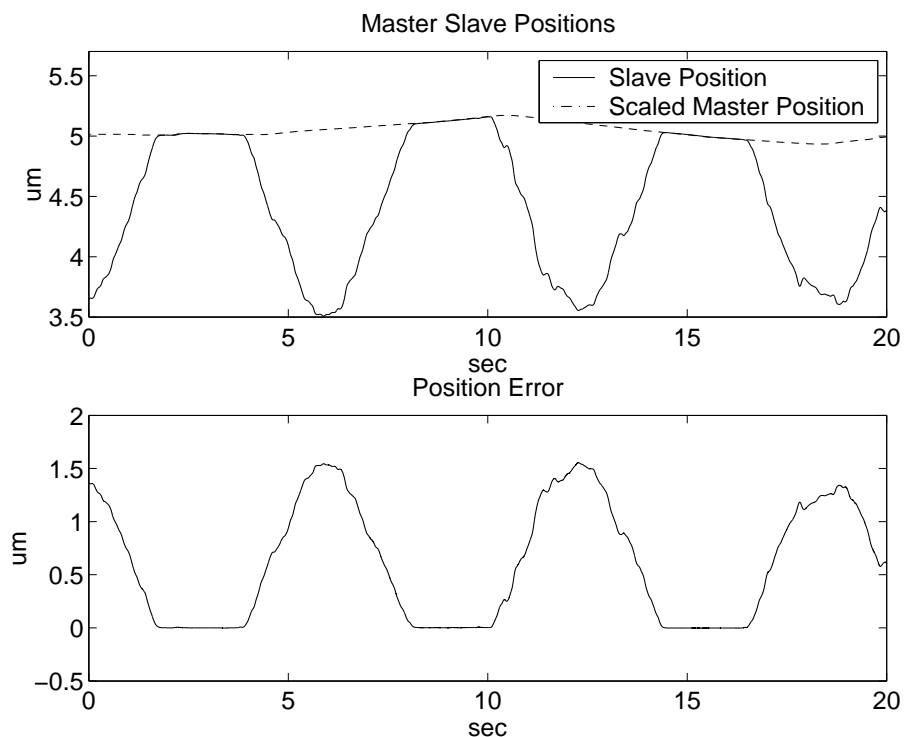


Figure 5.13: Scaled Safe Teleoperation Ex 2: Master (Scaled) and Slave Positions and Position Error Graphs

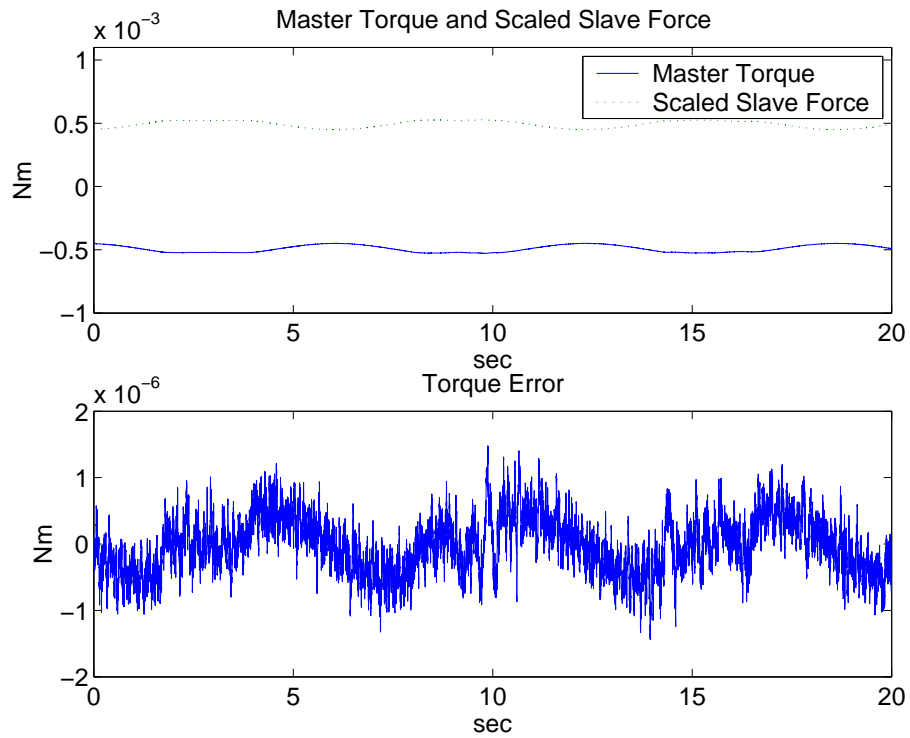


Figure 5.14: Scaled Safe Teleoperation Ex 2: Master and Slave (Scaled) External Torques and Torque Error Graphs

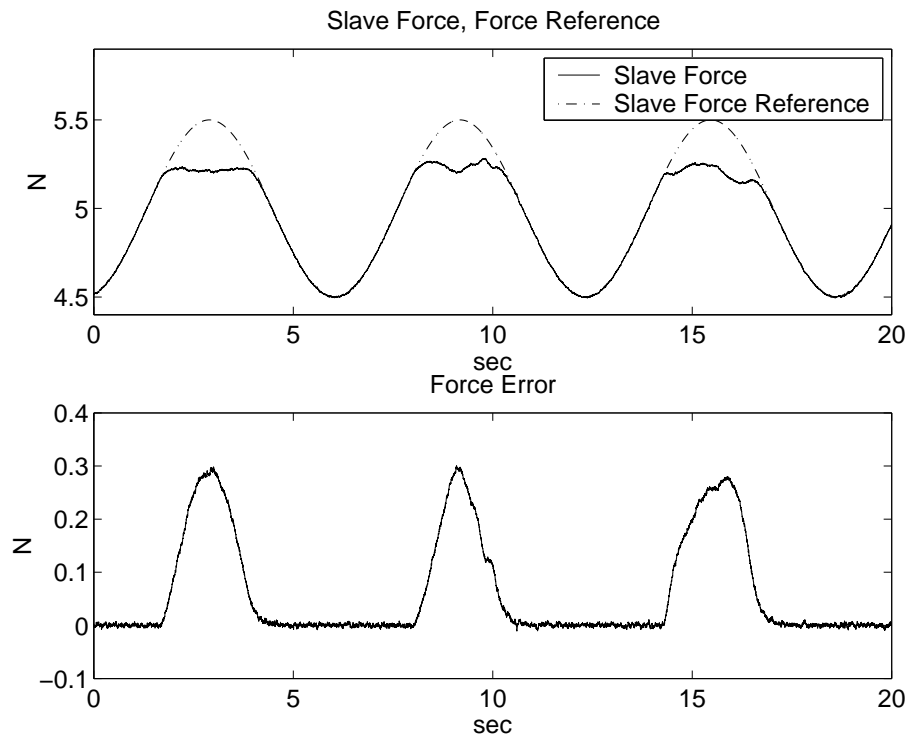


Figure 5.15: Scaled Safe Teleoperation Ex 2: Slave External Force, Hybrid Force Reference and Hybrid Force Error Graphs

## 5.5 Decentralized Bilateral Control

Considering the general vector plant model in (3.3) and environment model in (3.6) for fully actuated  $l$  dimensional (i.e.  $m = l$ ) electromechanical master and slave systems affine with respect to control, denoted as subscripts  $m$  and  $s$  respectively as follows,

$$\dot{\mathbf{x}}_m = F_m(\mathbf{x}_m, t) + B_m \mathbf{u}_m, \quad (5.10)$$

$$\dot{\mathbf{x}}_s = F_s(\mathbf{x}_s, t) + B_s \mathbf{u}_s. \quad (5.11)$$

Writing the unified overall plant consisting of the master and slave sides together in one vector equation would let one to treat the two subsystems as ‘peers’ (i.e. interchangeable master and slave sides) as:

$$\dot{\mathbf{x}} = F(\mathbf{x}, t) + B\mathbf{u}, \quad (5.12)$$

if a general state vector  $\mathbf{x} \in \mathfrak{R}^{2n}$  and the general control input  $\mathbf{u} \in \mathfrak{R}^{2m}$  are defined as  $\mathbf{x} = [\mathbf{x}_m \ \mathbf{x}_s]^T$  and  $\mathbf{u} = [\mathbf{u}_m \ \mathbf{u}_s]^T$  respectively for

$$F = [F_m \ F_s]^T \quad (5.13)$$

$$B = \begin{bmatrix} B_m & 0 \\ 0 & B_s \end{bmatrix} \quad (5.14)$$

if  $F \in \mathfrak{R}^{2n}$  and  $B \in \mathfrak{R}^{2n \times 2m}$ .

The requirements for bilateral action can be expressed as  $\mathbf{x}_s - \alpha \mathbf{x}_m = 0$  for position tracking and  $\mathbf{F}_m^{ext} + \beta \mathbf{F}_s^{ext} = 0$  for force tracking where  $\alpha$  and  $\beta$  are the scaling coefficients among actuators. Defining the errors,  $\mathbf{e}_x \in \mathfrak{R}^{2n}$  and  $\mathbf{e}_f \in \mathfrak{R}^{2l}$ , from the desired behaviour as

$$\mathbf{e}_x = \mathbf{x}_s - \alpha \mathbf{x}_m, \quad (5.15)$$

$$\mathbf{e}_f = \mathbf{F}_m^{ext} + \beta \mathbf{F}_s^{ext} \quad (5.16)$$

both systems can contribute to the task requirements using two virtual plants (“functions”) with a transformation from plant space to the “function” space as shown in [47] and in Fig 5.16, whose positions and external forces are essentially regulated. The derivation of the virtual plants are explained in the following sections.

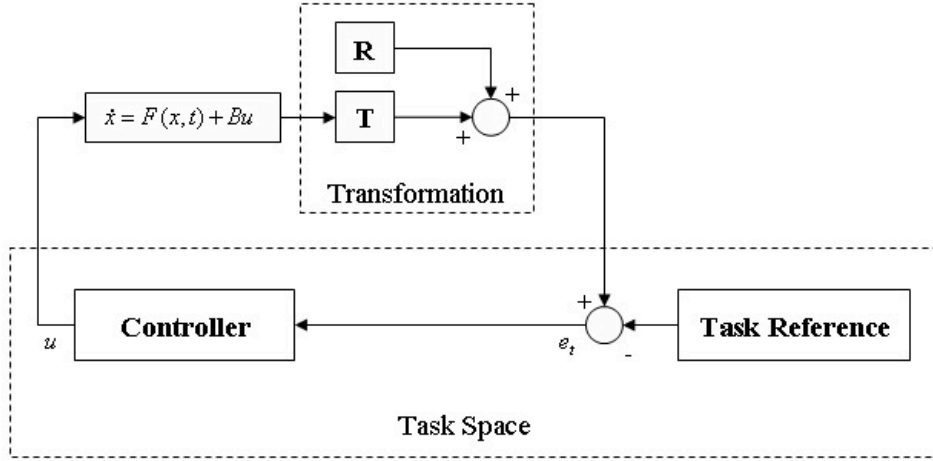


Figure 5.16: The general structure of Task Based Control with a Transformation to Task Space

### 5.5.1 Virtual Plant for Position Tracking

Defining the position tracking task function as

$$\sigma_x = G_x \mathbf{e}_x \quad (5.17)$$

for  $\sigma_x \in \mathfrak{R}^m$  and  $G_x \in \mathfrak{R}^{m \times 2n}$ , which realizes tracking of states between the two ‘peers’ of bilateral action on the sliding manifold  $\sigma_x = 0$  for  $G_x$  being a positive definite matrix in the form

$$G_x = K_x \begin{bmatrix} C_x & 1 \end{bmatrix} \quad (5.18)$$

for  $l = 1$ ,  $K_x$  and  $C_x \in \mathfrak{R}^+$ .

Inserting (5.15) into (5.17), the derivative of the position tracking task function could be expressed as

$$\dot{\sigma}_x = G_x \dot{\mathbf{x}}_s - \alpha G_x \dot{\mathbf{x}}_m. \quad (5.19)$$

If a state vector  $\mathbf{x} \in \mathfrak{R}^{2n}$  is defined as  $\mathbf{x} = [ \mathbf{x}_m \quad \mathbf{x}_s ]^T$ , then a transformation matrix  $T_x \in \mathfrak{R}^{m \times 2n}$  could be designated such as

$$T_x = \begin{bmatrix} -\alpha G_x & G_x \end{bmatrix} \quad (5.20)$$

which becomes

$$T_x = \begin{bmatrix} -\alpha K_x C_x & -\alpha K_x & K_x C_x & K_x \end{bmatrix} \quad (5.21)$$

for  $l = 1$ . Then the position tracking task function derivative can be restated as

$$\dot{\sigma}_x = T_x \dot{\mathbf{x}}. \quad (5.22)$$

Putting (5.12) into (5.22) the task function dynamics is written as:

$$\dot{\sigma}_x = T_x F(\mathbf{x}_m, \mathbf{x}_s, t) + T_x B(\mathbf{x}_m, \mathbf{x}_s, t) \mathbf{u} \quad (5.23)$$

yielding

$$\dot{\sigma}_x = F_x(\mathbf{x}_m, \mathbf{x}_s, t) + B_x(\mathbf{x}_m, \mathbf{x}_s, t) \mathbf{u}. \quad (5.24)$$

for  $F_x = T_x F$  and  $B_x = T_x B$ , with  $F_x \in \mathfrak{R}^m$  and  $B_x \in \mathfrak{R}^{m \times 2m}$ . Note that the final virtual plant whose output is to be regulated, which has two control inputs, has the same structure as (3.3).

### 5.5.2 Virtual Plant for Force Tracking

Selecting the force tracking task function as

$$\sigma_f = \mathbf{e}_f, \quad (5.25)$$

from (5.16), its derivative is

$$\dot{\sigma}_f = \mathbf{F}_m^{\dot{ext}} + \beta \mathbf{F}_s^{\dot{ext}}. \quad (5.26)$$

Putting (3.6) into (5.26)

$$\dot{\sigma}_f = A_m^{ext}(\dot{\mathbf{x}}_m - \dot{\mathbf{x}}_m^{env}) + \beta A_s^{ext}(\dot{\mathbf{x}}_s - \dot{\mathbf{x}}_s^{env}). \quad (5.27)$$

Defining a transformation matrix  $T_f \in \mathfrak{R}^{m \times 2n}$  as

$$T_f = \begin{bmatrix} A_m^{ext} & \beta A_s^{ext} \end{bmatrix} \quad (5.28)$$

which becomes

$$T_f = \begin{bmatrix} K_m^{ext} & b_m^{ext} & \beta K_s^{ext} & \beta b_s^{ext} \end{bmatrix} \quad (5.29)$$

for  $l = 1$ , external force error derivative can be restated as

$$\dot{\sigma}_f = T_f F(\mathbf{x}_m, \mathbf{x}_s, t) + T_f B(\mathbf{x}_m, \mathbf{x}_s, t) \mathbf{u} - T_f \dot{\mathbf{x}}^{env} \quad (5.30)$$

with the integration of (3.3), for  $\mathbf{x}^{env} = [ \mathbf{x}_m^{env} \quad \mathbf{x}_s^{env} ]^T$ ,  $\mathbf{x}^{env} \in \mathfrak{R}^{2n}$  yielding

$$\dot{\sigma}_f = F_f(\mathbf{x}_m, \mathbf{x}_m^{env}, \mathbf{x}_s, \mathbf{x}_s^{env}, t) + B_f(\mathbf{x}_m, \mathbf{x}_s, t) \mathbf{u}, \quad F_f \in \mathfrak{R}^m, B_f \in \mathfrak{R}^{m \times 2m}. \quad (5.31)$$

for  $F_f = T_f F + R_f$ ,  $R_f = -T_f \dot{\mathbf{x}}^{env}$  and  $B_f = T_f B$ . Note that the final virtual plant whose output is to be regulated, which has two control inputs, has the same structure as (3.3).

### 5.5.3 Task-Based Bilateral Control

Since a transformation scheme for the two tasks of bilateral control has been devised in sections 5.5.1 and 5.5.2, in this section a unification of the transformation from plant space to task (“function”) space of bilateral action will be explained. A graphical representation of this discussion is shown in Fig 5.17.

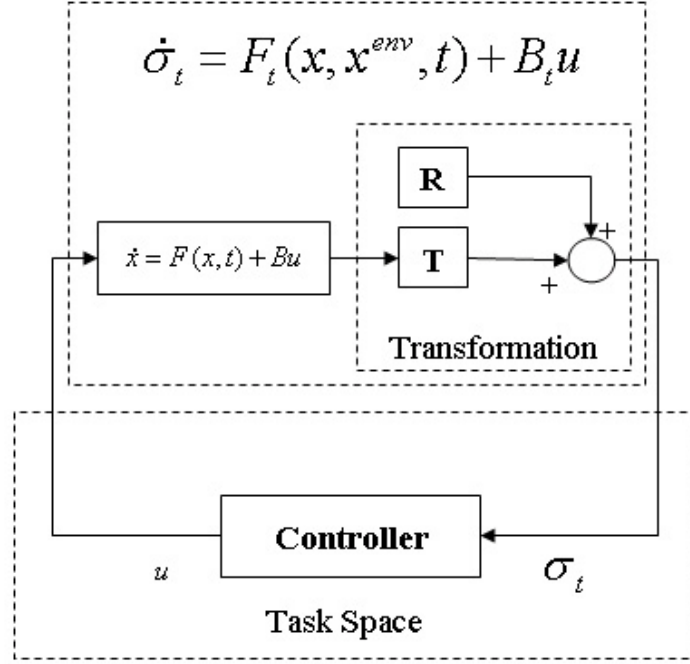


Figure 5.17: Task Based Bilateral Control

Note that, the amount of tasks a system can handle without problem is equal to the amount of control inputs to the plant, which is equal to  $2m$  according to (5.12). Therefore a unification of  $l = m$  position tracking and  $l = m$  force tracking tasks could be possible.

If

$$T = \begin{bmatrix} T_x \\ T_f \end{bmatrix}, R = \begin{bmatrix} R_x \\ R_f \end{bmatrix} \text{ and } \sigma_t = \begin{bmatrix} \sigma_x \\ \sigma_f \end{bmatrix}$$

are defined as the general Transformation Matrix  $T \in \mathfrak{R}^{2m \times 2n}$ , translation matrix  $R \in \mathfrak{R}^{2m}$  and task error  $\sigma_t \in \mathfrak{R}^{2m}$  respectively, note that  $R_x = \mathbf{0}$  for position tracking task, then the transformation from plant space to the task space is defined as

$$\dot{\sigma}_t = TF(\mathbf{x}_m, \mathbf{x}_s, t) + TB(\mathbf{x}_m, \mathbf{x}_s, t)\mathbf{u} + R \quad (5.32)$$

according to the generalized plant equation in (5.12). Defining

$$F_t = TF + R \quad (5.33)$$

and

$$B_t = TB, \quad (5.34)$$

for  $F_t \in \mathfrak{R}^{2m}$  and  $B_t \in \mathfrak{R}^{2m \times 2m}$  the unified bilateral task error dynamics could be written as

$$\dot{\sigma}_t = F_t(\mathbf{x}, \mathbf{x}^{env}, t) + B_t(\mathbf{x}, t)\mathbf{u} \quad (5.35)$$

and the controller could be designed in the same way as for the general fully actuated systems described as (3.3). Next, an iterative sliding mode controller will be derived for this plant in task space.

#### 5.5.4 Sliding Mode Controller Derivation for Task Based Bilateral Control

The transformation to task space enables one to write the most general dynamical relationship between the two control inputs  $\mathbf{u}_m, \mathbf{u}_s$  and the task error functions  $\sigma_x, \sigma_f$  in the combined system (5.35). Therefore, realizing bilateral control means to regulate  $\sigma_t$  with  $\mathbf{u}$ .

For stability, a non-negative Lyapunov Function is typically selected as

$$\nu_t = \frac{\sigma_t^T \sigma_t}{2}, \quad (5.36)$$

whose derivative is nothing but

$$\dot{\nu}_t = \sigma_t^T \dot{\sigma}_t. \quad (5.37)$$

If the sliding manifold is chosen to be

$$\dot{\sigma}_t + D_t \sigma_t = 0 \quad (5.38)$$

stability is ensured on this sliding manifold for positive definite  $D_t \in R^{2m \times 2m}$  yielding the Lyapunov Function derivative

$$\dot{\nu}_t = -\sigma_t^T D_t \sigma_t, \quad (5.39)$$

which is non-positive. As equivalent control  $\mathbf{u}_{eq}$  is defined as the amount of control input  $\mathbf{u}$  that enforces the system to remain on the manifold, (5.35) can be restated with the inclusion of  $\mathbf{u}_{eq}$  as,

$$\dot{\sigma}_t = B_t(\mathbf{x}, t)(-\mathbf{u}_{eq} + \mathbf{u}). \quad (5.40)$$

Solving for  $\mathbf{u}_{eq}$  in (5.40) reveals

$$\mathbf{u}_{eq} = \mathbf{u} - B_t^{-1}\dot{\sigma}_t. \quad (5.41)$$

if  $B_t^{-1}$  exists. For the sliding manifold to be reached and motion on it to be maintained, one has to calculate the necessary control input  $\mathbf{u}$  according to (5.38). When (5.40) is placed in (5.38) to solve for  $\mathbf{u}$

$$B_t(\mathbf{x}, t)(-\mathbf{u}_{eq}(t) + \mathbf{u}(t)) + D_t\sigma_t = 0, \quad (5.42)$$

the only unknown is  $\mathbf{u}_{eq}(t)$ . However, since  $\mathbf{u}_{eq}(t)$  is a continuous and bounded function, it can be considered almost constant for the sample time, making it possible to use the equivalent control of the previous time step, namely,  $\mathbf{u}_{eq}(t - \Delta t)$  calculated according to (5.41). Putting  $\mathbf{u}_{eq}(t - \Delta t)$  for  $\mathbf{u}_{eq}(t)$  and solving for  $\mathbf{u}$  yields the iterative controller as

$$\mathbf{u}(t) = \mathbf{u}(t - \Delta t) - B_t^{-1}(\dot{\sigma}_t + D_t\sigma_t). \quad (5.43)$$

for  $rank(B_t) = 2m$ .

### 5.5.5 Experimental Results

#### Two Maxon RE-40 DC Motors

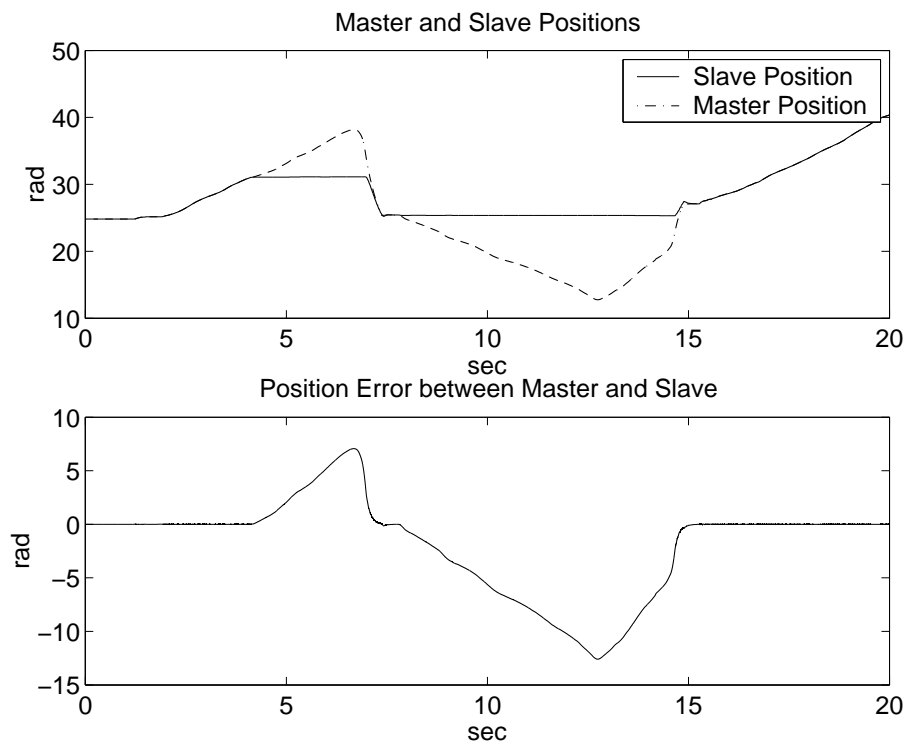


Figure 5.18: Task Based Bilateral Control Ex 1 (Two RE-40's): Master and Slave Positions and Position Error Graphs

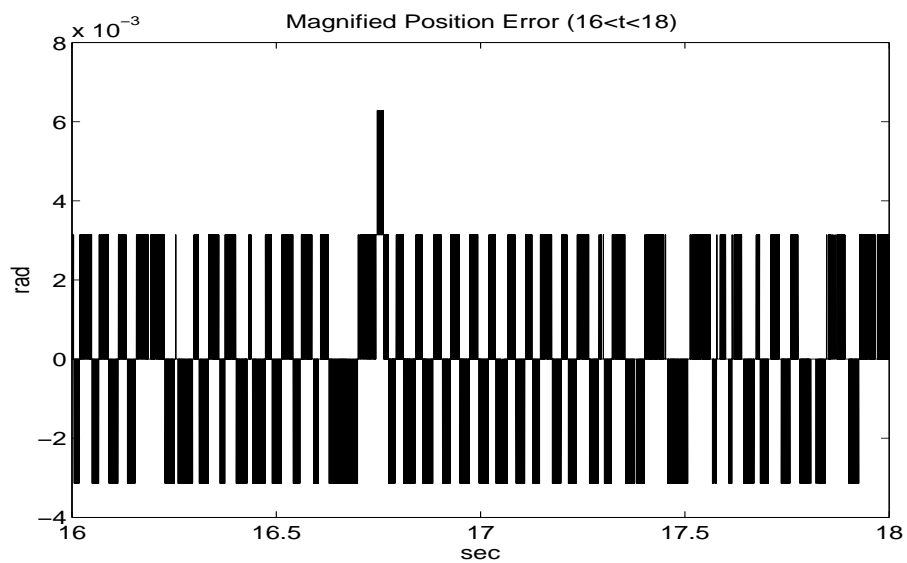


Figure 5.19: Task Based Bilateral Control Ex 1 (Two RE-40's): Magnified Position Error between Master and Slave Sides for  $16 < t < 18$

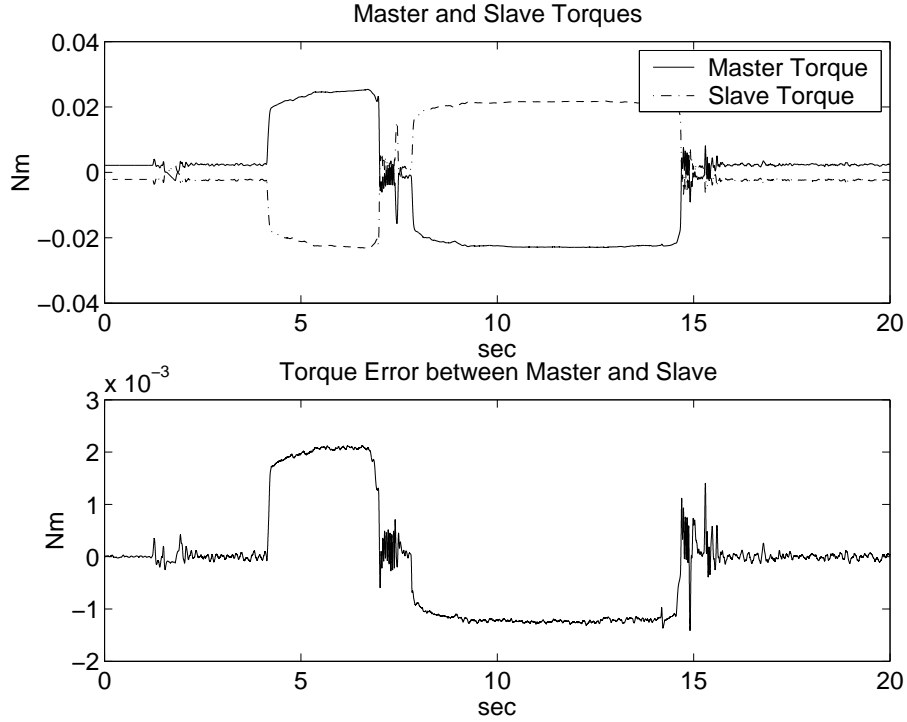


Figure 5.20: Task Based Bilateral Control Ex 1 (Two RE-40's): Master and Slave Torques and Torque Error Graphs

### Scaled Teleoperation with a Maxon RE-40 DC Motor as the Master and a Piezoactuator as the Slave

In this experiment, scaling factors of  $\alpha = 1 \times 10^{-2} \frac{\mu\text{m}}{\text{rad}}$  and  $\beta = 1 \times 10^{-3} \frac{\text{Nm}}{\text{N}}$  are used, that is an angular displacement of 1 rad on the master side corresponds to a linear displacement of 10 nm on the slave side and a force of 1 N on the slave side corresponds to a torque of  $1 \times 10^{-3}$ . The objective of this experiment is to provide fine motion on the slave side for a relatively larger displacement on the master side, hence  $\alpha$  is selected according to this objective. Then the corresponding forces/torques for each amount of displacement were compared for the selection of  $\beta$ , keeping in mind that the DC motor on the master side has low torques as mentioned in Section A.1.

The obstacle is not stationary in this experiment, in fact it hits the PEA at  $t = 22$  and moves back at  $t = 48$ . Therefore, the capabilities of task based bilateral control to reflect sudden external forces to the operator are demonstrated. The results for position and force tracking are shown in Figures 5.21 and 5.22 respectively.

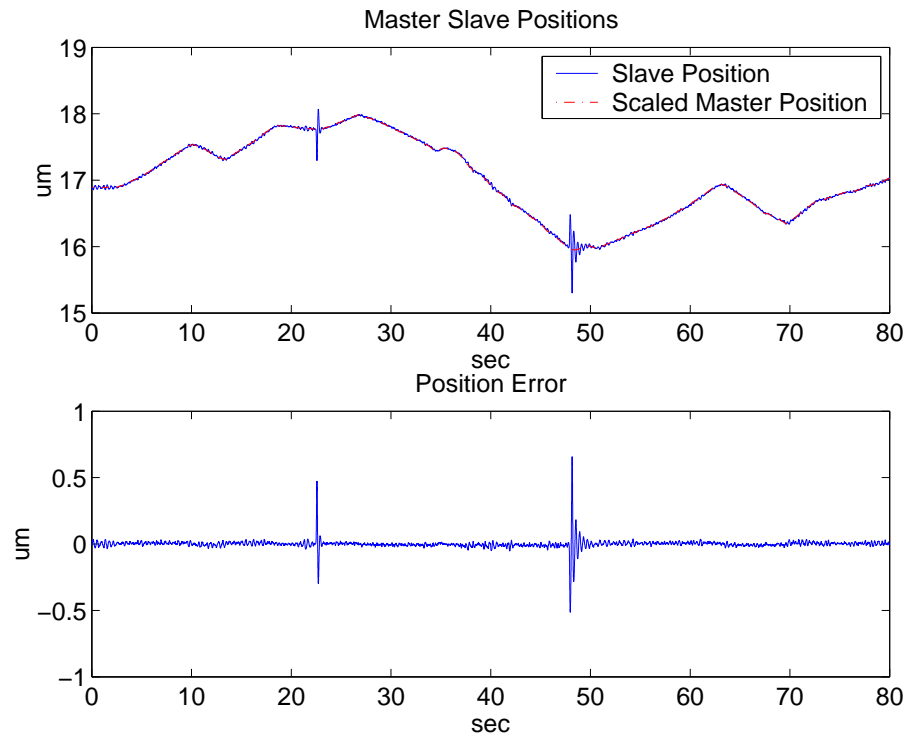


Figure 5.21: Task Based Bilateral Control Ex 2 (Scaled): Master (Scaled) and Slave Positions and Position Error Graphs

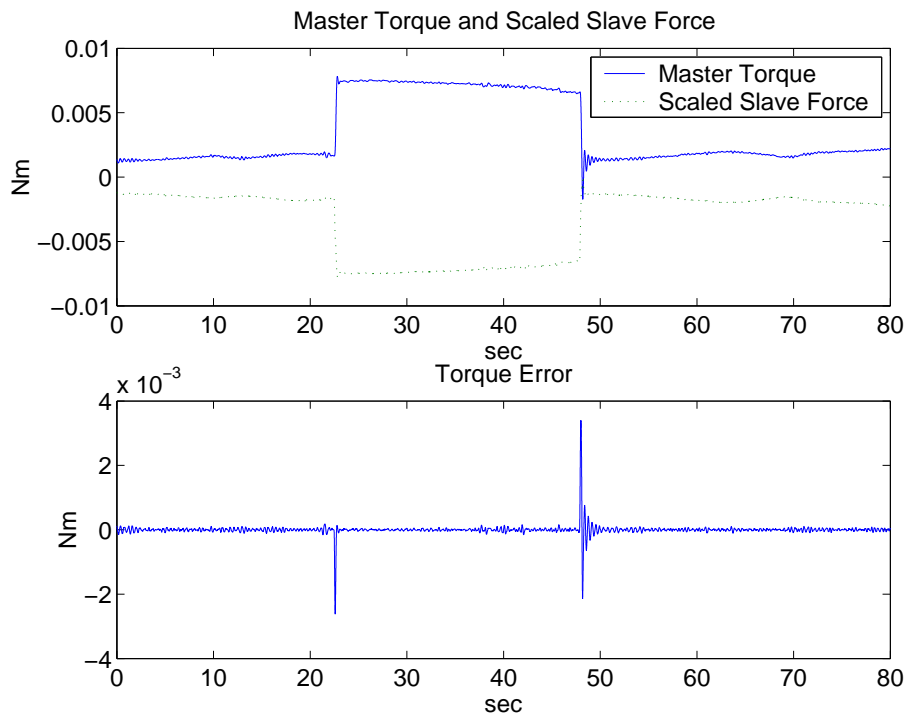


Figure 5.22: Task Based Bilateral Control Ex 2 (Scaled): Master and Slave (Scaled) Torques and Torque Error Graphs

## Chapter 6

### Conclusions

In this thesis, bilateral control has been addressed with two main approaches. In both approaches, discrete time sliding mode controllers were used to achieve high transparency since these controllers are invariant to nonlinearities and hence offer high precision in force and position tracking. The plants considered for the master and slave sides are taken to be fully actuated electromechanical systems affine with respect to control. For simplicity, experiments are held on 1D actuators (SISO systems) to demonstrate the practical application of the theories.

First approach proposes a force-hybrid structure for master-slave sides of the controller. The hybrid force/position controller on the slave side is handled by a novel cascaded sliding mode hybrid force/position controller. The controller designed with this approach has achieved high transparency. Scaling is also possible with the approach. Also, the external forces could be controlled, which means that slave side is able to protect itself from large external forces, which otherwise may not be reacted in time by the operator, due to possible time delay. Therefore, this approach provides a safety mechanism, which could be extended to applications on medical applications such as teleoperated minimally invasive surgery.

Second approach focuses on the tasks instead of plants to result in a decentralized structure. With this approach, the controllers are designed to regulate a sliding mode variable that defines the task at hand. As shown in respective sections, task variables of bilateral control are essentially linear transformations from plant space to task space. High transparency has been achieved and scaling is possible with this approach, too. The important property of the approach is that it can be generalized to a coordination or cooperation scheme of more than two systems, which then

could be referred to as multilateral control. A typical example is the coordination of mobile robots.

In addition to the bilateral control problem, some solutions were achieved for other problems. For instance, since the slave subsystem is run by a hybrid controller, a cascaded hybrid controller was designed. Some other problems arose on applications, such as the hysteresis nonlinearity of PEA or the different control input needs of Maxon DC Motor for small and large errors for best tracking performance. The first problem was solved by a sliding mode model reference controller, that essentially linearizes the system to a desired model by taking all the differences of actual plant from the desired model as disturbances and adding a compensation to the control input for them. The solution to second problem was handled in terms of a simple adaptation mechanism that changes the slope (gain) of sliding manifold for each dimension according to the error (hence, small control input for small errors and large control input for large errors has been obtained).

The work could be extended to teleoperation of robotic manipulators from a distance. Micromanipulation and nanomanipulation could be realized by human operators with the aid of the two approaches to bilateral control, proposed in this thesis.

## Appendix A

### Experimental Setup

#### A.1 Maxon RE-40 DC Motor

RE-40 DC motors produced by Maxon have 150 Watts assigned power rating with nominal parameters shown in Table A.1. These motors are known to have little torque as opposed to being able to reach high velocities. Therefore, using them for bilateral, hybrid and force control realization would be a challenge. ADS\_E 50/10 drivers and incremental encoders with 500 ticks per revolution, yielding a precision of  $\frac{2\pi}{2000} = 0.0031416$  rad for positioning are used with the motors. The controllers are implemented using a dSpace DS1103 board with a step time of 0.1 msec. The experimental setup structure is shown in Figure A.1.

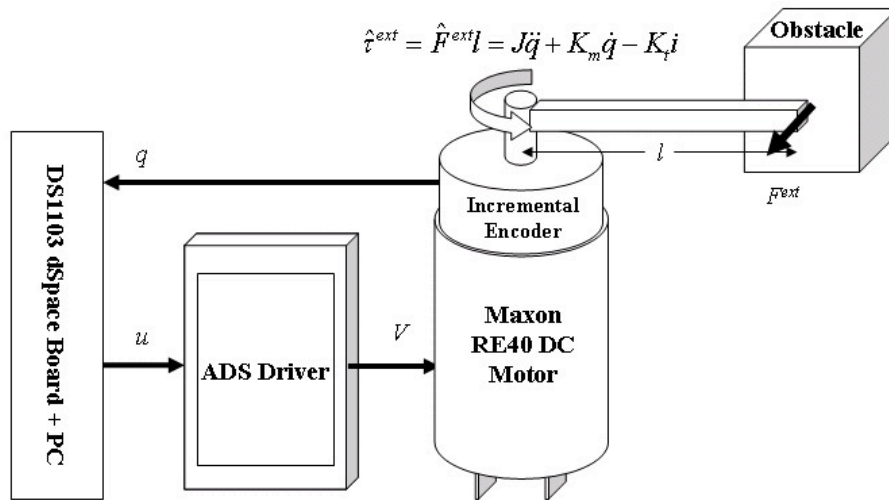


Figure A.1: Structure of the Maxon RE-40 Setup

The general model for the DC motors can be written as

$$J\ddot{q} + K_m\dot{q} = K_t i + \tau_{ext}. \quad (\text{A.1.1})$$

Parameter	Value
Assigned Power Rating	150 W
Rotor Inertia ( $J$ )	135.1 gcm <sup>2</sup>
Torque Constant ( $K_t$ )	16.45 mNm/A
Dynamical Friction Torque ( $K_m$ )	$2.7 \times 10^{-4}$ mNm/rpm
Max Continuous Torque	98.687 mNm

Table A.1: Maxon RE-40 DC Motor Parameters

Here,  $J$ ,  $K_m$  and  $K_t$  are the nominal values of the inertia, mechanical friction and torque coefficients of the motor shown in Table A.1 and  $i$  is the current or control input to the plant.  $q$  is the angle in radians and  $\tau_{ext}$  is the external torque applied to the motor shaft by the environment (i.e. obstacle, operator hand, etc.).

## A.2 Piezomechanik PSt150/5/60 Piezoelectric actuator

Micromanipulator applications require control actuators that can provide accurate position tracking performance in addition to robustly stable force control. These objectives are significantly compromised by the presence of backlash and Coulomb friction in the control plant, the effects of which are exaggerated in small scales. Since PZT stack actuators are monolithic and have no sliding or rolling parts, they exhibit no significant mechanical stiction or backlash. Additionally, a typical PZT stack actuator can perform step movements in nanometer resolutions with bandwidths on the order of a kilohertz. Consequently, PEA's are well suited for use as precision microactuators for micropositioning devices. In Figure A.2, the actuators used in the experiments are shown.

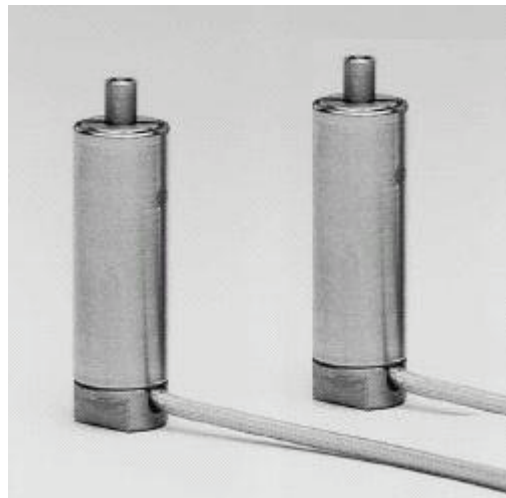


Figure A.2: Piezostack Actuators Used in the PEA Experiments

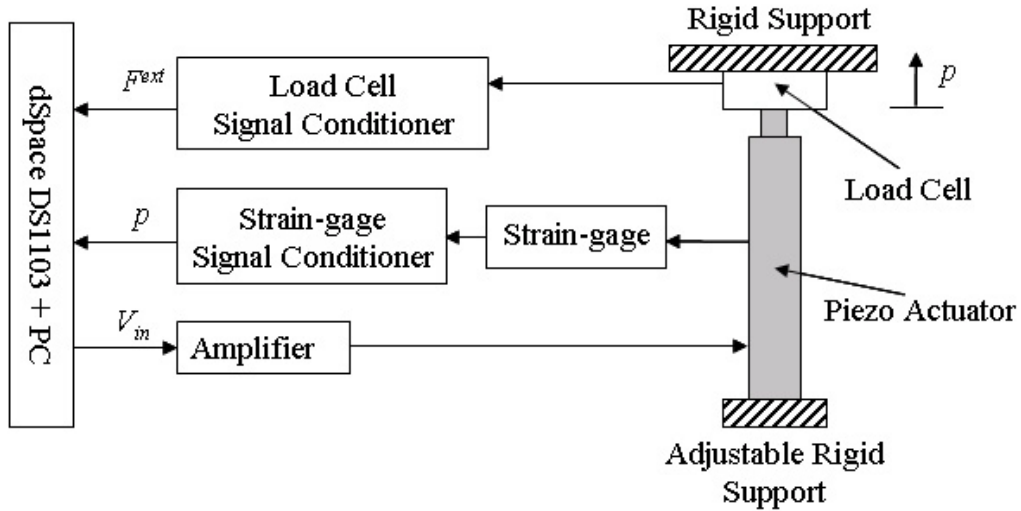


Figure A.3: Structure of the PEA Setup

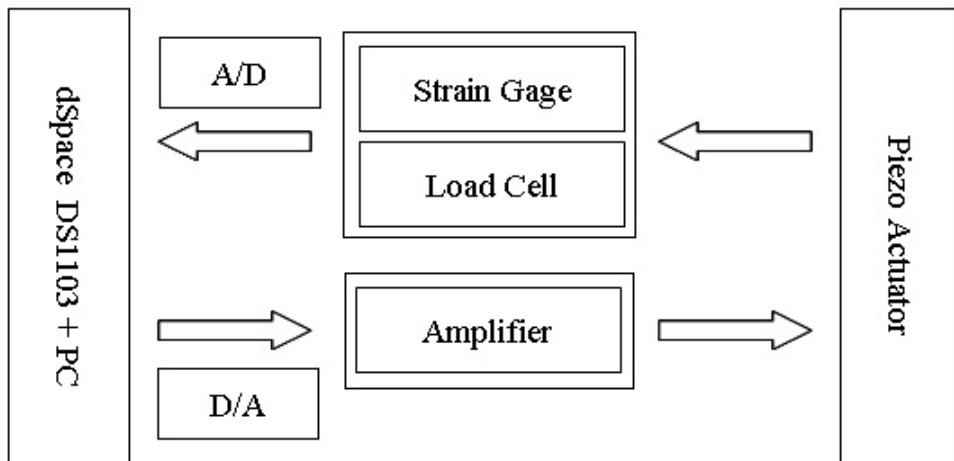


Figure A.4: Simplified Structure of the PEA Setup

An inherent nonlinearity in especially man-made piezoceramic actuators is hysteresis. This hysteresis nonlinearity is usually about 15-20% of the output thereby greatly reducing the performance of the actuators. Additionally, many attempts of modeling this behavior have been fruitless due to its peculiarities. In [26] and [27] attempts were made to model the voltage-to-displacement behavior of PZT actuators using Bond-Graph and Priesach models. These models proved effective, however, they failed to explain the physical behavior of the actuators. In [24] and [25] models were made based on the physics of the actuators and these models proved to be effective in modeling the behavior of these actuators under different excitations. Additionally, they claim that the hysteresis behavior exists in the electrical domain

of the actuator and is between voltage and charge. In [25], a simple differential equation was used to model the voltage-charge hysteresis behavior. This model proved simple to implement in real-time applications due to the simplicity of the equation representing the hysteresis. However in this work, a simpler linear motion equation with nominal parameters is used as a model of the PEA instead of a more accurate model involving the hysteresis function to demonstrate the efficiency of SMC in case of highly nonlinear plants to be controlled.

The experimental setup consists of a PSt150/5/60 stack actuator ( $p_{max} = 60\mu\text{m}$ ,  $F_{max} = 800\text{N}$ ,  $V_{max} = 150\text{V}$ ) produced by Piezomechanik connected to a LE150HYB/020 Hybrid (Voltage/Current) Amplifier, with a voltage range of 20 V through 150 V and a voltage gain of 50, produced by Piezomechanik. The piezoelectric actuator has built-in strain-gages for position measurement. Force measurement is accomplished with the help of a load cell that is placed against the actuator as shown in Figure A.3 and Figure A.4 presents a simplified version. Any motion on the tip of the actuator will exert a force on the load cell which is equal and opposite of the force on the actuator. Hence, the force measured by the load cell is nothing but the force acting on the actuator.

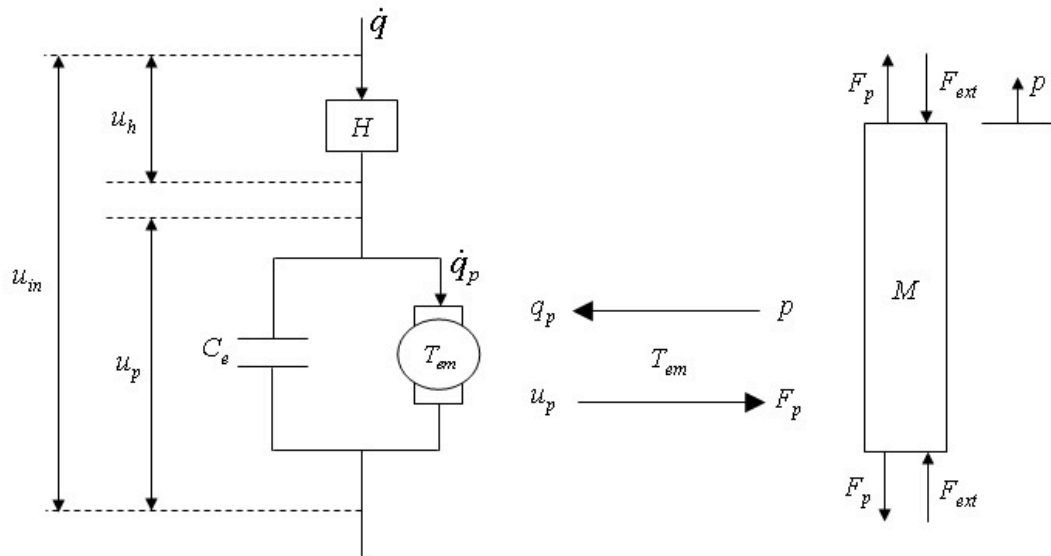


Figure A.5: Electromechanical Model of PEA

The piezoelectric ceramic has elasticity modulus  $E$ , viscosity  $\eta$ , and mass density  $\rho$ . The geometrical properties of the PEA are length  $L$  and cross-sectional area  $A_p$ .

The mechanical parameters, mass  $m_p$ , stiffness  $k_p$ , and damping coefficient  $c_p$  can be calculated from these material and geometrical properties as (A.2.2 - A.2.4).

$$m_p = \rho A_p L, \quad (\text{A.2.2})$$

$$c_p = \frac{\eta A_p}{L}, \quad (\text{A.2.3})$$

$$k_p = \frac{E A_p}{L}. \quad (\text{A.2.4})$$

Though, it will be safer to experimentally measure those using FRF analysis, since, some of the parameters needed above are not easily available.

As shown in [25] and referring to the model shown in Figure A.5, the complete set up electromechanical equations are written as (A.2.5 - A.2.10).

$$u_i n = u_h - u_p, \quad (\text{A.2.5})$$

$$q = H(u_h), \quad (\text{A.2.6})$$

$$q = C_e u_p + q_h, \quad (\text{A.2.7})$$

$$q_p = T_{em} p, \quad (\text{A.2.8})$$

$$F_p = T_{em} u_p, \quad (\text{A.2.9})$$

$$m_p \ddot{p} + c_p \dot{p} + k_p p = F_p - F_{ext}. \quad (\text{A.2.10})$$

In these equations,  $u_i n, u_h$  and  $u_p$  are the total applied voltage, the voltage spent by the hysteresis and the effective voltage applied to the PEA, respectively.  $q$  denotes the charge,  $C_e$  is the effective capacitance of the dielectric (piezo) material and  $T_{em}$  is the force constant of the electromechanical model. In this work, the motion equation is incompletely defined as

$$m_p \ddot{p} + c_p \dot{p} + k_p p = T_{em} u_{in} - F_{ext}, \quad (\text{A.2.11})$$

assuming that  $u_{in} = u_p$ , disregarding the hysteresis behaviour to be compensated later by a sliding mode model reference controller (SMMRC). The parameters of this nominal linear motion model, (A.2.11) are given in Table A.2.

Parameter	Value
Mass ( $m_p$ )	$9.24 \times 10^{-4}$ kg
Damping Coefficient ( $c_p$ )	685 Ns/m
Dynamical Friction Coefficient ( $k_p$ )	$8.0 \times 10^6$ N/m
Force Constant ( $T_{em}$ )	3.9 N/V

Table A.2: Nominal Parameters of the PEA Model

To test and demonstrate the hysteresis behaviour of the used model (A.2.11), a varying amplitude 1 Hz sinusoidal voltage input is given to the plant to yield the Figures A.6, A.7, and A.8.

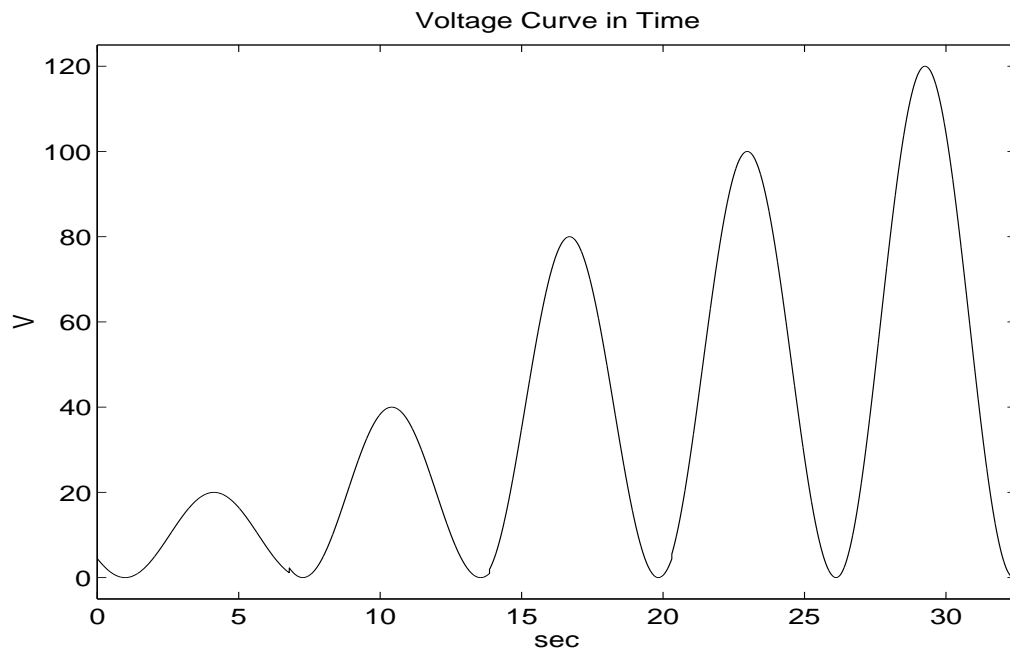


Figure A.6: 1 Hz Sinusoidal Voltage Input with Varying Amplitude for Hysteresis Analysis of PEA

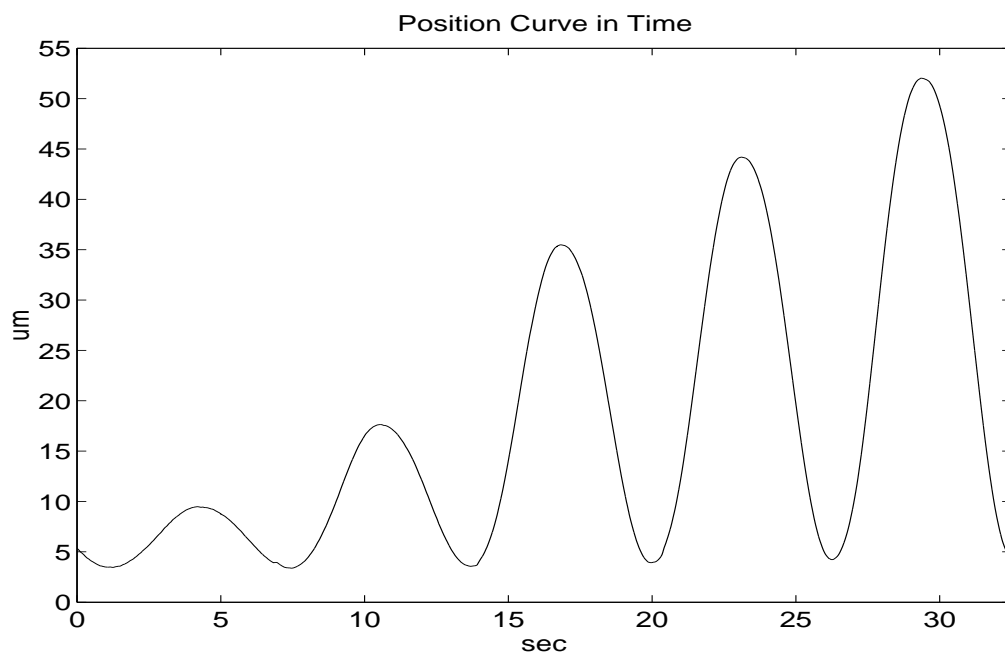


Figure A.7: Position Output of PEA for 1 Hz Sinusoidal Voltage Input with Varying Amplitude

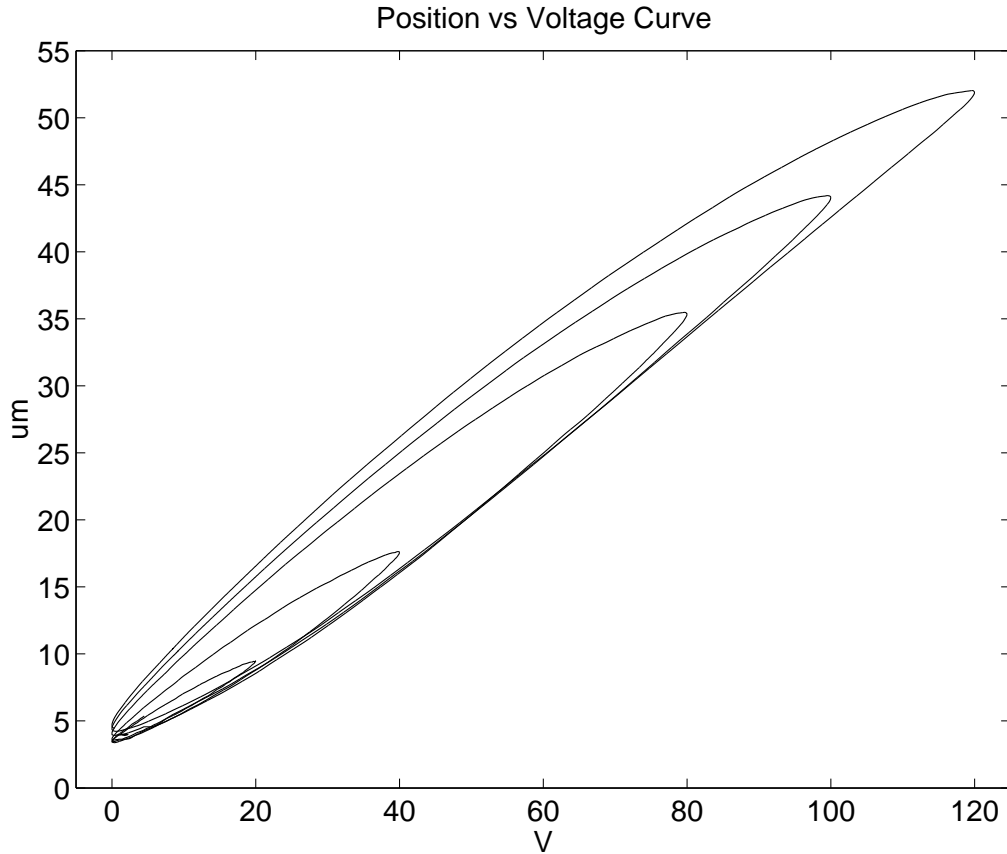


Figure A.8: PEA Position Voltage (Hysteresis) Curve for 1 Hz Sinusoidal Voltage Input with Varying Amplitude

### A.3 Unscaled Bilateral Control Experimental Setup

In the bilateral control experiments, for the unscaled case (i.e.  $\alpha = \beta = 1$ ), the experimental setup shown in Figure A.9 was used. In this setup, master and slave sides are identical Maxon RE-40 DC motors, hence no scaling is performed.

### A.4 Scaled Bilateral Control Experimental Setup

In the bilateral control experiments, for the scaled case, the experimental setup shown in Figure A.10 was used. In this setup master side is the Maxon RE-40 DC motor and the slave side is the PEA, which enables scaled teleoperation experiments.

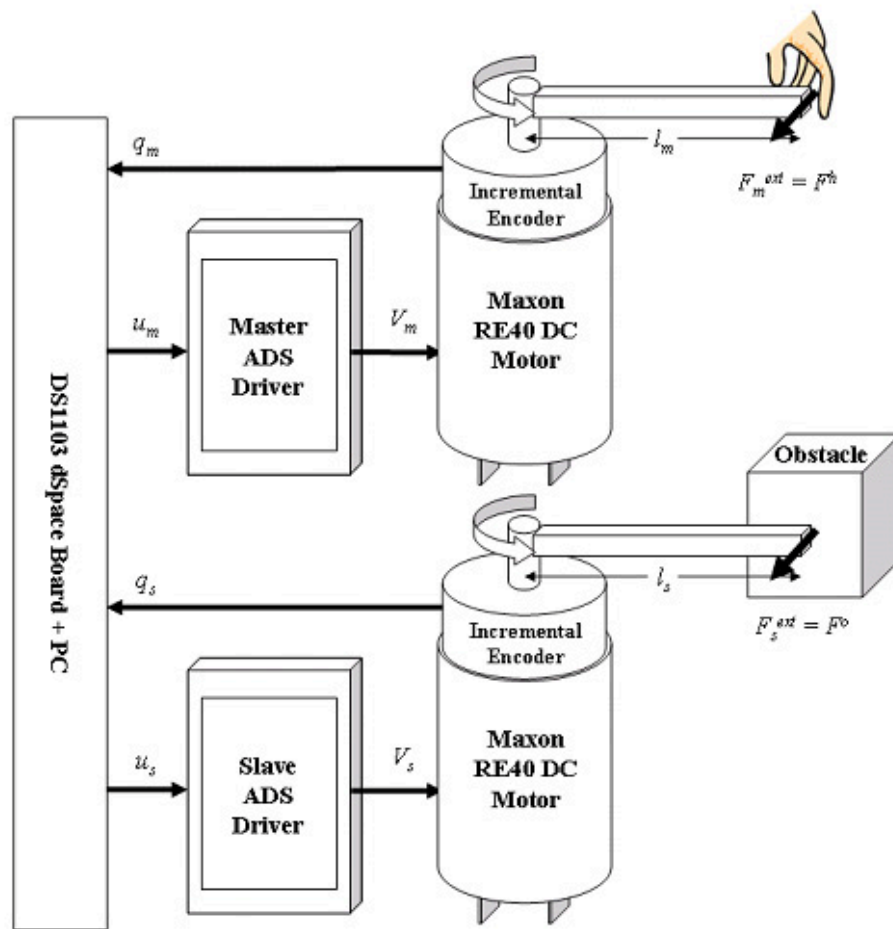


Figure A.9: The Experimental Setup for Unscaled Bilateral Control

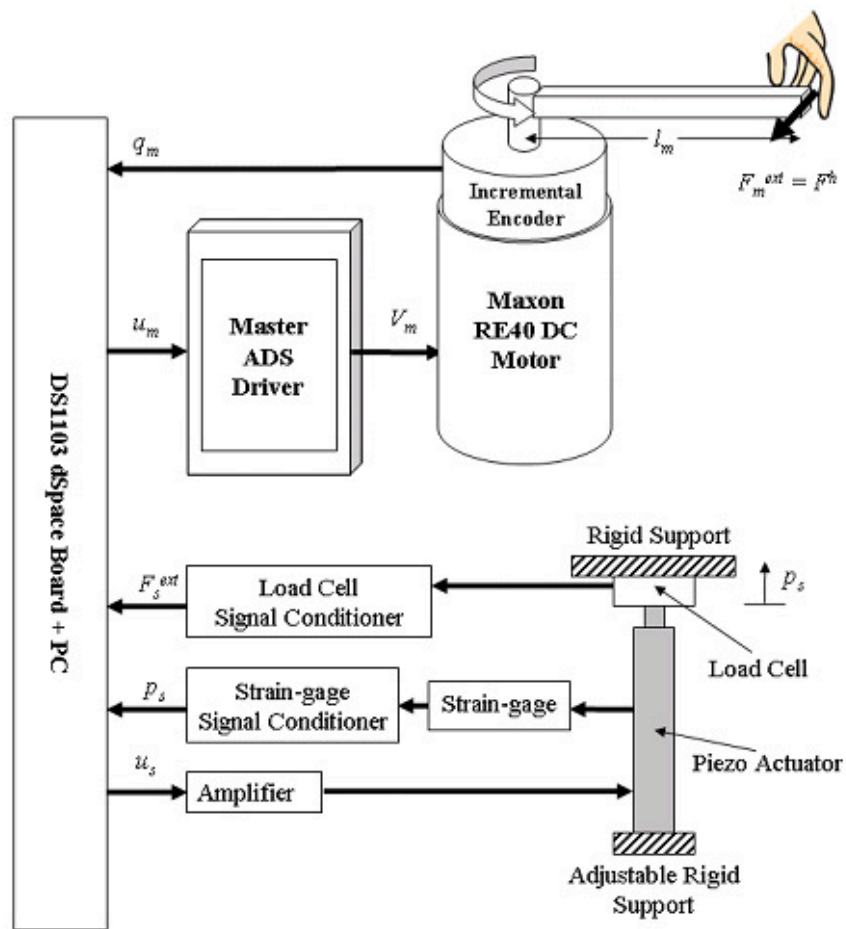


Figure A.10: The Experimental Setup for Scaled Bilateral Control

# Bibliography

- [1] J. Amat, A. Casals, M. Frigola and E. Martin, “Experimental Bilateral Control Telemanipulation Using a Virtual Exoskeleton,” *Springer Tracts in Advanced Robotics*, vol. 5, pp. 350–361, 2003.
- [2] R. J. Anderson and M. W. Spong, “Bilateral Control of Teleoperators with Time Delay,” *Proceedings of the 27th Conference on Decision and Control*, 1988.
- [3] I. Elhajj , W. K. Fung and Y. Liu, “Real-Time Bilateral Control of Internet-Based Teleoperation,” *Proceedings of the 3rd World Congress on Intelligent Control and Automation*, 2000.
- [4] K. Yamada, N. Iida and N. Kudou, “Design of Bilateral Control for a Certain Class of Non-Minimum Phase Time-Delay System –The Parameterization Approach–,” *Proceedings of the 2002 IEEE International Symposium on Intelligent Control*, 2002.
- [5] Y. Yokokohji and T. Yoshikawa, “Bilateral Control of Master-Slave Manipulators for Ideal Kinesthetic Coupling,” *IEEE International Workshop on Intelligent Robots and Systems*, pp. 355–362, 1990.
- [6] T. Tsuji, K. Natori and K. Ohnishi, “A Controller Design Method of Bilateral Control System,” *EPE-PEMC04*, Vol. 4, pp. 123–128, 2004.
- [7] M. H. Raibert and J. J. Craig, “Hybrid position/force control of manipulators”, *ASME Journal of Dynamic Systems, Measurement and Control*, Vol. 102, pp. 126–133, 1981.

- [8] J. J. Craig and M. H. Raibert, “A systematic method of hybrid position/force control of a manipulator”, *Proc. IEEE Computer Software and Applications Conference, COMPSAC 79*, pp. 446–451, 1979.
- [9] P.B. Goldsmith, B.A. Francis, and A.A. Goldenberg, “The cause of kinematic instability in hybrid position/force control: contact compliance”, *Intelligent Information Systems, IIS '97 Proceedings*, pp. 594-598, 8–10 Dec. 1997.
- [10] Luya Li, “Stable hybrid position/force control for redundant manipulators”, *IEEE International Conference on Systems, Man, and Cybernetics*, Vol. 4, pp. 3261–3266, 1997.
- [11] D. Xiao, B. K. Ghosh, N. Xi, T. J. Tarn, “Sensor-based hybrid position/force control of a robot manipulator in an uncalibrated environment”, *IEEE Transactions on Control Systems Technology*, Vol. 8, pp. 635–645, 2000.
- [12] N. Hogan, “Impedance control: an approach to manipulation”, *ASME Journal of Dynamic Systems, Measurement and Control*, Vol. 107, pp. 1–7, 1985.
- [13] N. Hogan, “Stable execution of contact tasks using impedance control”, *Proceedings of the IEEE International Conference of Robotics and Automation*, pp. 1047–1053, 1987.
- [14] F. Y. Hsu, L. C. Fu, “Intelligent robot deburring using adaptive fuzzy hybrid position/force control”, *IEEE Transactions on Robotics and Automation*, Vol. 16, pp. 325–335, 2000.
- [15] R. G. Gilbertson and J. D. Busch, “A survey of micro-actuator technologies for future spacecraft missions”, *The Journal of The British Interplanetary Society*, Vol. 49, pp. 129–138, 1996.
- [16] K. Abidi, A. Sabanovic and S. Yesilyurt, “Sliding-mode based force control of a piezoelectric actuator,” *ICM04, Proceedings of the IEEE International Conference on Mechatronics*, pp. 104–108, 2004.
- [17] C. D. Onal, K. Abidi, A. Sabanovic, “A Cascaded Sliding Mode Hybrid Force/Position Controller,” *International Symposium on Industrial Electronics, ISIE05*, pp. 183–188, June 2005.

- [18] A. Sabanovic and C. D. Onal “Hybrid Control - SMC Point of View,” *IPEC’05, Proceedings of the International Power Electronics Conference*, pp. 1815–1822, 2005.
- [19] V. Utkin, “Variable structure systems with sliding modes”, *IEEE Transactions on Automatic Control*, Vol. 22-2, pp. 212–222, 1977.
- [20] V. Utkin, J. Guldner and J. Shi, *Sliding Modes in Electromechanical Systems*, Taylor and Francis, London, 1999.
- [21] A. Sabanovic, L. M. Fridman, and S. Spurgeon, *Variable Structure Systems: from Principles to Implementation* IEE Control Series, Vol. 66, The Institute of Electrical Engineers, London, 2004.
- [22] Y. Matsumoto, S. Katsura and K. Ohnishi, “An analysis and design of bilateral control based on disturbance observer,” *2003 IEEE International Conference on Industrial Technology*, Vol. 2 pp. 802–807, Dec 2003.
- [23] D. A. Lawrence, “Stability and Transparency in Bilateral Teleoperation,” *IEEE Transactions on Robotics and Automation*, Vol. 9 No. 5 pp. 624–637, Oct 1993.
- [24] M. Goldfarb and N. Celanovic, “Modeling Piezoelectric Stack Actuators for Control of Micromanipulation,” *IEEE Control Systems Magazine*, Vol. 17 Issue 3 pp. 69–79, June 1997.
- [25] J. M. T. A. Adriaens, W. L. Koning and R. Banning, “Modeling Piezoelectric Actuators,” *IEEE/ASME Transactions on Mechatronics*, Vol. 5 No. 4 pp. 331–341, Dec 2000.
- [26] H. Jung, J. Y. Shim and D. Gweon, “Tracking control of piezoelectric actuators,” *Institute of Physics Publishing, Nano-technology*, Vol. 12 pp. 14–20, 2001.
- [27] R. B. Mrad and H. Hu, “A Model for Voltage to Displacement Dynamics in Piezoceramic Actuators Subject to Dynamic-Voltage Excitations,” *IEEE/ASME Transactions on Mechatronics*, Vol. 7 No. 4 pp. 479–489, Dec 2002.

- [28] I. Flgge-Lotz, *Discontinuous Automatic Control*, Princeton: Princeton University Press, 1953.
- [29] Z. Ya Tsytkin, *Discontinuous Automatic Control*, Gostekhizdat, Moscow (in Russian), 1955.
- [30] S. V. Emelyanov and A. I. Fedotova, “Design of astatic tracking system with variable structure”, *Automat. Remote Contr.*, Vol. 10 pp. 1223–1235, 1962.
- [31] S. V. Emelyanov and N. E. Kostyleva, “Design of variable structure control systems with discontinuous switching function.”, *Eng. Cybern.*, Vol. 1 pp. 156–160, 1964.
- [32] S. V. Emelyanov, *Variable Structure Control*, Nauka, Moscow (in Russian), 1967.
- [33] U. Itkis, *Control systems of variable structure*, John Wiley & Sons, New York, Toronto, 1976.
- [34] J. Y. Hung, W. Gao and J. C. Hung, “Variable Structure Control: A Survey”, *IEEE Transactions on Industrial Electronics*, Vol. 40 No. 1, pp. 2–22, 1993.
- [35] H. Kiendl, *Suboptimale Regler mit abschnittweise linearer Struktur*, Springer, New York, 1972.
- [36] H. Kiendl and G. Schneider, “Synthese nichtlinearer Regler für die Regelstrecke  $\text{const}/s^2$  aufgrund ineinandergeschachtelter abgeschlossener Gebiete beschränkter Stellgröße,” *Regelungstechnik und Prozeß-datenverarbeitung*, Vol. 20 No. 7 pp. 289–296, 1972.
- [37] J. Adamy, “Soft Variable-Structure Controls: A Survey,” *Automatica : (Oxford)*, Vol. 40 No. 11, pp. 1821–1844, 2004.
- [38] J. J. Slotine, and W. P. Li, *Applied Nonlinear Control*, Prentice-Hall Inc., New Jersey, 1991.
- [39] S. V. Drakunov and V. Utkin, “A Semigroup Approach to Discrete-Time Sliding Modes,” *Proceedings of the American Control Conference*, June 1995.

- [40] K. Ohnishi, N. Matsui and Y. Hori, “Estimation, identification, and sensorless control in motion control system,” *Proceedings of the IEEE*, Vol. 82 No. 8 pp. 1253–1265, 1994.
- [41] T. Tsuji, A. Kato, K. Ohnishi, A. Hase, and K. Jazernik, “Safety control of teleoperation system under time varying communication delay,” *The 8th IEEE International Workshop on Advanced Motion Control, AMC '04*, pp. 463–468, March 2004.
- [42] D. J. Lee and M. W. Spong, “Passive Bilateral Control of Teleoperators under Constant Time Delay,” *IEEE Transactions on Robotics*, submitted, June 2004.
- [43] D. J. Lee and M. W. Spong, “Bilateral Teleoperation of Multiple Cooperative Robots over Delayed Communication Networks,” *IEEE Transactions on Robotics*, submitted, November 2004.
- [44] Jin-Quan Huang and F. L. Lewis, “Neural-network predictive control for non-linear dynamic systems with time-delay,” *IEEE Transactions on Neural Networks*, Vol. 14 No. 2, pp. 377–389, March 2003.
- [45] A. K. Bejczy, W. S. Kim and S. C. Venema, “The phantom robot: predictive displays for teleoperation with time delay,” *IEEE International Conference on Robotics and Automation*, Vol. 1, pp. 546–551, May 1990.
- [46] J. Sheng and M. W. Spong, “Model predictive control for bilateral teleoperation systems with time delays,” *Canadian Conference on Electrical and Computer Engineering*, Vol. 4, pp. 1877–1880, May 2004.
- [47] T. Tsuji, K. Natori and K. Ohnishi, “A Controller Design Method of Bilateral Control System,” *EPE-PEMC04*, Vol. 4, pp. 123–128, 2004.